NASA CR-72402

FINAL REPORT
For the period
1 May 1966 to 2 July 1967

# VOLUME I - LITERATURE REVIEW OF ADSORPTION ON METAL SURFACES



By

L. W. Swanson
A. E. Bell
C. H. Hinrichs
L. C. Crouser
B. E. Evans

27 July 1967

CONTRACT NAS3-8910



Technical Management
NASA Lewis Research Center
Cleveland, Ohio
Electric Propulsion Office

Field Emission Corporation
McMinnville, Oregon

FINAL REPORT
For the period
1 May 1966 to 2 July 1967

# VOLUME I - LITERATURE REVIEW OF ADSORPTION ON METAL SURFACES

By

L. W. Swanson
A. E. Bell
C. H. Hinrichs
L. C. Crouser
B. E. Evans

27 July 1967

CONTRACT NAS3-8910

Technical Management
NASA Lewis Research Center
Cleveland, Ohio
Electric Propulsion Office

FIELD EMISSION CORPORATION
Melrose Avenue at Linke Street
McMinnville, Oregon

TABLE OF CONTENTS

TABLE OF CONTENTS (cont'd)

TABLE OF CONTENTS (cont'd)

TABLE OF CONTENTS (cont'd)

TABLE OF CONTENTS (cont'd)

## LIST OF ILLUSTRATIONS

LIST OF ILLUSTRATIONS (cont'd)

LIST OF ILLUSTRATIONS (cont'd)

LIST OF ILLUSTRATIONS (cont'd)

LIST OF ILLUSTRACTIONS (cont'd)

## LIST OF TABLES

## LIST OF SYMBOLS

The following is a list in alphabetical order of symbols used in the text. Some symbols have different meanings in various sections of the report. A number in the last column indicates the section in which the symbol has a particular meaning.

| Symbol | Meaning | Section |
|---|---|---|
| A | surface area in $cm^2$ | A-2, 3, 7 |
| | theoretical Richardson constant | A-6 |
| $A_f$ | pre-exponential in Fowler-Nordheim equation | A-4 |
| $A_r$ | experimental Richardson constant | A-6, B |
| a | slope of Fowler-Nordheim plot | A-4 |
| | radius of electron path in a magnetic field | A-6 |
| $a_d$ | average jump length of migratory atoms | A-4 |
| $a_M$ | maximum radius of electron path in a magnetic field | A-6 |
| $a_0$ | slope of Fowler-Nordheim plot for surface whose work function is $\phi_o$ | A-4 |
| $a_1$ | slope of Fowler-Nordheim plot for surface whose work function is $\phi_1$ | A-4 |
| B | arbitrary constant | A-6 |
| C | total heat capacity | A-7 |
| c | arbitrary constant | A-3 |
| | $-4/3\left[(2m\phi^3)^{1/2} v(y)/\hbar eF\right]$ | A-4 |
| D | diffusion coefficient | A-4, B |

LIST OF SYMBOLS (cont'd)

| Symbol | Meaning | Section |
|---|---|---|
| $D_o$ | diffusion constant | A-4, B |
| d | $\hbar eF/(2m\phi)^{1/2}t(y)$ | A-4 |
| | resolution limit of FIM | A-5 |
| $d_{hk}$ | interrow spacing between atoms | A-1 |
| E | metal-adsorbate binding energy | A-2, B |
| $E_a$ | activation energy for neutral desorption | A-4, 7, B |
| $E_d$ | activation energy for surface diffusion | A-4, B |
| $E_o$ | zero coverage desorption activation energy | B |
| $E_p$ | activation energy for ionic desorption | B |
| $E_d^f$ | field dependent activation energy for surface diffusion | B |
| Eff | ionization efficiency | A-3 |
| e | electronic charge | A-3, 4, 5, 6 |
| F | electric field | A-4, 5, B |
| | Helmholz potential | A-6 |
| F(X) | function in basic equation for Fowler-analysis | A-6 |
| $f_i$ | fraction of total field emission current coming from a single plane | A-4 |
| g | constant in equation for coverage dependent desorption activation energy | B |
| H | magnetic field | A-6 |
| $H_{111}$ | heat of adsorption on the (111) plane | B |

LIST OF SYMBOLS (cont'd)

| Symbol | Meaning | Section |
|---|---|---|
| $\Delta H$ | equilibrium heat of adsorption | A-7 |
| $h$ | Planck's constant<br>average hopping height | A-4, 6<br>A-5 |
| $\hbar$ | Planck's constant divided by $2\pi$ | A-4 |
| $I$ | electron current | A-3, 4, 6 |
| $I^+$ | positive ion current | A-3, 7 |
| $I_o^+$ | $\sigma_o Q^+ I$ | A-3, 7 |
| $J$ | electron current density | A-3, 6 |
| $J_{OF}$ | field emission current density at $0^oKelvin$ | A-4 |
| $J_{TF}$ | thermal-field emission current density | A-4 |
| $J_e$ | thermionic current density in retarding potential | A-6 |
| $J_o$ | thermionic current density | A-6 |
| $K$ | $(kT/2\pi m)^{1/2}$<br>constant in Equation (70) | A-2<br>A-6 |
| $k$ | Boltzmann's constant | A-2, 4, 5, 6, 7, B |
| $k_t$ | image compression factor | A-5 |
| $M$ | effective dipole moment | A-4, 6, B |
| $M_t$ | total dipole moment | A-6 |
| $M_{virgin}$ | dipole moment of virgin layer | B |
| $M_\alpha$ | dipole moment for $\alpha$ phase | B |
| $M_\beta$ | dipole moment for $\beta$ phase | B |

LIST OF SYMBOLS (cont'd)

| Symbol | Meaning | Section |
|---|---|---|
| $m$ | particle mass | A-2, 4 |
| $n$ | order of the diffraction image | A-1 |
| | density of molecules in gas phase | A-2, 3 |
| | number of electrons | A-6 |
| $n_a$ | number of adsorbed particles | A-7 |
| $P(\epsilon)$ | number of electrons whose energy relative to the Fermi level lies between $\epsilon$ and $\epsilon + d\epsilon$ | A-4 |
| $p$ | pressure | A-2, 3, 7 |
| | $kT/d$ | A-4 |
| $Q$ | total electron desorption cross section | A-3, B |
| $Q^+$ | electron desorption cross section for ionic desorption | A-3 |
| $Q_{virgin}$ | electron desorption cross section for "virgin" layer | B |
| $Q_a$ | electron desorption cross section for $a$ phase | B |
| $q$ | rate of gas influx into the system | A-2 |
| | influx of gas due to electron impact desorption | A-3 |
| | heat of adsorption | A-7 |
| $q_a$ | adiabatic heat of adsorption | A-7 |
| $q_d$ | differential heat of adsorption | A-7 |
| $q_{iso}$ | isoteric heat of adsorption | A-7 |
| $q_o$ | gas influx responsible for background pressure | A-2, 3 |
| $q_1$ | adsorbate gas influx admitted externally | A-2 |
| $q_2$ | gas evolving from the surface | A-2 |

LIST OF SYMBOLS (cont'd)

| Symbol | Meaning | Section |
|---|---|---|
| R | gas constant | A-7 |
| $R_1, R_2$ | gas reservoirs of constant volume | A-7 |
| r | tip radius | A-5 |
| S | system pumping speed<br>entropy | A-2, 3<br>A-6 |
| $S_a$ | pumping by adsorbate on surface | A-2 |
| s | sticking coefficient<br>transition probability or entropy factor | A-2, B<br>A-4 |
| s(y) | tabulated function in Equation (39) | A-4 |
| T | temperature in degrees Kelvin | A-2, 3, 4, 5, 6, 7, B |
| $T_p$ | temperature at constant pressure | A-2 |
| t | time in seconds | A-2, 3 |
| t(y) | slowly ranging function of $\emptyset$ and F | A-4 |
| U | potential energy | A-6 |
| V | voltage, or potential difference | A-1, 4, 5, 6 |
| $V_a$ | voltage applied to anode | A-6 |
| $V_{AB}$ | contact potential difference | A-6 |
| $V_c$ | voltage applied to central accelerating electrode | A-6 |
| $V_e$ | potential of electron relative to anode | A-6 |
| $V_I$ | ionization potential | A-4, 5 |
| $V_{in}$ | potential inside the metal | A-6 |

LIST OF SYMBOLS (cont'd)

| Symbol | Meaning | Section |
|---|---|---|
| $V_{out}$ | potential outside the metal | A-6 |
| $V_R$ | retarding potential | A-6 |
| $V_1, V_2, V_3, V_4, V_5$ | gas inlet valves | A-7 |
| v | volume of the system | A-2, 3, 6 |
| v(y) | slowly varying function of $\emptyset$ and F | A-4 |
| x | order of desorption process - equal to 1 for monatomic and 2 for diatomic molecules | A-2 |
| | distance travelled by adsorbate atom in time t | A-4 |
| | tip to screen distance | A-5 |
| $x_c$ | $x_o + \lambda$ | A-4 |
| | minimum distance at which field ionization can occur | A-5 |
| $x_o$ | equilibrium distance of the ion from the surface | A-4 |
| $\alpha$ | polarizability | A-5, B |
| | temperature coefficient of thermionic work function in Equation (74) | A-6 |
| | surface phase of various adsorbates | B |
| $\alpha_a$ | effective adsorbate polarizability | A-4 |
| $\alpha_i$ | ionic polarizability | A-4 |
| $\beta$ | arbitrary constant | A-2 |
| | geometrical factor equal to F/V | B |
| | surface phase of various adsorbates | B |
| $\gamma$ | surface phase of various adsorbates | B |
| $\epsilon$ | energy | A-4, 7 |
| | numerical constant | A-5 |

LIST OF SYMBOLS (cont'd)

| Symbol | Meaning | Section |
|---|---|---|
| $\epsilon(T)$ | temperature dependent energy | A-6 |
| $\epsilon_o$ | permittivity of free space | A-6 |
| $\theta$ | relative surface coverage equal to $\sigma/\sigma_o$ | A-6, B |
| $\theta_m$ | relative coverage at maximum work function change | B |
| $\theta_{hk}$ | diffraction angle measured relative to surface normal | A-1 |
| $\lambda$ | wavelength for electrons<br>Thomas-Fermi screening length | A-1<br>A-4 |
| $\bar{\mu}$ | electrochemical potential | A-6 |
| $\mu$ | chemical potential | A-6 |
| $\nu$ | pre-exponential frequency factor<br>photon frequency for photoemission | A-2, 4<br>A-6 |
| $\nu_o$ | threshold frequncry for photoemission | A-6 |
| $\pi$ | spreading pressure | A-7 |
| $\sigma$ | surface coverage density<br>dipoles per unit area | A-2, 3, 4, 7, B<br>A-6 |
| $\sigma_o$ | defined by Equation (14)<br>number of adsorption sites | A-2, 3<br>A-6 |
| $\tau$ | reciprocal frequency defined by Equation (44) | A-4, 7 |
| $\tau_i$ | lifetime with respect to field ionization | A-5 |
| $\tau_o$ | pre-exponential factor | A-7, B |
| $\phi$ | work function | A-3, 4, 5, 6, B |

LIST OF SYMBOLS (cont'd)

| Symbol | Meaning | Section |
|---|---|---|
| $\phi_o$ | work function of clean surface | A-4, B |
| $\phi_1$ | work function of adsorbate covered surface | A-4 |
| $\phi_a$ | work function of anode | A-6 |
| $\phi_c$ | work function of cathode | A-6 |
| $\phi_{oc}$ | temperature independent work function of thermionic cathode | A-6 |
| $\phi_m$ | work function at $\theta_m$ | B |
| $\phi_{min}$ | minimum work function due to adsorption | B |
| $\Delta\phi_m$ | maximum work function change due to adsorption | B |
| $\phi_r$ | experimentally determined thermionic work function; obtained from Richardson plot | A-6 |
| $\phi_{110}; \phi_{100}; \phi_{111}$ | single crystal face work functions on the (110), (100), and (111) planes respectively | B |
| $\chi$ | surface potential | A-6 |

# INTRODUCTION

The importance of the solid surface in present day technology is not easily overestimated. Indeed, it seems possible that the surface properties of a solid affect technology as much as bulk properties, an observation which is all the more surprising when one compares the amounts of time and money spent on surface research with that devoted to the investigation of the bulk properties of the solid state. Of the several reasons for the fact that the bulk properties of solids have been studied more extensively than have their surface properties, the importance of the bulk properties to the field of solid state electronics is predominant. Also, the properties of solids are often more easily measured than effects which occur at the surface. In fact, the ability to study surfaces has been very dependent upon the ability of the researcher to invent tools suitable to surface research. The field electron microscope, one of the first of the new tools, has been followed in recent years by such novel devices as the field ion microscope, the low energy electron diffraction analyzer and others.

The role played by surfaces in electron emission, ion emission, catalysis, vacuum technology, corrosion, bonding (both adhesive and cohesive), contact charging, and friction, not to mention the basic insights gained, may all be cited as reasons for studying interactions involving surfaces. However, before questions concerning these various surface problems can be adequately answered, a great deal of basic information must be acquired concerning surface interactions. As it now stands, surface physics is still in a primitive state; and a great deal must still be done, both theoretically and experimentally, if we expect to be able to attack the important problems of surface physics and chemistry.

In spite of the difficulties, surface research has grown rapidly in

recent years. Along with the rapid advances taking place in the field of surface physics, has come the need for a comprehensive compilation of experimental results, an endeavor that is necessary before a satisfactory understanding of surface phenomena is possible.

Although experimental investigations of metal surface-adsorbate interactions have been conducted for many years, very few experiments carried out prior to the advent of ultra-high vacuum technology may be regarded as having meaning. This may be understood readily if reference is made to the length of time required for a monolayer of residual gas to be formed on a freshly-cleaned metal surface. If the pressure is of the order of $10^{-4}$ torr, a pressure within the capabilities of mechanical pumps, a monolayer is formed in less than 0.01 seconds. At $10^{-7}$ torr, a region commonly referred to as the high vacuum region, 10 seconds are required, while in the ultra-high vacuum region of $10^{-10}$ torr or better a monolayer is formed only after about 3 hours. Thus, it becomes clear that one of the first considerations in evaluating the merits of an experimental technique is that of the static vacuum conditions prevailing during the course of the experiment. This factor also established a reasonable starting point for a literature review since it was not until 1953 that the methods of measuring pressures in the ultra-high vacuum were well established. This is not to say that ultra-high vacuum had not been obtained prior to this date, but only that it was difficult to demonstrate. No effort has been made here to describe the vacuum techniques since a number of excellent reviews are already in existence.

A second consideration which bears heavily upon the reliability of the experimental results is that of the condition of the surface. Since the interaction of the adsorbate with the surface is affected strongly by the presence of a contaminant, it is important that the surface be clean prior to adsorption. Thus, methods must be available for cleaning the

surface if the experimental technique is to be acceptable. While the most direct method of cleaning the surface is by heating, it is not possible to clean some metals this way and other methods must be devised such as sputtering. Accepted methods of cleaning metal surfaces are described in the data section of this report.

In most cases, the interpretation of the experimental results is complicated by the uncertainty associated with the structure of the surface. For example, if the surface is polycrystalline, it is difficult to identify the relationship between the experimental results and the surface structure. Total emission measurements of work function yield only weighted averages over all the crystal faces present. Therefore, priority is given to experimental techniques which permit studies to be made on smooth single crystallographic planes.

A clear understanding of metal surface-adsorbate interactions can come only after an adequate store of experimental data have been collected. This report represents an initial attempt to collect under one cover all important metal surface adsorption data. This is not to say that the experimental results have been presented indiscriminately, since one of the objectives of this report is to select the most reliable data for tabulation. Because metal surfaces represent the simplest surfaces to study, it is not surprising that much of the reliable adsorption data have been obtained for such surfaces. Single crystals of nearly all metals may be grown, and there are cases where the experimental techniques dictate that the surface material be a conductor of electricity. Of those metals receiving attention, by far the greatest amount of research has been performed on tungsten because it is easily cleaned. The quality of the experimental data depends in an important way upon the techniques used to obtain them. Indeed, the slow progress in understanding surface interactions may be attributed to the lack of sensitive techniques with which to obtain the experimental data; therefore, Section A of Volume I is designed to point

out the important features of the various experimental methods used to obtain the experimental data listed in Section B of this report.

## SECTION A-EXPERIMENTAL TECHNIQUES

The objectives of this section of the report are to outline the acceptable methods of acquiring the data listed in Volume I, Section B of this report. An attempt has been made to present each experimental technique clearly enough that a reader may be able to read the pertinent papers with understanding. In each instance, the description has been treated in as elementary a fashion as possible. Because of the elementary nature of the description, it is anticipated that the reader may wish to refer to some of the original papers or the several excellent reviews which have been written on the respective topics.

Presented in this section are the separate descriptions of five experimental techniques which have found favor among experimental surface scientists and which are considered to be among the more important techniques currently in use. In addition, there are other techniques which have not been used widely, but which still merit discussion. These methods have been added under the general topics of work function measurements, binding energies, etc.

Attention has been given to the mathematical methods used in experimental analysis, particularly for those experimental techniques which require the use of kinetic equations for the interpretation of the results. One must understand the way in which the kinetic equations have been derived in order to fully appreciate the benefits and shortcomings of an experiment. Only a general discussion is given on details of the experimental apparatus since these vary with experiment and the original papers should be consulted for further clarification.

# 1 - LOW ENERGY ELECTRON DIFFRACTION

## Introduction

When a directed beam of low energy electrons (usually between 20 and 300 eV) is incident upon a crystal surface, a back reflected diffraction image is formed which, when properly analyzed, yields information concerning the atomic structure of the surface. The use of low energy electron diffraction to investigate surfaces had its beginning in 1927 with the experiments of Davisson and Germer[1] in which the wave description of electrons was confirmed. During the 40 years since those historical experiments, the application of low energy electron diffraction to the study of surfaces has continued, primarily through the efforts of Farnsworth[2]. Within the past fifteen years, important advances in vacuum practice and certain experimental techniques associated with low energy electron diffraction have inspired others to use this technique, making it currently the fastest growing field of surface-research[3, 4, 5].

Diffraction effects become important when the wave length of the incident beam is of the order of the spacing of the diffraction centers. The wave length in Angstroms for electrons accelerated through a potential difference of V volts is computed from

$$\lambda = (150.4/V)^{1/2}$$

and if $d_{hk}$ is the interrow spacing of atoms in a two-dimensional array, the conditions for diffraction maxima (Figure 1) are given by the Bragg condition

$$n\lambda = d_{hk} \sin \theta_{hk}$$

where $\theta_{hk}$ is the diffraction angle measure relative to the surface normal and n is the order of the diffraction image.

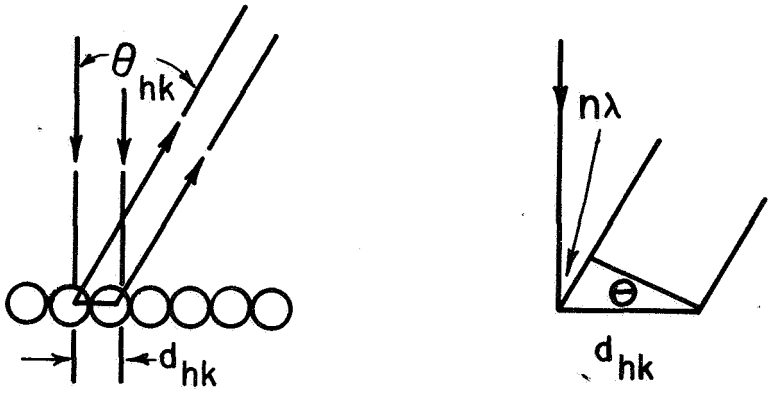


Figure 1. Illustration of conditions for diffraction image maxima.

To a first approximation, the electron diffraction centers have the periodicity of the substrate lattice parallel to the surface and, consequently, the surface serves as a two-dimensional diffraction grating. Idealized diffraction images for two different cases of a surface parallel to a (100) plane and one parallel to a (111) plane are illustrated in Figure 2. The interpretation of these patterns is discussed in further detail below.

The scattering of the incident electrons occurs as a result of charge sensitive interactions at the surface; therefore, low energy electron diffraction effects are sensitive to perturbations in the surface charge distribution due to the presence of foreign atoms on the surface or other factors. For example, it is possible, under favorable conditions to detect the presence of a few percent of a monolayer of adsorbate. In addition, it is possible to observe the effects of temperature on the lattice vibrations of the surface atoms in which the intensity of the diffracted beam is found to depend upon temperature, a phenomenon referred to as the Debye-Waller effect.[6] Although the primary value of low energy electron diffraction has been in providing information concerning surface structure, improvements in technique promise to make possible the investigation of such phenomena as catalysis, adsorption, epitaxy, chemical reaction, and order-disorder transitions.[3,4,5] Furthermore, low energy electron diffraction is a useful method for a wide variety of surface materials, provided a suitable method of cleaning is available. Dielectric surfaces may be investigated if the secondary electron coefficient is equal to or in excess of unity or if the surface is sprayed with electrons to prevent surface charging during the experiment.[7,8]

Although low energy electron diffraction is a highly sensitive method, it is difficult to arrive at a completely fool-proof interpretation of the observed diffraction pattern which can be more complex than the three-dimensional pattern because of a larger number of permissible

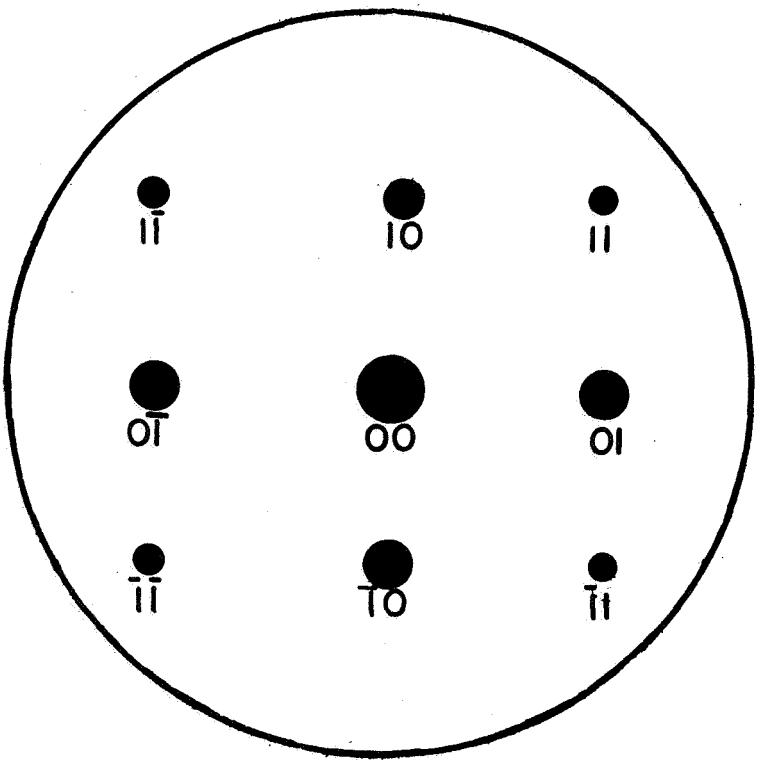


Figure 2a. Diffraction pattern characteristic of (100) plane.

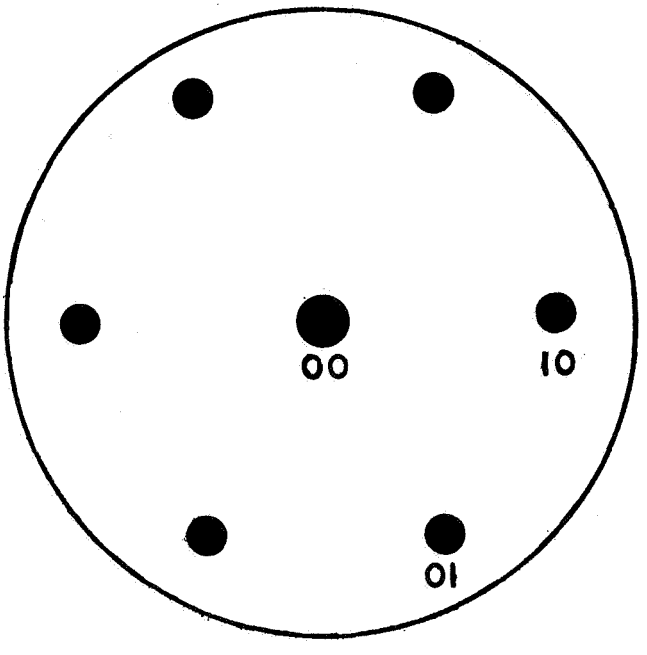


Figure 2b. Diffraction pattern characteristic of (111) plane.

structures.[9] Furthermore, the problem of interpretation is complicated by the fact that diffraction does not occur from the top layer of atoms alone, but second and third atomic layers may also contribute. In addition, there are numerous other factors which add to the complexity of the diffraction image such as secondary electrons, interference effects, due to scattering from steps in the surface layers, temperature effects, and uncertainty in the contact potential.[10] At present, these inherent complications make quantitative analysis of the diffraction image virtually impossible;[11] however, as these problems become better understood, more precise measurements are to be expected.

## Surface Crystallography

As with three-dimensional crystallography, certain conventions have been established for the description of two-dimensional crystal structures. Actually, the conventions used in three-dimensional crystallography have been carried over to two dimensions with only minor modifications or extensions being required. These conventions have been discussed in detail by E. A. Wood[12] and will be introduced here for the convenience of the reader.

In discussing two-dimensional structures, it is convenient to use the term diperiodic to describe any structure, not necessarily with all atoms lying in a plane, which has only two-dimensional symmetry (i.e., no symmetry in the direction normal to the surface). It has been suggested that the transition from the symmetry of the bulk lattice to the extreme of the surface be called the selvedge. The selvedge may be very thin as in the case of metal surfaces or may be three or more atomic layers thick as in the case of certain semi-conductors and compounds.

The terms lattice and unit cells are reserved for three-dimensional symmetry and the corresponding terms to be used in the two-dimensional case are the net and unit mesh respectively. Here, a net is a two-dimensional array of points such that each has an identical environment.

Note this is different from a diperiodic array which may be composed of atoms lying in more than one plane; diperiodic structures are formed by associating with each net point an assembly, or basis, of atoms. In two-dimensional crystallography five nets may be distinguished and are shown in Figure 3. The letter c denotes the use of a centered mesh while p indicates that the net is a primitive mesh. In all cases the convention requires that $a \leq b$.

Listed below is a set of standard symbols, based on the work of Wood, which appear frequently in the literature.

a, b: Lengths of unit-mesh edges such that $a \leq b$. Subscript s may be used to distinguish surface structure from underlying structure where necessary.

$\bar{a}, \bar{b}$: Unit-mesh vectors.

$\gamma$: Interaxial angle xy, ab.

x-, y-: Directions of crystallographic axes of coordinates.

x, y: Coordinates of any point within the unit mesh, expressed in terms of a and b units.

z-: Direction normal to x- and y- directions.

z: Coordinate of any point in this direction.

u, v: Coordinates of any net point, expressed in terms of a and b as units.

uv: Indices of a direction in the direct net.

h, k: Two-dimensional Miller indices of mesh points.

(hk): Indices of a set of parallel rows.

hk: Indices of the reflection from a set of parallel rows; coordinates of a line or "rod" in the reciprocal-lattice as measured on any plane normal to the lines.

{hk}: Indices of equivalent rows with different indices.

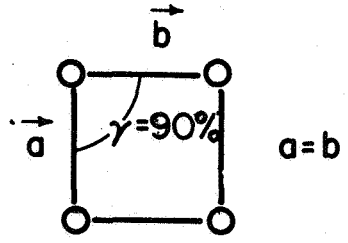


(a) SQUARE

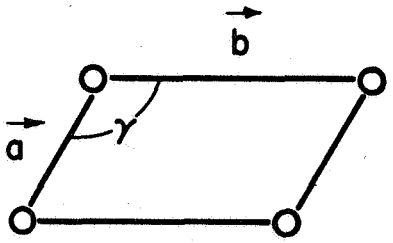


(b) OBLIQUE

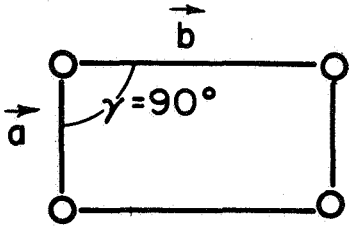


(c) RECTANGULAR

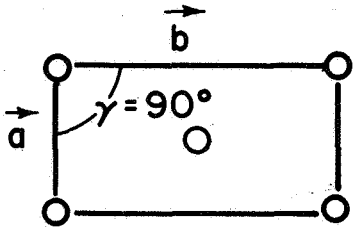


(d) CENTERED RECTANGULAR

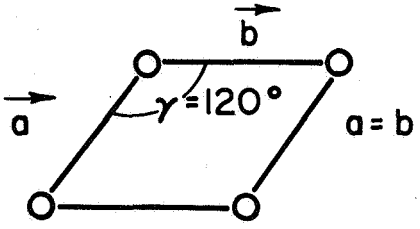


(e) HEXAGONAL

Figure 3. The five two-dimensional nets.

$*$: Starred quantities refer to quantities in reciprocal space.

$d_{(hk)}$: Interrow spacing of rows hk.

p, c: Primitive and centered nets.

The interrow spacings for the five nets are:

Oblique:

$$1/d^2_{(hk)} = (h^2/a^2\sin^2\gamma) + (k^2/b^2\sin^2\gamma) - (2hk\cos\gamma/ad\sin^2\gamma)$$

Rectangular: p and c

$$1/d^2_{(hk)} = (h/a)^2 + (k/b)^2$$

Hexagonal:

$$1/d^2_{(hk)} = 4/3 \left[(h^2 + hk + k^2)/a^2\right]$$

Square:

$$1/d^2_{(hk)} = (h^2 + k^2)/a^2$$

As in the triperiodic case, it is convenient to introduce the concept of a reciprocal lattice in the analysis of diperiodic structures. This, coupled with the Ewald sphere, provides a powerful aid in the reconstruction of the surface structure or net. The Ewald sphere is a sphere of radius $1/\lambda$ intersecting an arbitrarily chosen origin of the reciprocal net such that the incident beam passes through the geometric center of the sphere and the origin of the reciprocal net. In the diperiodic case, the requirements for diffraction are not quite so severe as for the triperiodic lattice so that the reciprocal lattice goes over from a set of lattice points to a set of lines or one-dimensional "rods" extending indefinitely in a direction normal to the plane. The various spots of the diffraction image may then be found from use of the Ewald sphere as shown in Figure 4, for the case of an electron beam incident normal to the (100) surface of a cubic crystal. Notice that in this case, spots corresponding to the 00, 10, 01, $\bar{1}0$, and $0\bar{1}$ reciprocal

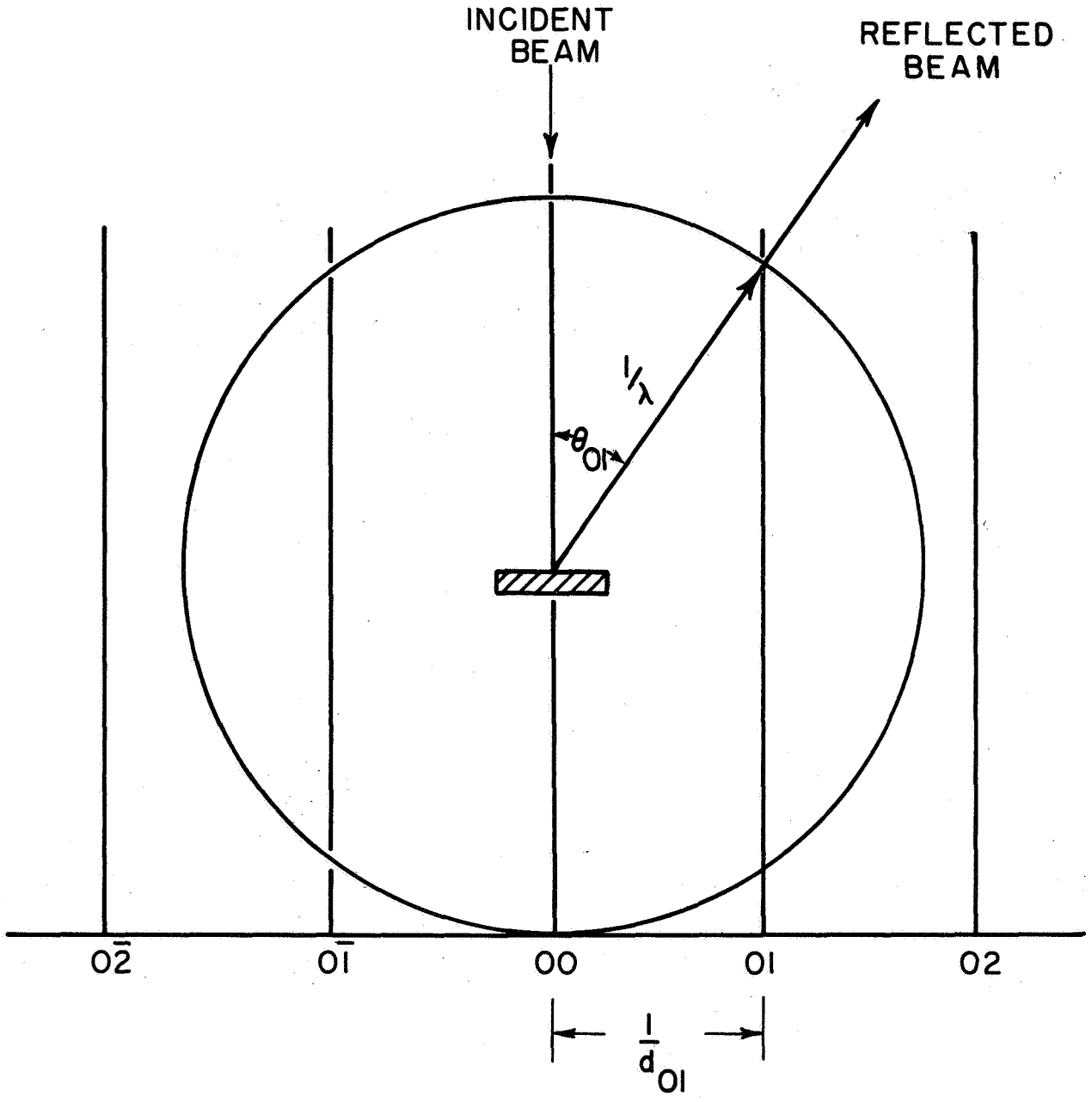


Figure 4. A section of the reciprocal lattice of a diperiodic structure with the Ewald sphere. For the special case of normal incidence and $\lambda = d_{hk} \sin \theta_{hk}$.

lattice lines will be present in the diffraction pattern, but the 02, 20, $0\bar{2}$ and $\bar{2}0$ spots will be absent.

It sometimes happens that the surface mesh and the mesh of the corresponding plane in the bulk are different and it is useful to refer the surface mesh to that of the substrate. This situation arises in at least two ways; when the clean surface structure differs from the bulk and also as a result of adsorption. It is customary to describe the surface mesh in terms of the known substrate mesh. Here the reference net is the net parallel to the surface. Thus, if the substrate net is a square array and the surface is a square array with dimensions twice as large, the surface mesh will be designated 2 x 2 (See Figure 5a). Or in the case of the hexagonal structure shown in Figure 5b, the surface mesh is 3 x 1. The information contained in this short hand notation can be extended by including both the substrate material and the adsorbate. Thus, oxygen adsorbed on the (110) face of nickel is found to have the structure described by Ni(110) 3 x 1-O, meaning that when oxygen is adsorbed on the (110) face of nickel the resulting diperiodic surface structure has a mesh with edges parallel to the edges of the clean surface net but with $a_s$ equal to 3a. If a centered mesh is chosen, the designation would be c(2 x 2) and is shown in Figure 5c. When a simplification results from consideration of a mesh whose sides are turned at an angle with respect to the substrate structure, the designation 3 x 1-R(30°) has been used. This would indicate that the surface mesh with the indicated dimensions is rotated 30° with respect to the substrate mesh.

## Experimental Technique

Three basic experimental approaches have been developed for employing low energy electron diffraction techniques in surface studies. The first approach resembles that of Davisson and Germer in its utilization of a Faraday collector to analyze the diffraction image as illustrated in

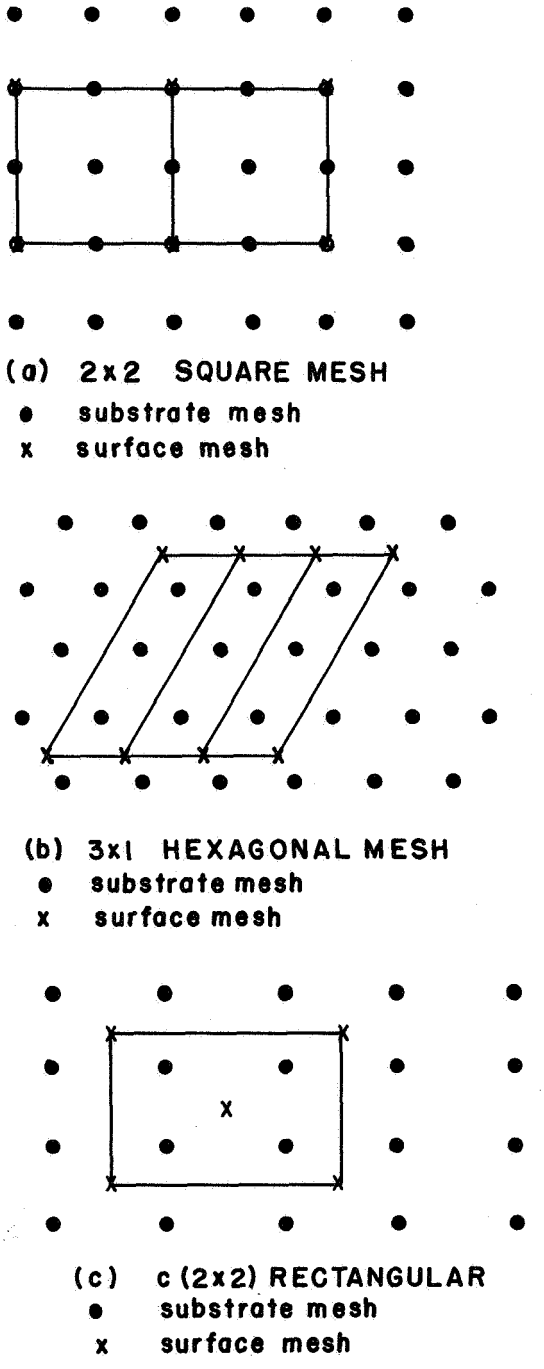


Figure 5. Illustrations of shorthand designation of relationship between surface mesh and substrate mesh.

Figure 6. This method has been used successfully by Farnsworth[4] and it is especially suited to the precise measurement of diffracted beam intensities, an important consideration when one wishes to make a quantitative interpretation of the diffraction image. Measurements made by this method tend to be time consuming unless an automatic or semi-automatic scan is used. In one such system, the sample is rotated about the beam axis at several thousand rpm while the Faraday collector is moved in and out in the azimuthal direction. The results may be read out on an oscilloscope.[13]

The second method of analyzing the diffraction effects is based on a design proposed by Ehrenberg in 1934 in which the diffraction pattern is displayed on a flourescent screen. Since the energy of the diffracted electrons is insufficient (typically a few hundreds of eV) to excite the phosphors used in the screen, it is necessary to accelerate the diffracted electrons to an energy of a few thousand volts. This technique, known as the postacceleration display method, was perfected by Lander et al.[14] and a typical experimental tube design is shown in Figure 7. In this system an electron beam is directed onto the crystal at normal incidence and is diffracted into a nearly field free region. The diffracted beam passes through a spherically shaped grid maintained at the potential of the crystal and exit electrode of the electron gun, and is retarded by the suppressor grid to eliminate secondary radiation. Finally, it is accelerated to the flourescent screen and the resulting pattern is viewed or photographed through a window located behind the crystal.

A major advantage of the display system is its ability to display the entire diffraction pattern instantaneously, a feature which represents a considerable saving in time. This is particularly important if the characteristics of the surface are changing for some reason, as for example, during adsorption. Intensity measurements are readily made with a spot photometer, although the results are not as reliable as those obtained directly with a Faraday collector.

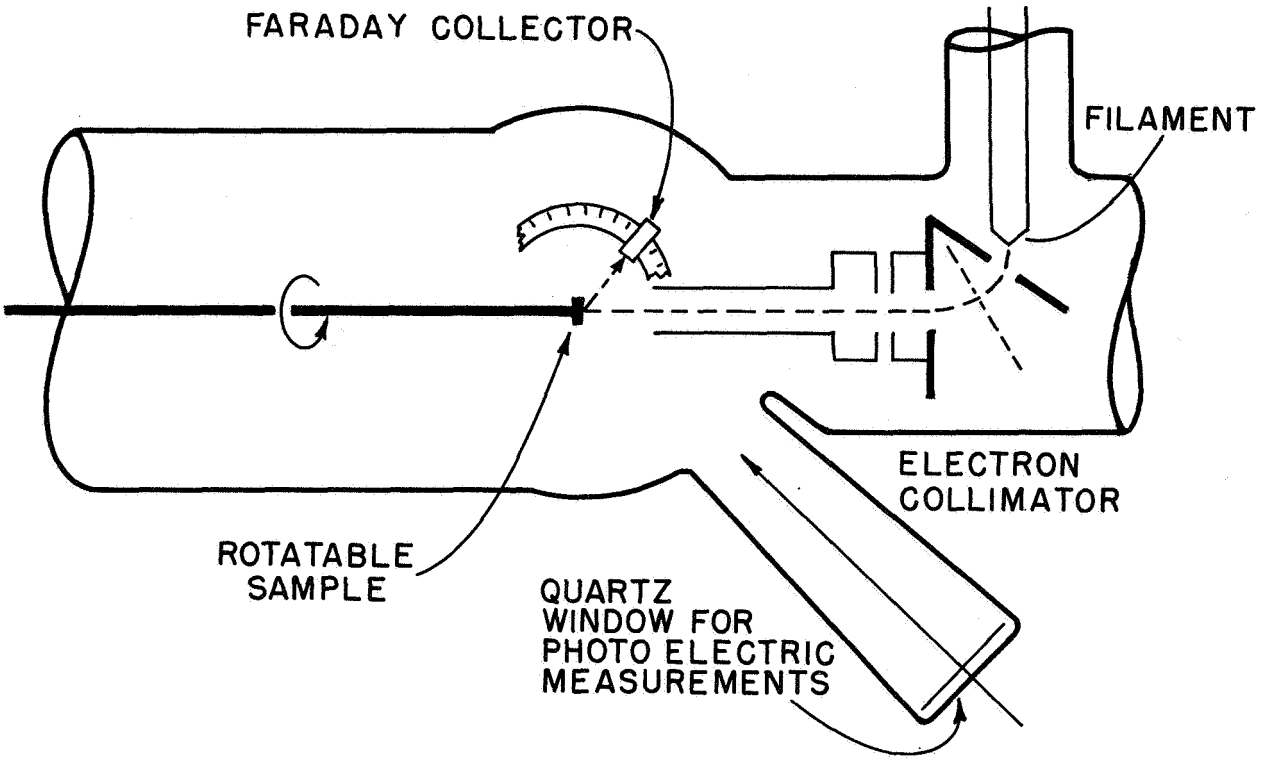


Figure 6. Diagram of Faraday-collector type low energy electron diffraction tube used by Farnsworth and co-workers.

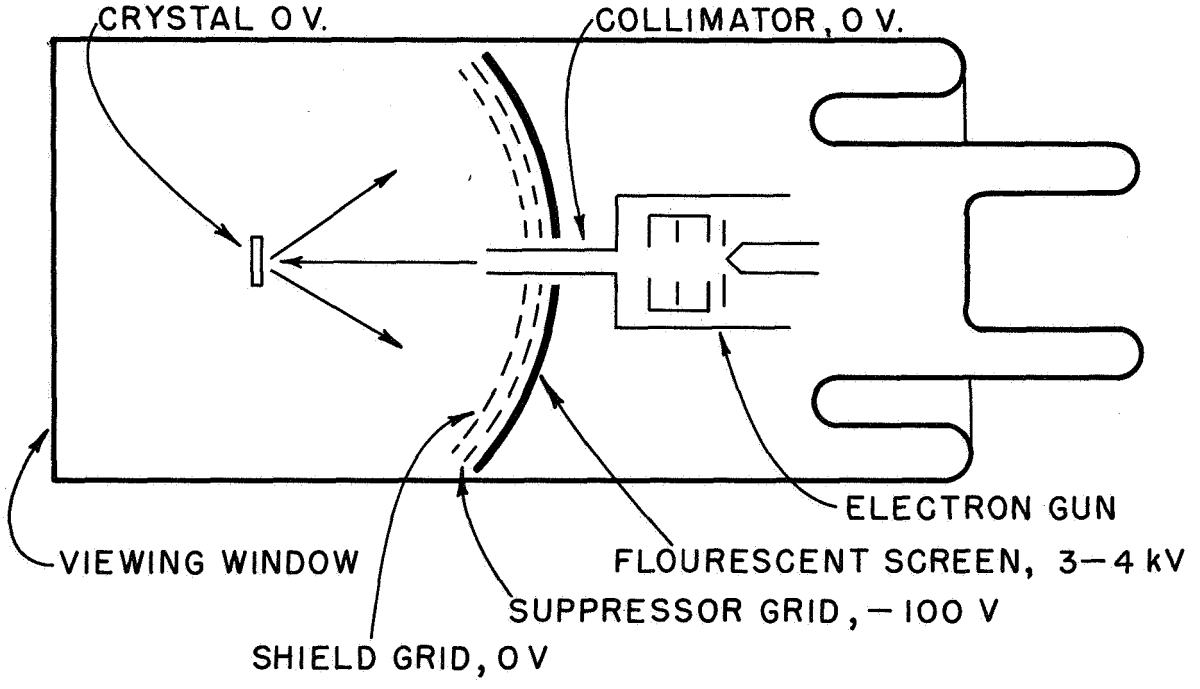


Figure 7. Basic components of a post acceleration display low energy electron diffraction tube similar to that used at Bell Laboratories.

The use of spherical geometry, although highly desirable from an experimental point of view, is difficult to achieve because of problems associated with the fabrication of the spherical grids. A modified form of the spherical low energy electron diffraction system has been presented by Fujiwara et. al.[15] In this system (Figure 8) the difficulty of constructing the grids was reduced through the use of cylindrical symmetry. An added advantage of this system is that it permits observation of the diffraction patterns over a wide range of scattering angles, from $0^{o}$ to $130^{o}$ and the angle of incidence can be changed.

Recently, C. W. Tucker[16] described a display type tube which eliminates the need for complicated grid structures by employing a magnetic deflection scheme, as illustrated in Figure 9. Upon emerging from the gun, the electron beam is deflected by an external magnetic field (2 - 8 Oe. for electron energies ranging from 20-300 eV) onto the crystal. The electrons scattered from the crystal are subsequently deflected through a grid located in front of the flourescent screen, and accelerated to 3KeV onto the screen. In this tube, secondary electrons are removed from the diffracted beam by the magnetic field.

## Summary

Low energy electron diffraction techniques have done much to further our knowledge of the surface-adsorbate interaction. In particular, low energy electron diffraction may be used to study adsorption, yielding information about adsorption sites, as well as coverage, and sticking probabilities. This technique is especially powerful when used in conjunction with other techniques such as flash desorption or work function measurements. In addition, valuable information concerning epitaxy, lattice vibrations, chemical reactions, catalysis and order-disorder transitions may be obtained. Although much may be learned from such studies, quantitative measurements are not yet possible due to the complexity of the electron scattering process at the surface.

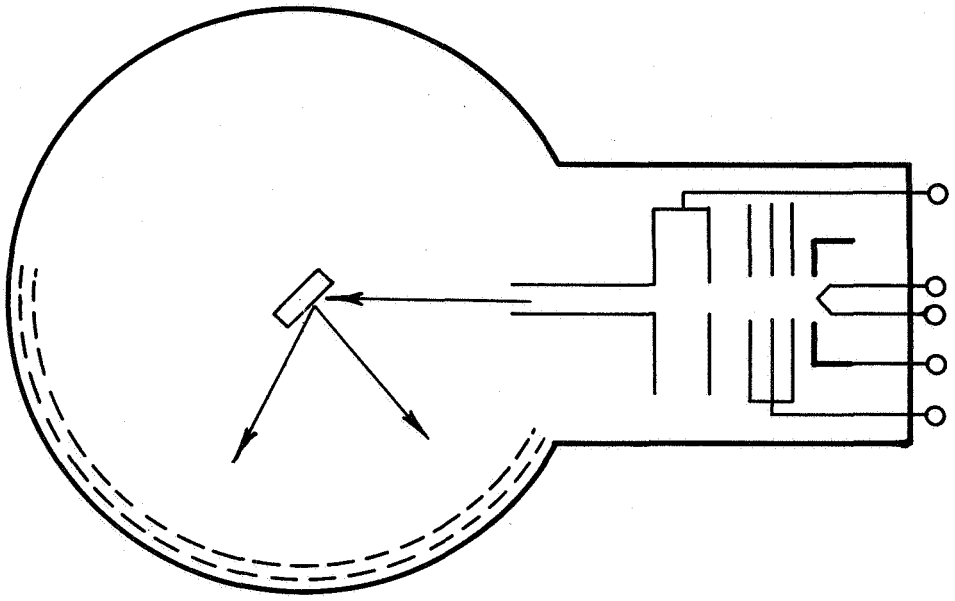

Figure 8. Diagram of low energy diffraction system designed by Fujiwara, et al. This system utilizes cylindrical symmetry and the crystal may be rotated to vary the angle of incidence.

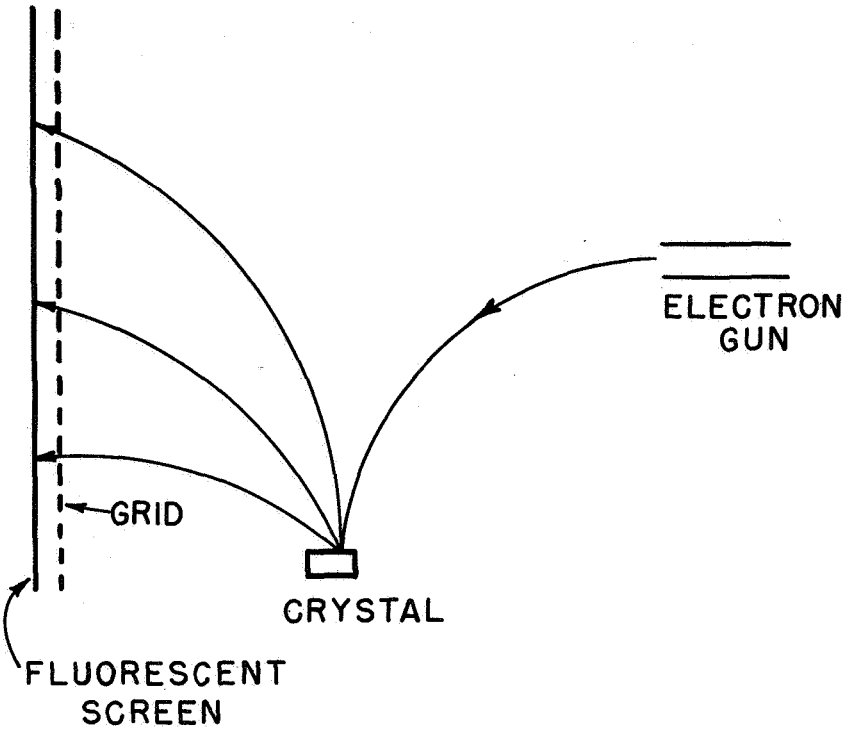


Figure 9. Diagram of low energy electron diffraction display type tube described by C. W. Tucker. The electron beam is deflected by an external magnet and the resulting pattern displayed on a fluorescent screen.

# 2 - FLASH FILAMENT TECHNIQUES

## Introduction

Measurements of adsorption-desorption phenomena involving the use of a heated solid surface play an increasingly important role in the investigation of the physical and chemical properties of surfaces.[17] The flash filament technique consists of using a test cell of known volume (one to two liters), containing a temperature controlled surface (usually, but not always in the form of a filament or ribbon) and some means of measuring pressure changes as the adsorption and desorption take place. The most widely used pressure detector has been the Bayard-Alpert ionization gauge, whose advantages and disadvantages have been discussed in the literature.[18] Use of a partial pressure analyzer adds considerable refinement because it removes much of the uncertainty in the identification of the species being adsorbed or desorbed. Mass spectrometers have also made it possible to study replacement,[19] isotopic mixing on the surface,[20] and coadsorption.[21] As with all reliable surface measurements, considerable care must be exercised to ensure the cleanest possible conditions during the experiments.

The flash filament technique has the advantage that considerable information can be obtained in a system that is relatively inexpensive and simple to construct. Important parameters readily obtained by analysis include the binding energy, sticking probability, the entropy of adsorption, and information concerning replacement and coadsorption. The physical quantities of interest are not measured directly, but must be derived from the kinetics of the process.

Despite its advantages, there are certain limitations to the flash method. By its very nature, it must be possible to heat the surface to a relatively high temperature, thus confining measurements to the refractory metals. Resistive heating of a filament or ribbon has been most widely used.

Such surfaces are inherently polycrystalline, making interpretation of experimental results somewhat doubtful. It is possible to make flash measurements on single crystals if special considerations are given to the desorption tube design.[22] Surfaces of ribbons have been found to approximate single crystal planes (often (113) or (114)), but in general, the orientation depends upon the prior treatment.[23, 24] Because the physical quantities are not measured directly, special consideration must be given to the derivation of the kinetic equations for adsorption and desorption.[17]

## Kinetics of the Flash Technique

In developing the kinetic equations for the flash technique, the following symbols will be chosen:

n - density of molecules in the gas phase in molecules/$cm^2$

$\sigma$ - surface coverage density in molecules/$cm^2$

v - volume of the sorption chamber in $cm^3$

A - total surface area in $cm^2$

S - system pumping speed in $cm^3$/sec

$S_a$ - pumping due to adsorption on a surface

q - rate of gas influx into the system in molecules/sec

t - time in sec

T - temperature in degrees Kelvin

$T_p$ - temperature at constant pressure

k - Boltzman s constant in appropriate energy units

s - sticking probability

E - metal-adsorbate binding energy

$\nu$ - pre-exponential frequency

$\beta$ - arbitrary constant

The rate of increase in the number of molecules per volume in the gas phase may be written generally as

$$v\frac{dn}{dt} = -Sn - S_a n + \sum_{i=o}^{n} q_i \qquad (1)$$

where the $q_i$ take into account all sources of gases, including the desorption from the surface of the filament under investigation. Only three types of sources need be considered, $q_o$, $q_1$, and $q_2$, corresponding respectively to the influx of gas responsible for the background pressure (i.e., wall effects, gauge interactions, virtual leaks, etc.) the influx of the adsorbate gas externally admitted to the system, and the gas evolving from the surface. In the following discussion, it will usually be assumed that $q_o$ is negligibly small and special consideration must be given to those situations for which this condition is not met. The gas evolution from the surface may be written as $q_2 = A(d\sigma/dt)$, while the quantity $S_a$ is the pumping due to adsorption on the surface. Specifically,

$$S_a = As(\sigma)K(m, T)$$

where from kinetic theory

$$K(m, T) = \left(\frac{kT}{2\pi m}\right)^{1/2}$$

The general expression for the kinetics then becomes

$$v\frac{dn}{dt} = -Sn - sAKn + A\frac{d\sigma}{dt} + q_1 \qquad (2)$$

As it stands, the above expression does not lend itself to easy analysis; however, considerable simplification results by suitable choice of experimental procedure. Both adsorption and desorption experiments are conducted by the flash filament technique and since they involve slightly different procedures as well as kinetics they will be described individually.

Adsorption kinetics have been investigated by two methods referred to as the closed system and the continuous flow methods.[17] As implied

the closed system method is one in which gas (or vapor) is admitted to the test chamber while the filament is too hot for adsorption to occur. When the gas has reached the desired pressure, the volume is sealed off and the filament temperature is dropped suddenly to some prescribed value. As the temperature of the filament begins to decrease, the gas is pumped by the filament, leading to a characteristic decrease in the pressure within the test cell. (Figure 10) For this case, with S and $q_1$ set equal to zero, Equation (2) reduces to

$$v\frac{dn}{dt} = - sAKn + A \frac{d\sigma}{dt} \tag{3}$$

If re-evaporation of the adsorbed gases is ignored (i.e., $d\sigma/dt = 0$), then the sticking probability may be found from

$$s = \frac{v}{KA} \frac{d\ln [n(t)]}{dt} \tag{4}$$

The surface coverage density at any time is given by

$$\sigma(t) = v [n(o) - n(t)] /A \tag{5}$$

In the event that re-evaporation is not negligible, it is still possible to analyze the pressure vs time curve as follows: It is usually assumed that the rate of decrease in coverage is governed by an Arrhenius law of the form

$$\frac{d\sigma}{dt} = \sigma^x \nu_x \exp [-K/kT] \tag{6}$$

where x = 1 or 2 (for monatomic and diatomic molecules) is the order of the desorption process. Rewrite Equation (3) in the form

$$\frac{dn}{dt} = \frac{-sKAn}{v} + \frac{1}{v} \frac{d(A\sigma)}{dt} \tag{7}$$

then by measuring dn/dt for various values of n(o) and plotting a family of curves of dn/dt vs n for a constant number adsorbed (i.e., $A\sigma$ = constant) it is possible to obtain s from

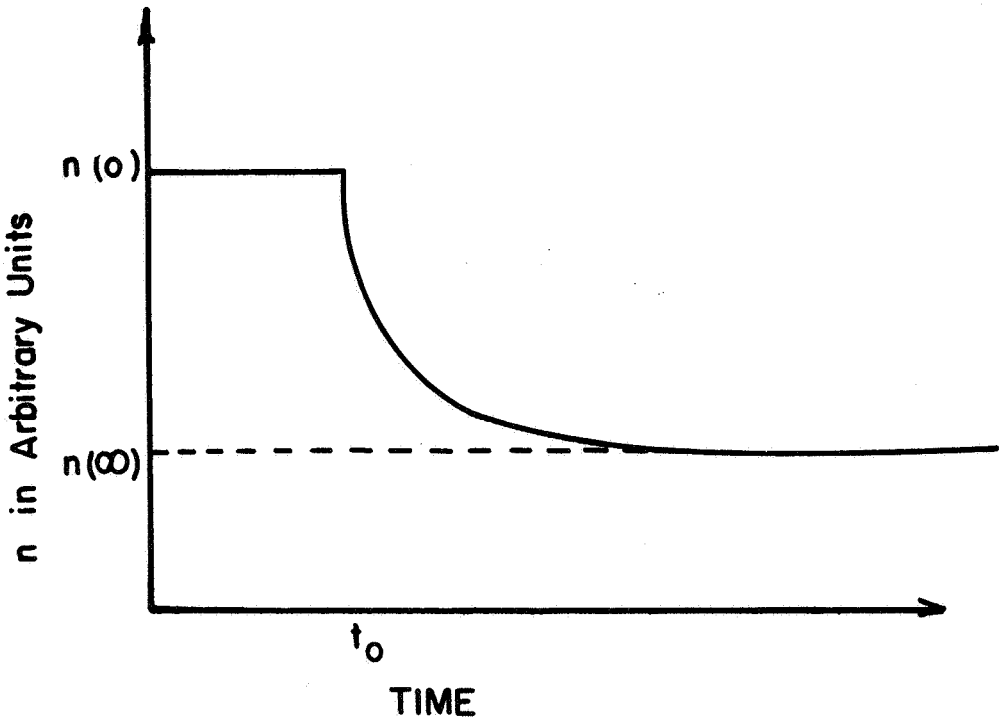


Figure 10. A typical n vs t curve for adsorption in a closed system in which the surface was suddenly cooled at time $t_o$.

$$s = \frac{-v}{KA} \left[\frac{d}{dn}\left(\frac{dn}{dt}\right)\right]_{A\sigma} \qquad (8)$$

and in addition, extrapolation of the curves through n = o yields for first order desorption

$$\left(\frac{dn}{dt}\right)_{n=o} = \frac{A}{v}\frac{d\sigma}{dt} = \frac{A\sigma\nu}{v} \exp\left[-E/kT\right] \qquad (9)$$

which permits E to be determined as a function of $A\sigma$ assuming a value of $\nu$.*

Unfortunately, it is difficult to achieve the conditions of the ideal closed system. One important problem is that gases adsorbed on the walls of the test volume may evolve as the pressure on the cell decreases thereby leading to an erroneous interpretation of the pressure vs time curve. In addition, ion gauge pumping can be considerable although precautions can be taken to reduce this effect substantially. In addition, impurities can build up rather rapidly. Impurity problems such as CO buildup due to hot filament degassing can be minimized by using continuous flow techniques, where gas is continually passing through the system.

Continuous flow studies have been performed both by maintaining the flow rate constant and the pressure constant.[25,26] In the constant flow method, the adsorbing vapors are allowed to flow at a constant rate through the system as determined by the rate of input through a suitable leak and the rate of removal by the pumping system and by adsorption on the surface. With the filament initially hot, a reference pressure is reached by careful adjustment of the leak and pumping rates which, once adjusted, remain constant for the duration of the experiment. The filament is then allowed to cool, leading to a sudden decline in the pressure due to the onset of adsorption (Figure 11).

---

*Usually one assumes $\nu = 10^{13}$ sec$^{-1}$

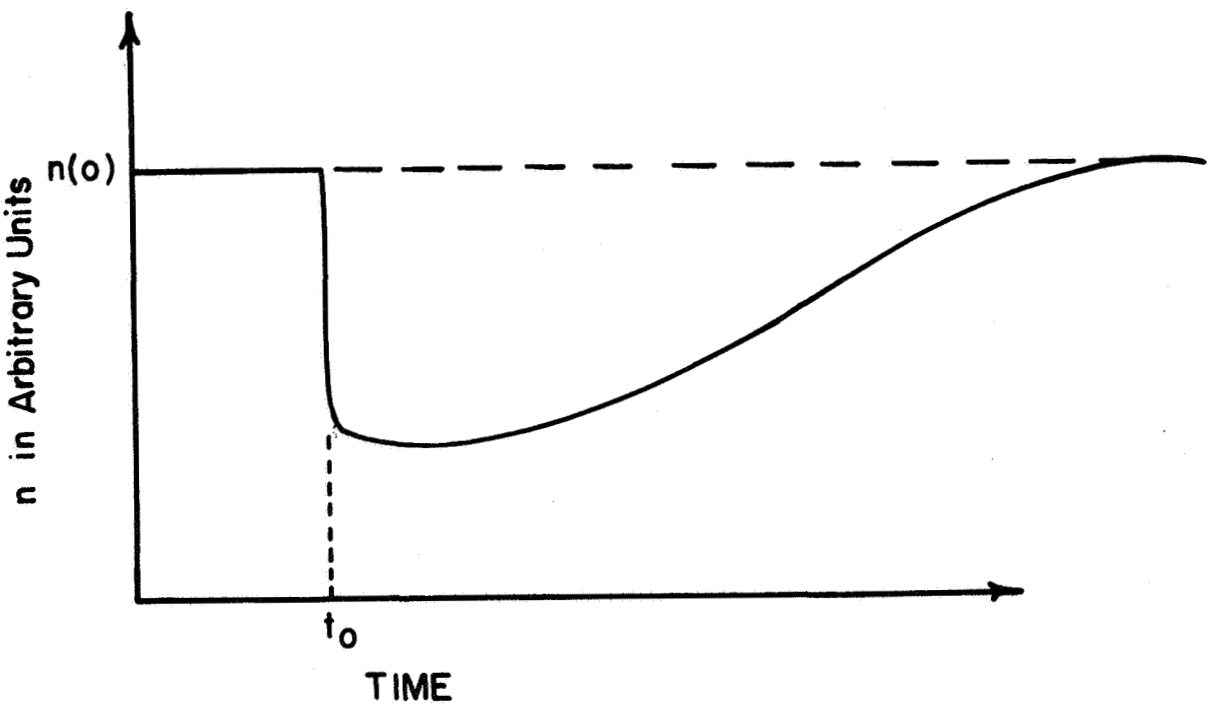


Figure 11. Typical n vs t curve for adsorption at constant flow rate.

As the filament becomes covered, the rate of adsorption decreases until finally the pressure returns asymptotically to the initial steady state value. For this case, the rate equation is

$$v \frac{dn}{dt} = -Sn - sAKn + q_1 + A \frac{d\sigma}{dt} \qquad (10)$$

Now the pumping speed may be readily found by introducing a small quantity of gas with conditions such that no filament pumping (i. e., with a monolayer adsorbed) or readsorption occurs and then plotting ln p vs t, as gas is pumped from the system. In this case

$$\frac{S}{v} = \frac{-d\ln(n)}{dt} = -\frac{d\ln(p)}{dt} \qquad (11)$$

The value of $q_1$ is determined by considering the steady state situation for which

$$q_1 = Sn(o) \qquad (12)$$

so that if re-evaporation is negligible,

$$\frac{dn}{dt} = \frac{S}{v}\left[n(t) - n(o)\right] - \frac{sKA\, n(t)}{v}$$

or

$$s = \frac{v}{KA}\frac{d\ln(n)}{dt} - \frac{S}{KA}\left[\frac{n(t)-n(o)}{n(t)}\right] \qquad (13)$$

$$\sigma_o = \frac{v}{A}\left[n(o) - n(\infty)\right] \qquad (14)$$

Use of a constant pressure flow system minimizes problems of gauge and wall interactions and provides a means of direct measurement of pressure dependent parameters.[26] In this system, gas flows from a reservoir through a servo-controlled leak valve into a small chamber containing an ion gauge, then through a capillary of known conductance and into the sample chamber. Regulating the flow rate allows a constant pressure to be maintained in the sample chamber.

The flow rate through the system is represented by the expression:

$$q_1 = Sn + v\frac{dn}{dt} - q_o + sAKn - A\frac{d\sigma}{dt} \qquad (15)$$

By using high flow rates, vdn/dt is negligible. Interactions of the walls and gauges are small because impurities are continuously pumped out. By allowing the system to equilibrate at constant pressure, errors due to gauge pumping and degassing can be eliminated. The net sorption rate by the sample is proportional to the upstream pressure, since Sn is a constant in this system.

## Kinetics of Flash Desorption

The kinetics of flash desorption may be studied by heating a sample at a controlled rate and analyzing the resulting p vs t curves as gas evolves from the surface. The type of system used is shown schematically in Figure 12. The general rate expression is

$$v\frac{dn}{dt} = -Sn + A\frac{d\sigma}{dt}, \qquad (16)$$

provided readsorption and gas influx from the reservoir are negligible during the heating time.

Again, it is found that analysis of the desorption kinetics may be simplified by making the proper design considerations. Desorption experiments are normally conducted in systems operating under one of two possible extremes, namely the conditions of $Sn \ll vdn/dt$ and $Sn \gg vdn/dt$. Since both of these approaches are used commonly, it is worthwhile to consider each in some detail.

Pumping Speed Small Compared to Rate of Gas Evolution. - When the pumping rate is slow compared to the rate of gas evolution,[27] $Sn \ll vdn/dt$ and Equation (16) reduces to

$$v\frac{dn}{dt} = A\frac{d\sigma}{dt} = A\sigma^x \nu_x \exp\left[-E/kT(t)\right]$$

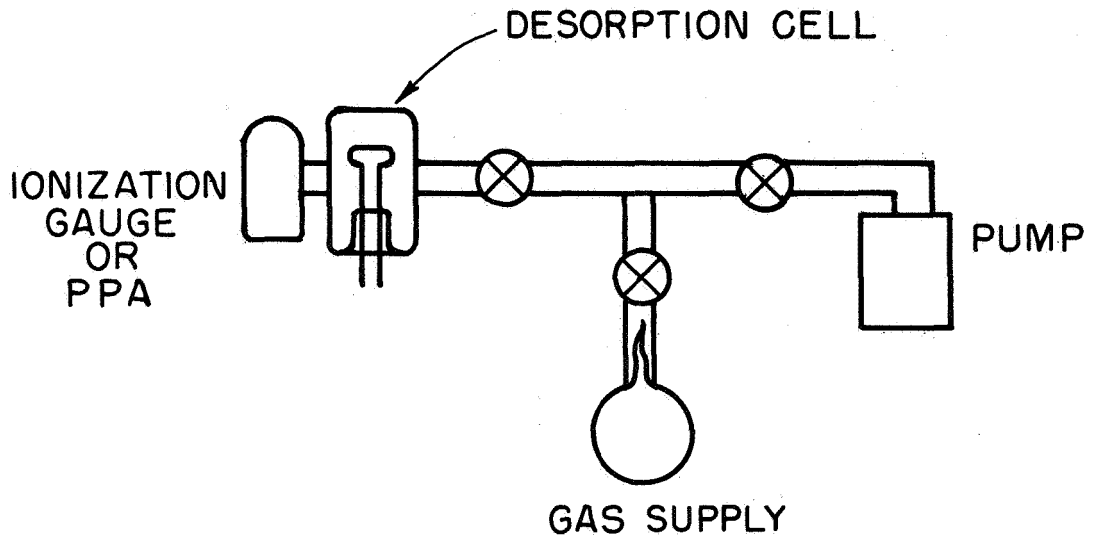


Figure 12. Schematic representation of closed flash desorption system.

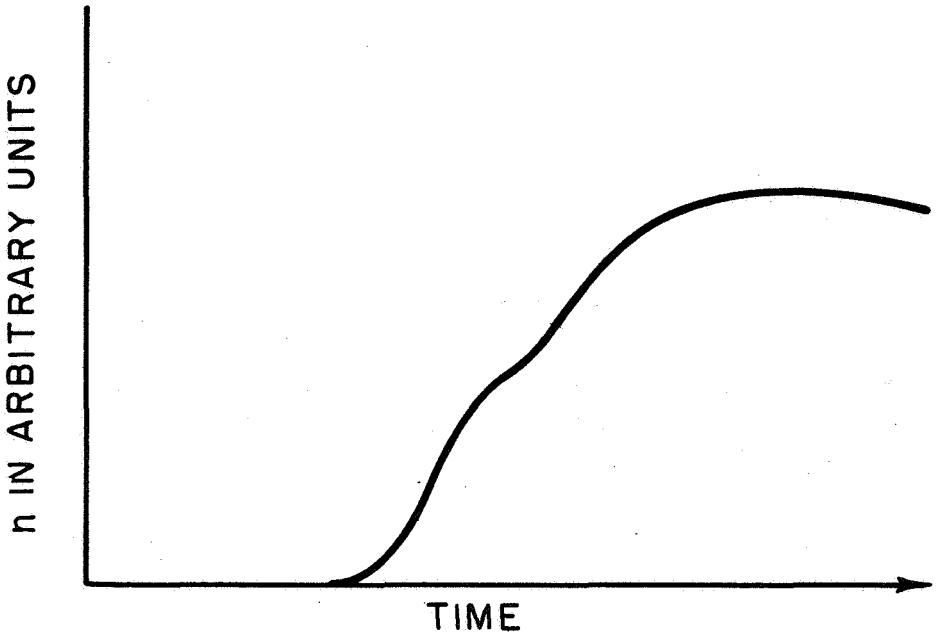


Figure 13. Hypothetical n vs t curve for flash desorption in a closed system from two adsorbed states.

A typical pressure vs time curve for this situation is shown in Figure 13. It will be observed that at points of maximum evolution rate, $d^2n/dt^2 = 0$, which leads to the result

$$\frac{E}{kT_p} = \ln(x\sigma^{x-1}) + \ln\left[\nu_x T_p / (dT/dt)\right] - \ln(E/kT_p) \tag{17}$$

Before carrying this development further, it is convenient to consider the second case:

Pumping Speed High Compared to the Rate of Gas Evolution. - In this case,[28] $Sn >> vdn/dt$ and the Equation (16) simplifies directly to

$$Sn = A\frac{d\sigma}{dt} = -A\nu_x \sigma^x \exp\left[-E/kT(t)\right]$$

Here the pressure vs time curve assumes the structure shown in Figure 14 and the peaks occur at times (temperatures) for which

$$\frac{dn}{dt} = 0$$

which leads to

$$\frac{E}{kT_p} = \ln(x\sigma^{x-1}) + \ln\left[\nu_x T_p / dT/dt\right] - \ln(E/kT_p)$$

This is identical to the result obtained above for the opposite extreme and so the analyses for both situations are identical. It is well at this point to continue the analysis for first and second order kinetics separately. For the case, x=1, Equation (17) becomes

$$\frac{E}{kT_p} = \ln\left[\nu_1 T_p / (dT/dt)\right] - \ln(E/kT_p)$$

The last term is small which permits one to rewrite the above expression in the form

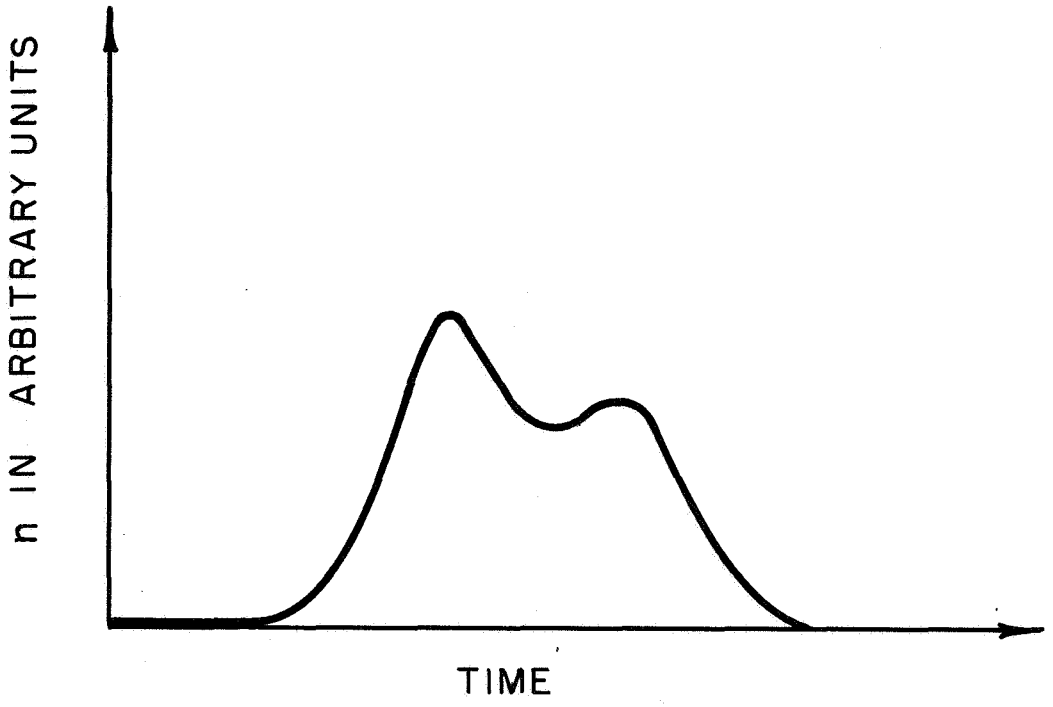


Figure 14. n vs t curves for flash desorption from two adsorbed states for the case of large pumping speed.

$$\frac{E}{kT_p} = \ln\left[\nu_1 T_p/(dT/dt)\right] - \ln\left\{\ln\left[\nu_1 T_p/(dT/dt)\right]\right\}$$

If a linear heating schedule is used, i.e., $T = T_o + \beta t$ then $dT/dt = \beta$ and

$$\frac{E}{kT_p} = \ln\frac{\nu_1 T_p}{\beta} - \ln\left[\ln\left(\frac{\nu_1 T_p}{\beta}\right)\right]$$

or for $10^8 \leq \nu_1/\beta \leq 10^{13}$ $^oK^{-1}$

$$\frac{E}{kT_p} \cong \ln\frac{\nu_1 T_p}{\beta} - 3.64; \quad \pm 1.5\% \tag{18}$$

This may be used in this form if a value for $\nu_1$ is assumed (usually $\nu_1 = 10^{13}$ $sec^{-1}$ is assumed). It is still possible to obtain a value of E without assuming a value for $\nu_1$ by varying the heating rate $\beta$, in which case it is found that

$$\frac{E}{kT_p} = \frac{d \ln \beta}{d \ln T_p} - 2$$

If the desorption process is second order i.e., x=2, Equation (17) must be rewritten in the form

$$\frac{E}{kT_p} = \ln 2\sigma_p + \ln\frac{\nu_2 T_p}{dT/dt} - \ln E/kT_p$$

where $\sigma_p$ is the surface coverage at a time corresponding to the peak desorption rate. With a linear heating schedule this equation reduces to

$$E/kT_p = \ln \sigma_o T_p^2 + \ln \nu_2/\beta - \ln E/k \tag{19}$$

where because of symmetry, $\sigma_o$ is assumed to be equal to $2\sigma_p$. Thus a linear plot of $\ln(\sigma_o T_p^2)$ vs $1/T_p$ may be used to demonstrate second order kinetics. The intercept gives $\nu_2$ and the slope yields E.

## Summary

Experiments using flash filament techniques provide highly sensitive means of acquiring information necessary for the complete identification of states of adsorption. From such measurements, it is possible to determine the binding energy, the entropy of adsorption, the molecular form of the adsorbate, the sticking co efficient, and the maximum coverage in each state. Recent improvements in technique make possible the separation of states differing in binding energy by only a few eV. However, in spite of its usefulness, the flash filament technique is limited to the refractory metals and it is not possible to relate the information gained directly to the microscopic structure of the surface.

# 3 - ELECTRON IMPACT DESORPTION

## Introduction

Under certain conditions, desorption is induced by the interaction of incident low energy electrons with molecules adsorbed on a metal surface. The earliest reports of electron impact desorption were made by workers using mass spectrometers in which gases desorbed from various electrodes by the ionizing electron beam produced spurious effects in their measurements.[29] Since these early findings, many have observed and reported similar effects, all of which have considerable practical importance. J. R. Young[30] and G. E. Moore[31] made mass spectrometric investigations of electron impact desorption of gases from various anode materials and at least partially confirmed the long-held belief that gases desorbed from anodes were responsible for the observed poisoning of thermionic oxide cathodes. Later studies by Degras, et al,[32] and by Redhead[33] led to the conclusion that electron impact desorption affected the operation of an ionization gauge, while more recently, electron impact desorption has been recognized as an important contributor to gas contamination in high current electron storage rings[34] and controlled fusion chambers.[35] In spite of the extensive number of observations of electron impact desorption, relatively few investigations have been made to determine the basic nature of the effect, and credit must be given to Redhead[33] and Menzel and Gomer[36] who appear to have concluded independently that the desorption is a direct result of electronic excitation to repulsive surface states.

Basically, the experimental arrangement for studying electron impact desorption consists of a specimen on which gases are adsorbed, a source of electrons with which to bombard the specimen, and some means of detecting the desorption products, all in an ultra-high vacuum environment maintained at pressures at least in the $10^{-10}$ torr range.

In general, the techniques of different investigators differ only in the method of detecting the desorption products and four methods have been used. For example, in the work of Degras, et al,[32] an ionization gauge was used to measure the total pressure change resulting from bombarding the surface with electrons. Moore[31] and Petermann[37] used mass spectrometric techniques to identify the desorbed species. Redhead[33] utilized the fact that under certain conditions the desorption products are ions which can be measured directly, and Menzel and Gomer[36] used the field electron microscope, which permits visual observation of the desorption process on a microscopic scale.

While it is possible that desorption of very loosely bound adsorbates may result from direct momentum transfer, in the majority of cases electron impact desorption must be explained in terms of electronic excitation of the adsorbed molecule to a repulsive molecular or ionic state. This is made clearer by referring to the potential energy curves shown in Figure 15, which represent various quantum states of a hypothetical metal-adsorbate system. The curves shown correspond respectively to the ground state $(M + A)$, the antibonding state $(M + A)^{\ddagger}$, an excited state of the ground state species $(M + A)^{*}$, and an ionic state $(M^{-} + A^{+})$. It is assumed that transitions from one state to another occur vertically within the shaded or Franck-Condon region. Observe that transitions to the states $(M + A)^{\ddagger}$ and $(M^{-} + A^{+})$ are to repulsive portions of the respective potential energy curves and consequently result in desorption, either as a neutral for the former case or as a positive ion for the latter. The probability for desorption of the ion will be reduced in this example because it must cross the potential energy curve corresponding to the $(M + A)^{*}$ binding state where it can become bound and subsequently return to the ground state. Although a number of modes of desorption can be visualized, only desorption from an ionic state has been positively identified at this time. However, it seems quite unlikely that ionic desorption accounts for all the electron impact desorption. There is some evidence

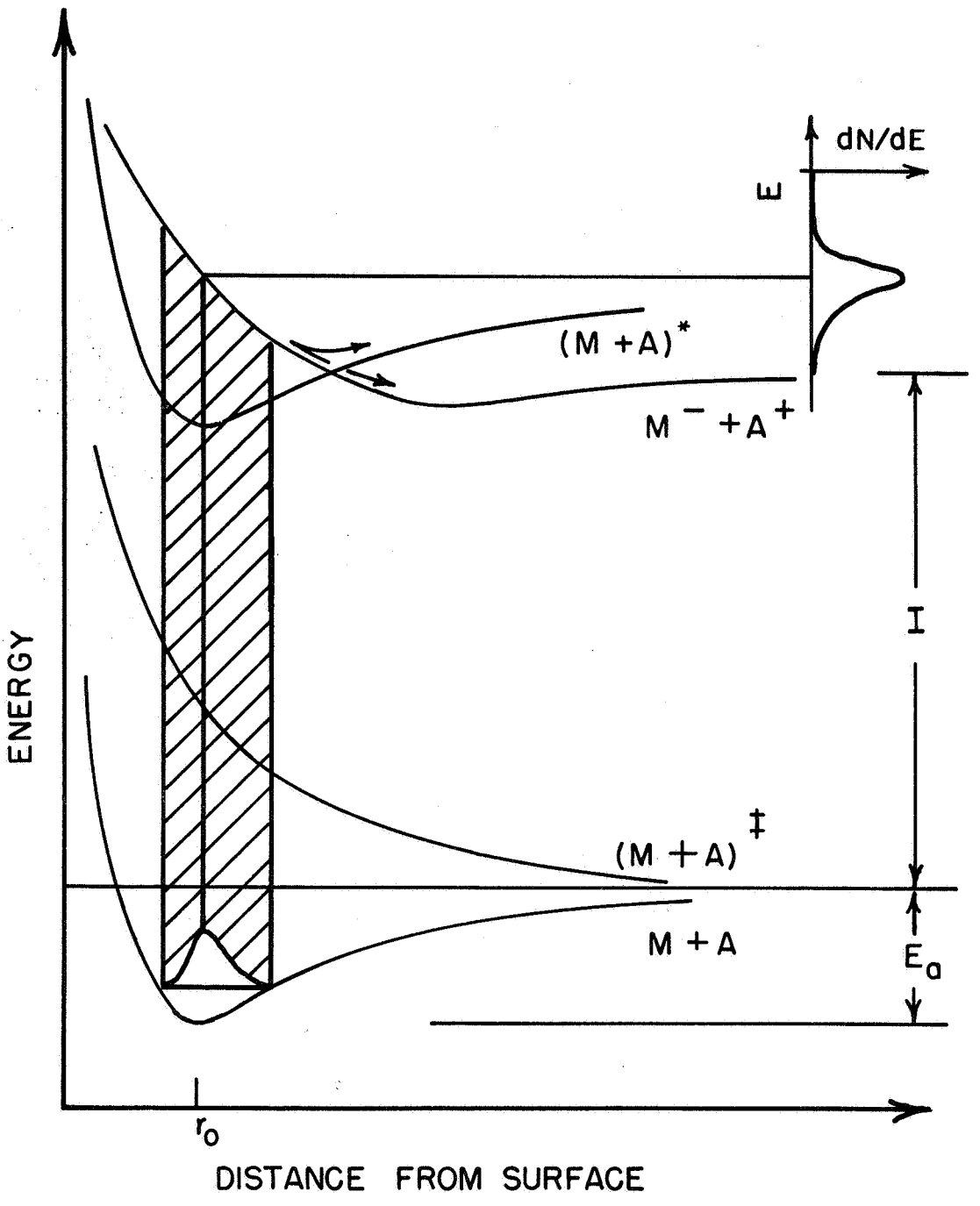


Figure 15. Potential energy curves for metal-adsorbate states at a hypothetical surface.

suggesting that excitation to a loosely bound state followed by thermal desorption might also be possible.[38]

If the energies of the desorption products can be analyzed, it is possible to acquire additional information about the ground state of the adsorbed species. This may be seen by referring once again to Figure 15. Suppose desorption from the ionic state, preceded by electron impact ionization, is considered. Since there is a certain spread in the positions of the ground state atoms, depending upon their vibrational energies and the shape of the potential well for this state, there will be a corresponding spread in the energies of the desorbed ions. In other words, knowledge of the energy distribution of the desorbed ions permits one to approximate the square of the ground state vibrational eigenfunction for the adsorbed species. Similar arguments hold for the desorption of neutral molecules as well, but such information is not easily obtained due to the difficulty with which energy measurements are made on neutral atoms.

Although the electron impact desorption process has not been placed on a firm theoretical basis, a few qualitative remarks are possible in light of earlier work by Redhead[33] and by Menzel and Gomer.[36] Menzel and Gomer argue quite convincingly that the cross section for excitation to the repulsive state cannot differ by more than a factor of ten from the cross section for excitation to the corresponding state of the molecule in the gas phase, which is of the order of $10^{-16}$ $cm^2$. This conclusion is arrived at by approximating ground and excited state wave functions for the bound molecule by a linear superposition of a set of carefully chosen basis states. The transition probabilities calculated in this way seem to be at least as large as the corresponding transitions in the gaseous state. Thus, in view of the fact that observed cross sections for electron impact desorption are often several orders of magnitude lower than the cross sections for the corresponding transitions in the gas phase, it would appear that the competing process of readsorption plays an important role.

Further conclusions are that the probability for desorption will increase with increasing lifetime of the adsorbed molecule in the excited state and will decrease with increasing mass and binding energy of the adsorbed species. In addition, the probability for desorption will depend rather sensitively on the equilibrium position of the adsorbed molecule, the probability decreasing with decreasing distance.

In his investi gation of the electronic desorption of oxygen adsorbed on molybdenum, Redhead found that ions and neutrals were desorbed in the ratio of one ion for every 50 neutrals. Furthermore, it was noted that the energy threshold for the onset of desorption was the same for both the ions and the neutrals which led him to propose, with excellent experimental verification, that the desorption for both species occurred from the same ionic state but that the ions were neutralized by Auger transitions as they moved away from the surface.

## The Kinetics of Desorption

As with flash filament desorption, the important parameters for electron impact desorption are obtained from the kinetic equations for the desorption process. Here one must take into account the kinetics for the three methods of measurement, namely, measurement of pressure change, measurement of work function change, and detection of desorbed ions.

The following symbols will be used:

$n$ = the number of molecules per unit volume in the gas phase.

$S$ = the pumping speed of the vacuum system in $cm^3/sec$.

$v$ = the volume of the system in $cm^3$.

$q$ = the influx of gas into the gas phase due to electron desorption.

$q_o$ = the influx of gas into the gas phase in molecules/sec, responsible for the background pressure.

$\sigma$ = surface coverage density in molecules/$cm^2$.

$J$ = electron current density (assumed uniform over the surface) in charge/$cm^2$-sec.

$A$ = target area in $cm^2$.

$e$ = electronic charge.

$Q$ = the total electron desorption cross section in $cm^2$.

$\phi$ = work function of the metal in electron volts.

In addition, the following assumptions will greatly simplify the calculations appearing below:

(1) The electron current density is uniform over the surface.

(2) The desorption rate is proportional to current in the first order.

(3) Diffusion of gas out of the bulk or along the surface is considered to have a negligible effect on the results.

(4) Readsorption from the gas phase is neglected, a valid assumption for pressures in the $10^{-10}$ torr range.

(5) Thermal desorption is not considered.

Pressure Change. - The time rate of change in the number density of molecules in a vacuum system is described by

$$v \frac{dn}{dt} = -Sn + q_o + q \tag{20}$$

If first order electronic desorption processes are assumed, then

$$q = \sigma Q J A / e \tag{21}$$

The surface coverage density will change with time according to the expression

$$\frac{d\sigma}{dt} = - \sigma Q J / e \tag{22}$$

which has the immediate solution

$$\sigma = \sigma_o \exp(-QJt/e) \tag{23}$$

Combining Equations (20), (21), and (23) one obtains the differential equation

$$\frac{dn}{dt} = -Sn/v + q_o/v + (\sigma_o QJA/eV) \exp(-QJt/e)$$

A solution to this equation is readily obtained and, if $n_o = q_o/S$, the final result is

$$n(t) = n_o + \frac{\sigma_o AQJ}{eS-QJv} \left[ \exp(-QJt/e) - \exp(-S/v)t \right] \tag{24}$$

This may be simplified; for example, if S/v is much larger than QJ/e, one obtains

$$n(t) = n_o + \frac{\sigma_o AQJ}{eS} \exp(-QJt/e) \tag{25}$$

From this equation, the following information is derived

$$Q = -\frac{e}{J} \frac{d\ln\left[ n(t) - n_o \right]}{dt} \tag{26}$$

and

$$\sigma_o = \left[ n(0) - n_o \right] eS/AQJ \tag{27}$$

which may be used to compute the cross section and initial coverage respectively. Note that the quantity, n, may be related at room temperature to the pressure, p, in torr, by the kinetic theory expression

$$n = 3.3 \times 10^{19} p$$

On the other hand, if S/v is very small compared to QJ/e,

$$n(t) = n_o + \frac{\sigma_o A}{v} \left[1 - \exp(QJt/e)\right] \tag{28}$$

from which

$$Q = -\frac{J}{e}\frac{d}{dt} \ln \left[\frac{n(t) - n_o + \frac{\sigma_o A}{v}}{\frac{\sigma_o A}{v}}\right] \tag{29}$$

and

$$\sigma_o = \frac{V}{A}\left[n(\infty) - n_o\right] \tag{30}$$

Work Function Change. - For small coverage changes, it is reasonably valid to assume that the work function is related linearly to coverage through the expression

$$\phi = \phi_\infty + c\sigma$$

where c is a constant and $\phi_\infty$ is the value of $\phi$ when $\sigma = 0$. With this assumption then, Equation (23) may be rewritten to yield

$$Q = \frac{e}{J} \ln \left[\frac{\phi(t) - \phi_\infty}{\phi(0) - \phi_\infty}\right] \tag{31}$$

Detection of Ions. - The ion current arising from electron impact ionization on the surface of the metal follows the rule

$$I^+ = \sigma Q^+ I \tag{32}$$

where $I^+$ is the positive ion current, I is the electron current and $Q^+$ is the cross section for an adsorbed molecule to be desorbed as an ion. Application of Equation (23) then leads to

$$I^+ = I_o^+ \exp(-QJt/e) \tag{33}$$

where $I_o^+ = \sigma_o Q^+ I$. From this expression the total cross section for electron desorption may be obtained:

$$Q = - \frac{e}{J} \frac{d \ln I^+}{dt} \tag{34}$$

The ionization efficiency is

$$\text{Eff} = I_o^+ / I = \sigma_o Q^+ \tag{35}$$

Knowledge of the initial coverage allows one to use the latter expression to compute $Q^+$.

## Experimental Considerations

It must be emphasized, that in the application of the kinetic equations derived in the preceding section, care must be taken to ensure that the conditions specified by the assumptions are satisfied for the particular experimental circumstances in question. An important consideration is that of readsorption which is inherently connected with the vacuum conditions; for, since the cross sections for electronic desorption are quite small, it is often necessary to carry out the measurements over extended periods of time in order to desorb an appreciable amount of gas. In addition, it seems almost certain that desorption occurs from more than one state, a fact which manifests itself in nonlinear ln $I^+$ vs t curves, for example. With proper analysis, however, it is usually possible to separate the effects of more than one state without undue difficulty. Recent experiments indicate that electron impact desorption may be coupled with flash filament techniques to good advantage, making it possible to gain further insight into the adsorption and desorption processes.[39]

The designs of three experimental electron impact desorption tubes are shown in Figures 16, 17, and 18. The tube shown in Figure 16 was used by Redhead [33] to measure the electronic desorption of oxygen and carbon monoxide adsorbed on molybdenum. Here, the surface being studied was in the form of a polycrystalline ribbon which could be heated, both resistively and by electron bombardment. The desorbing electrons

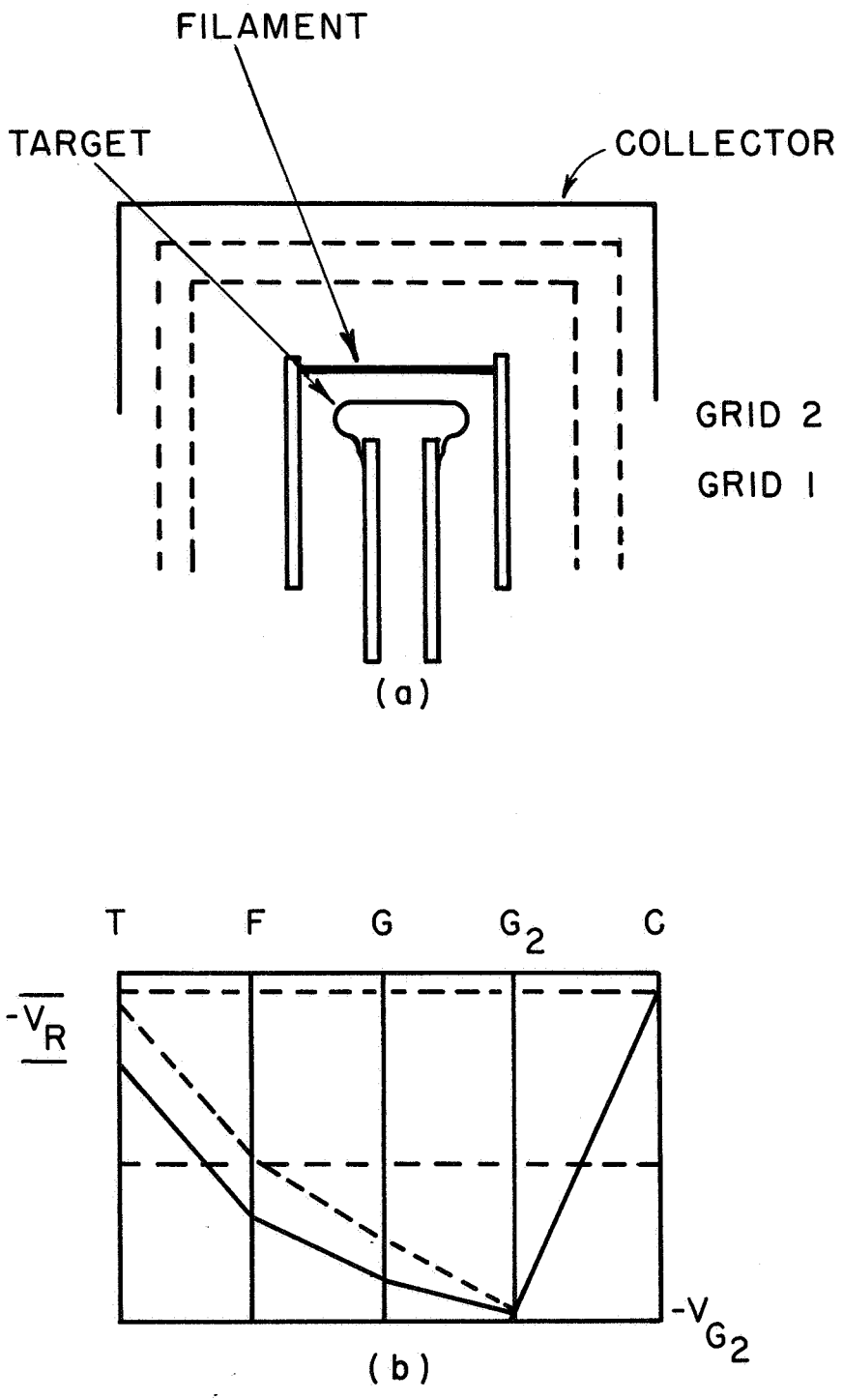


Figure 16. (a) Schematic diagram of experimental electron impact desorption tube used by Redhead. (b) Representation of electrode potential configuration used in Redhead's tube.

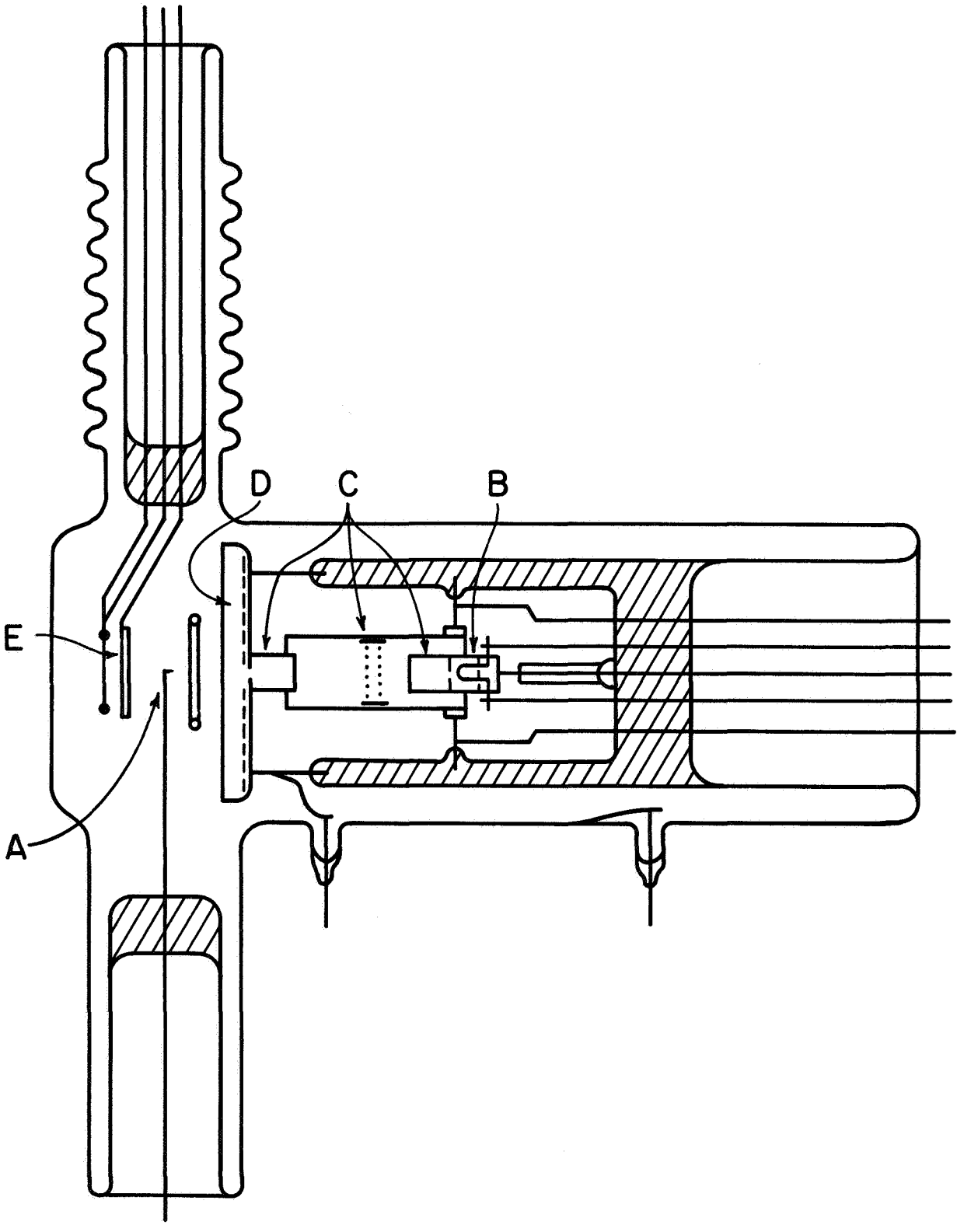


Figure 17. Field emission tube used by L. W. Swanson, et al., for electron desorption studies. A is a tungsten field emitter, B is a tungsten filament used as the electron source, C is a lens arrangement that can be used either to focus the electron beam or as a Faraday collector, D is a phosphor screen, and E is a collector.

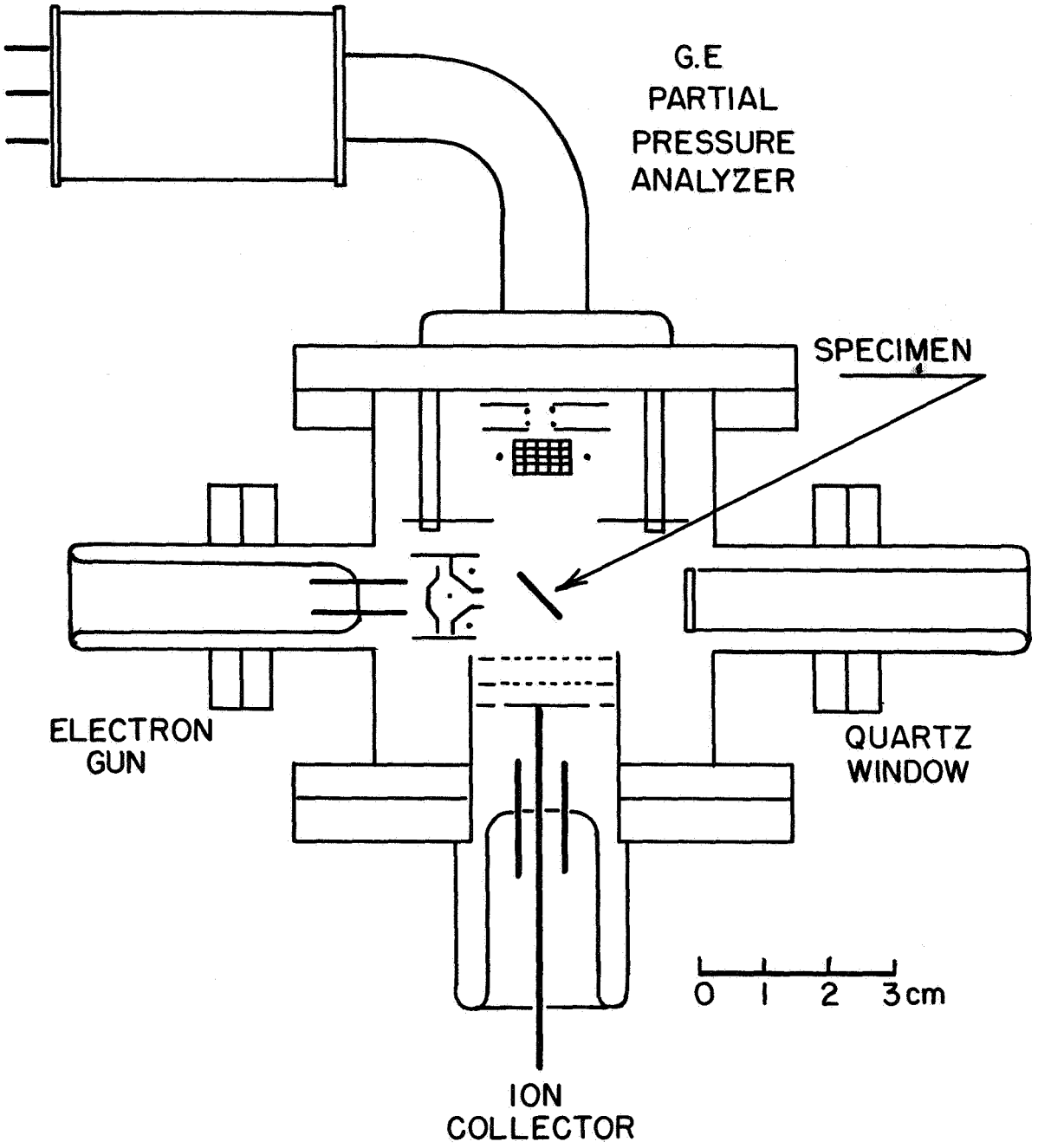


Figure 18. Electron impact desorption tube used by Hinrichs.

were emitted by a thoria coated tungsten filament with a spread in energy of about 0.8 eV, and the desorption process was studied by means of the ion current reaching the collector. Heating of the molybdenum ribbon permitted evaluation of the binding energies for the adsorbed molecules.

Figure 17 shows a tube used by the research group at Field Emission Corporation to investigate the electron impact desorption of coadsorbed alkali metal and electronegative adsorbates on various refractory metals.[40] In this tube, the electron beam is directed axially onto the apex of the emitter tip on which the adsorbate resides. With the arrangement shown, it is possible to select parts of the field emitted electron beam in order to determine changes caused by electron impact on single crystallographic planes. In field emission studies, use is made of the extreme sensitivity of the emission current on the work function of the surface so that the cross sections are determined using Equation 31. The field emission technique does not lend itself to the detection of ions nor to the identification of the desorbed species. However, it is a highly sensitive method of measuring cross sections as low as $10^{-23}$ $cm^2$.

The tube shown in Figure 18 was used in an investigation of the electron impact desorption of carbon monoxide adsorbed on nickel.[38] A mass spectrometer was incorporated in the design of the all stainless steel desorption chamber, which, along with the ion collector, permitted detection of both neutrals and ions.

## Summary

Electron impact desorption techniques yield information about excited and ionic states of the surface-adsorbate bond. By means of carefully taken threshold data, it is possible to deduce the binding energy of the ground state of the adsorbed species, thereby supplementing information derived from flash filament experiments. Finally, if the energy distributions for the desorbed ions are measured then the shape of the ground state potential energy curve may be estimated.

# 4 - FIELD ELECTRON MICROSCOPY

## Introduction

Field electron emission was discovered as early as 1897 by R.W. Wood of Johns Hopkins University, but it was not until after 1928 when R.H. Fowler and W. Nordheim of the University of Cambridge developed the wave mechanical concepts of field emission that earlier experimental results could be clarified. Although various aspects of the Fowler-Nordheim theory of field emission were confirmed in the 1930's the reproducibility and reliability of these early experiments were clouded by the inability to control and measure the vacuum conditions within the tube and the uncertainty as to the geometry of the emitting sites. The invention of the field electron projection microscope by Erwin W. Müller overcame many of these difficulties by providing a single crystal emitting surface of well-defined geometry and visual read-out of the work function topography of the emitting surface. The field electron microscope, which permits visualization of the effects of various phenomena at the surface of metallic crystals on what is nearly an atomic level, became an increasingly useful tool for analyzing physical and chemical phenomena that affect the work function or surface configuration. Subsequently, various investigators, principally Robert Gomer of the University of Chicago,[41] exploited the microscope to study such phenomena occurring at metal surfaces as catalysis, adsorption, desorption and epitaxy.

The extreme sensitivity of the field emission process on the degree of surface contamination provided early impetus for the obtaining and measurement of high vacuum, as well as the first visual demonstration of atomically clean surfaces. Perhaps the most important contribution of field electron microscopy to surface physics and chemistry was to provide a tool for obtaining and demonstrating well-defined surface conditions in performing investigations of surface adsorption and related phenomena.

## Theory of Field Emission

Field emission is a quantum mechanical phenomenon with no classical analogue. When a sufficiently high electric field is applied to the surface of a metal or semiconductor the surface potential barrier is deformed to provide a finite length through which an electron within the metal can "tunnel." This phenomenon (See Figure 19) can be formulated mathematically by considering a Fermi sea of electrons within the metal impinging on the surface.[42] Multiplying this impingement rate by the appropriate quantum mechanical transmission coefficient leads to the following expression for the number of field emitted electrons whose energy $\epsilon$ (relative to the Fermi level) lies between $\epsilon$ and $\epsilon + d\epsilon$:

$$P(\epsilon)\,d\epsilon = \frac{4\pi m d \exp(c\epsilon/d)}{h^3 \left[1 + \exp(\epsilon/kT)\right]}\, d\epsilon \qquad (36)$$

where

$$c = -\frac{4}{3}\,\frac{(2m\phi^3)^{1/2}}{\hbar\, e\, F}\, v(y)$$

and

$$d = \frac{\hbar\, e\, F}{2(2m\phi)^{1/2}\, t(y)}$$

and t(y) and v(y), (published in tabular form[42]), are slowly varying functions of the work function $\phi$ and applied electric field F.

Multiplying Equation (36) by the electronic charge, then integrating over the limits $-\infty$ to $\infty$, yields an expression for the current density of the field emitted electrons. This integration is conveniently accomplished by defining a dimensionless parameter $p = kT/d$ which leads to an expression for the current density $J_{TF}$ of T-F (thermal-field) emission of the following form:

$$J_{TF} = \frac{\pi p}{\sin \pi p}\,\frac{F^2 \exp(c)}{8\pi h \phi t^2(y)} = \frac{\pi p}{\sin \pi p}\, J_{0F} \qquad (37)$$

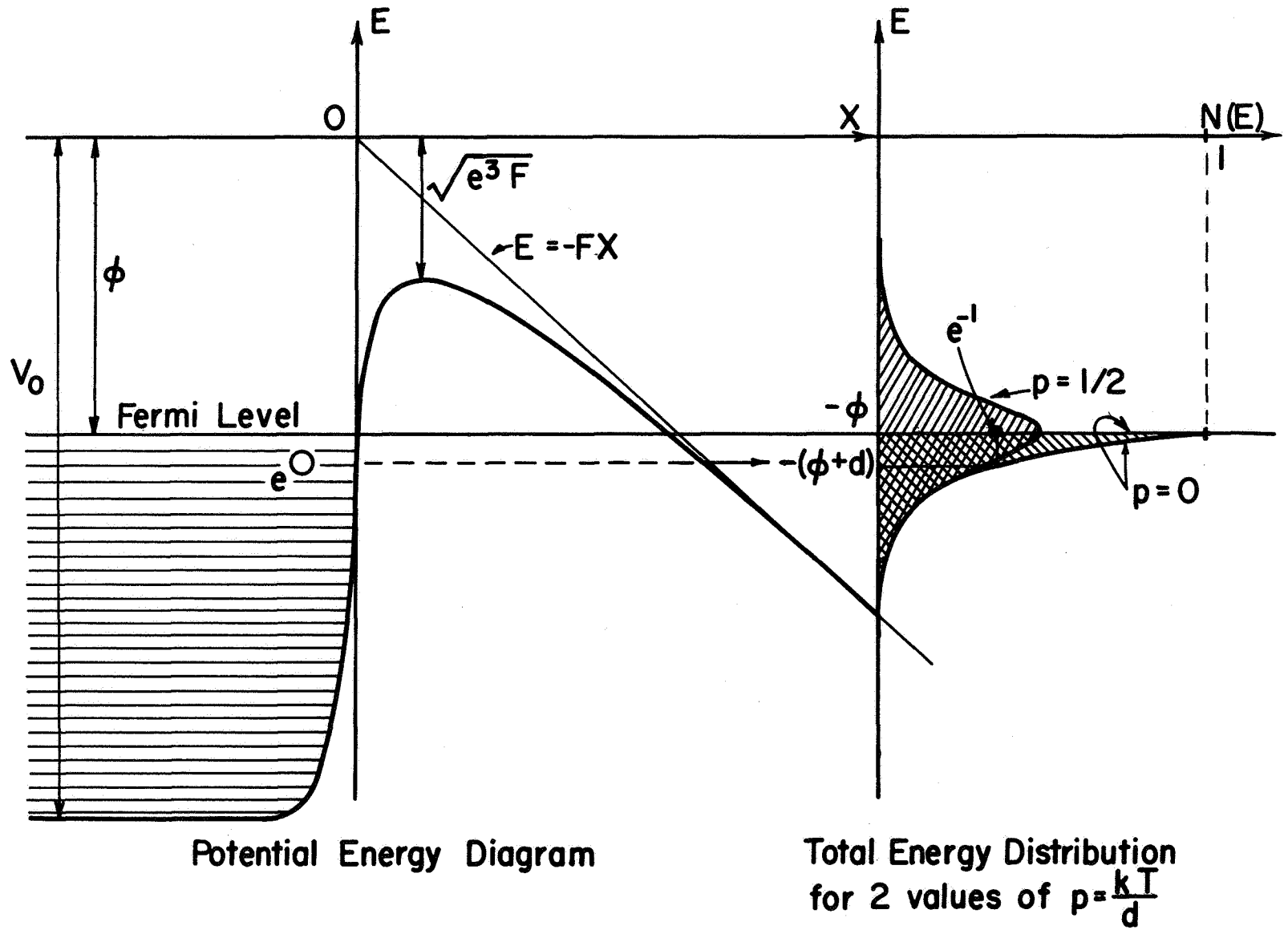


Figure 19. Potential energy diagram and total energy distribution for field of T-F emitted electrons.

which breaks down completely at p = 1 but is approximately valid up to $p \cong 2/3$. For small values of p (i.e., low temperatures or high fields) $\pi p/\sin\pi p \cong 1$ and one obtains the zero degree approximation of the Fowler-Nordheim formula for $J_{0F}$ which may be rewritten in terms of the directly measurable field emission current I and applied voltage V, as

$$I = A_f V^2 \exp\left[-a/V\right] \tag{38}$$

In view of this relation, it follows that a "Fowler-Nordheim plot" of the current-voltage relationship ($\ln(I/V^2)$ vs $1/V$) yields a straight line having a slope a and an intercept $A_f$ with the vertical axis at $\exp(-a/V) = 0$. The linearity of a Fowler-Nordheim plot is normally regarded as adequate proof that the emission is due to stable field emission. When the Fowler-Nordheim law is satisfied, it can be shown that $\phi$ is related to the slope a by the expression:

$$a = 2.96 \times 10^7 \frac{\phi^{3/2}}{\beta} s(y) \tag{39}$$

where s(y) is a tabulated function which is equal to $0.95 \pm 0.009$ over the range of current densities normally encountered. Using the work function $\phi_0$ for a clean surface as a reference, the work function $\phi_1$ of the surface when coated with an adsorbate can then be determined from

$$\phi_1 = \phi_0 \left[\frac{a_1 \, s(y_0)}{a_0 \, s(y_1)}\right]^{2/3} \tag{40}$$

where $a_0$ and $a_1$ are the slopes of the corresponding Fowler-Nordheim plots. Absolute determinations of the work function require a knowledge of the geometric factor $\beta$ (where $F = \beta V$), which can be determined from an electron micrograph of the emitter profile with an accuracy of about 15%; however, when the work function of the uncoated surface is well known, both $\beta$ and the work function of the coated surface can be determined with good accuracy.

## Techniques

General discussions of field electron microscopy and details on construction and processing have been presented in the literature.[41, 42] Briefly, the field electron microscope is a diode in which field emitted electrons are drawn from the single crystal hemispherical tip of a very sharp needle (tip radius usually below 1 micron) mounted in an evacuated bulb with a phosphor screen concentric with the cathode surface. When a sufficiently positive "viewing voltage" is applied to the phosphor screen, the field emitted electrons travel along nearly radial paths and form on the phosphor screen a visible, highly magnified emission image of the emitter surface. Such an image is shown in Figure 20 for a clean (110) oriented emitter. The field electron microscope is characterized by a high magnification, (typically $10^5$ to $10^6$ x) and a high resolving power for smooth surfaces, (typically 30 A, the limit determined by the initial energy spread (about 0.25 eV) of the field emitted electrons). Pattern detail arises from local variations in field and work function at the tip surface, and the pattern has a symmetry characteristic of the crystal structure of the tip material. Observation of the emission pattern of the uncoated tip provides a sensitive criterion for checking the smoothness and cleanliness of the substrate.

Emitter tips are easily fabricated from most refractory metals and many semiconductors. Although chemical or electrochemical etching techniques are usually employed, nearly all metals and semiconductors can be fabricated into clean emitters by vapor grown whiskers.[43] Thermal heating is normally employed for cleaning surfaces, although other methods, such as field desorption, must be used for low melting metals. When field desorption is used for cleaning, it is wise to cool the emitter to liquid nitrogen temperature to prevent surface migration of contaminants from the shank.

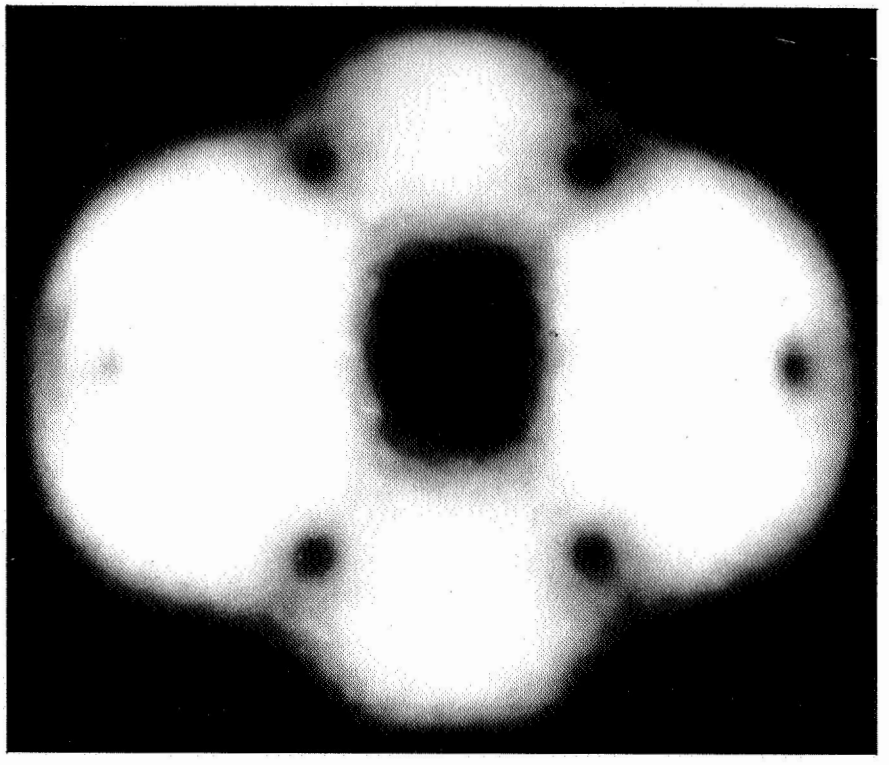

Figure 20. Field emission pattern of a clean (110) oriented tungsten emitter.

Adsorption, desorption and migration of adsorbates are measured through observation of the rate of change of the field electron pattern or current, which in turn, permits a determination of the associated physical constants (sticking probability, rate constants, and activation energies). However, at the high values of electric field required for emission, there is a possibility that the large electrostatic forces accompanying these fields may alter the processes under study and, at high temperatures may even alter the shape of the substrate. To avoid this, the "viewing field" required for field emission may be applied in the form of very short pulses at low duty factor (e.g., 1 microsecond pulses at a rate of 30 to 200 pulses per second), and the emission pattern is then viewed as a motion picture. This technique, introduced by Dyke[44] and co-workers, minimizes the perturbing effect of the viewing field on the event under study. Using a pulsed viewing voltage permits considerable freedom in the selection of the tip temperature (from $0^{\circ}K$ to the melting point of the emitter) and of the magnitudeand polarity of the dc voltage which may be applied at the tip surface.

Besides a high voltage supply for pattern viewing, additional equipment necessary for most field emission investigations include sensitive current and voltage measuring meters and provisions for measuring and controlling the emitter temperature. The latter is usually accomplished by resistively heating the supporting filament onto which the emitter is spot welded and accurately measuring the resistance of a small section of the filament. The resistance measurements can be related to temperature by precalibration or making use of the known variations of resistivity with temperature.

The vacuum requirements for performing meaningful investigations of surface phenomena by field emission are such that the surface must remain free of foreign contamination over the period of time the measurements are being performed. Residual gas pressures not only affect the

particular surface phenomenon under study, but also lead to sputtering of the emitter surface by the positive ions that are formed by electron impact ionization when steady field emission currents are drawn from the emitter. Residual helium pressures are particularly effective in leading to cathode sputtering during field emission but this problem is readily eliminated in sealed-off tubes by using glass of low helium permeability or immersing the tube in cryogenic liquids. Depending on the type of experiment contemplated, field emission investigations can be performed with evacuated sealed-off tubes or tubes attached to the vacuum system, but in either case it is desirable to have residual gas pressures well below $1 \times 10^{-9}$ torr. Investigations of the adsorption of volatile gases, such as hydrogen or neon, can be accomplished by immersing the tube in liquid helium and utilizing chemical or sublimation sources to deposit the desired adsorbate onto the emitter. A typical design of a field electron microscope used in adsorption studies is shown in Figure 21.

## Work Function-Coverage Relationships

The properties of the clean or contaminated emitter surface become apparent only through their effect on the electron emission. The precise evaluation of the work function is therefore of primary importance in the interpretation of the patterns observed in the field electron microscope. The variation in the electron emission over the surface of a smooth, atomically clean tungsten emitter is caused by variation of the work function with crystallographic direction. The use of Equation (40) to obtain the work function change due to adsorption is strictly correct only if F and the distribution of $\phi$ are constant over the emitting region, which is seldom the case. In general the electron emission is averaged over a variety of crystal faces with widely varying work functions. It can be shown that the slope of a Fowler-Nordheim plot yields an average value of $\phi^{3/2}\beta$ which is related to the individual regions as follows:

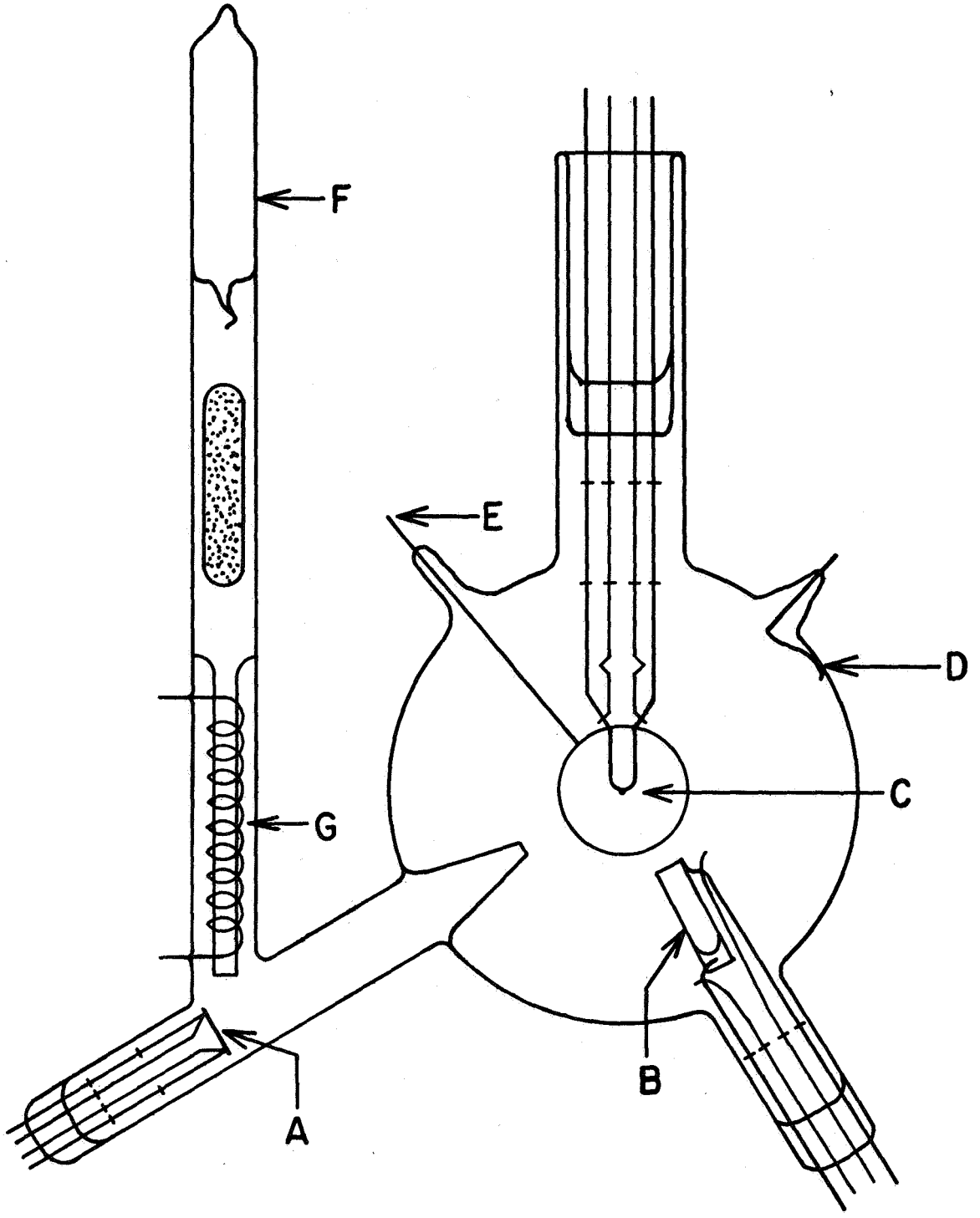


Figure 21. Front view diagram of field emission microscope for investigation of cesium and oxygen on tungsten. A, cesium source; B, oxygen source (heatable platinum crucible containing copper oxide); C, emitter assembly; D, electrical connection to conduction coating; E, anode ring; F, cesium reservoir; G, secondary cesium source.

$$\phi^{3/2}/\beta = \sum_i f_i \phi_i^{3/2}/\beta_i \qquad (41)$$

where $f_i$ is the fraction of the total current carried by the ith emitting region.

In practice, the curvature of the Fowler-Nordheim plot over the voltage range is negligible, so that its slope yields a constant $\phi^{3/2}/\beta$. It can be seen from Equation (41) that the experimentally obtained value is weighted heavily in favor of the highly emitting, or low work function, regions and may in practice be almost identical to the lowest $\phi$ encountered on the emitter surface. Thus, in utilizing Equation (40) to determine work function changes on adsorption it should be remembered that average values are obtained and when adsorption greatly alters the emission distribution from that of the clean surface, these values cannot always be related directly to contact potentials.

The difficulties inherent in the determination of averages can be overcome by measuring the electron current from individual crystal planes by suitably designed current probes. A tube designed for this purpose which allows measurement of total energy distrubutions as well as the emission from a single plane is shown in Figure 22.

Utilizing the average work function-coverage relationships and the results of probe tube measurements, it is possible to establish the relationship between the work function of individual crystal planes and average coverage. Although the field electron patterns give some indication as to the distribution of the adsorbate over the various crystallographic planes, only probe tube techniques will provide unequivocal measurements as to the atom density on various planes throughout the coverage range.[45]

## Surface Migration

One of the early uses of field electron microscopy was the investigation of surface migration of adsorbed layers on various substrates.

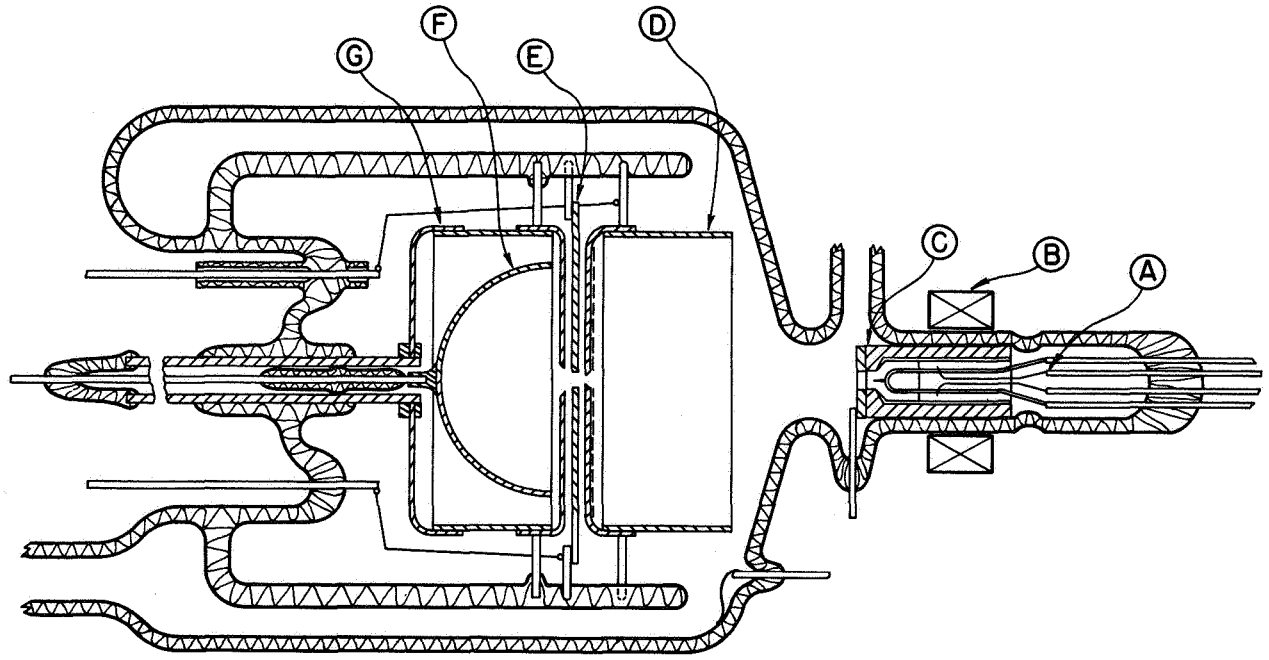


Figure 22. Energy analyzer tube designed to measure work function and energy distribution of single crystallographic planes. Provisions can be made for depositing adsorbates.

The activation energy for surface migration on various crystallographic planes can be readily determined by measuring the temperature dependence of the rate of diffusion of the adsorbate as it migrates across the emitter surface. Recently, it has been determined that the electric field necessary for field emission viewing can alter the rate of surface migration.[46] By applying the viewing voltage in pulses of low duty factor the time average field is negligible and such field effect problems are eliminated without sacrificing viewing. The activation energy for surface migration is determined by assuming a surface diffusion coefficient of the following form:

$$D = a_d^2 \ \nu_d \ \exp\left[-E_d/kT\right]$$

where $a_d$ is an average "jump" length of the migrating atoms and $\nu_d$ is a frequency factor of the order of $10^{12}$/sec. The distance x traversed by the adsorbate in time t is approximated by

$$x = (Dt)^{1/2}$$

The activation energy for surface diffusion is then determined from the combined equation

$$-\ln t = \ln \frac{a_d^2 \nu_d}{x^2} - E_d/kT \qquad (42)$$

The determination of surface diffusion rates thus involves the measurement of the time necessary for the adsorbate to travel a given distance across the emitter surface. This can be accomplished by visually choosing the end point when the advancing boundary travels a specified distance on the surface. In cases where the adsorbate migrates across the surface without a sharp boundary, visual end points cannot be easily employed. In this case one can make use of the fact that the field emission current (in this case the pulsed current) usually varies as the adsorbate migrates across the surface and can be utilized to establish the end point.

## Thermal Desorption

Field electron microsoopy lends itself to the measurement of thermal desorption rates and has been used in this connection for a variety of systems.[41] Typically, thermal desorption rates are determined by utilizing known relationships between work fucntion and coverage. In this fashion, rates of work function change over a small coverage increment at various temperatures lead to the determination of activation energies of desorption.

Pulsed electron microscopy can also be used to good advantage for desorption measurements for the following reasons: (1) it allows visual inspection of the pattern during desorption and use of pattern changes for end points and (2), either the variation of the pulse current $I_p$ at constant voltage $V_p$ or $V_p$ at constant $I_p$ can be followed and related to coverage-time plots for subsequent kinetic analysis. When using $I_p$ or $V_p$ to follow desorption rates care must be taken to allow for temperature effects on $I_p$ as shown in Equation (37) and also the temperature variations of the work function of the particular adsorbate-substrate system. Field emission determination of the binding energy is based upon the following analysis: Assuming first order kinetics, the rate of change of coverage is governed by

$$\frac{d\sigma}{dt} = -\sigma/\tau \tag{43}$$

where

$$\frac{1}{\tau} = \nu \exp\left[-E_a(\sigma)/kT\right] \tag{44}$$

By measuring sufficiently small coverage changes, it is possible to replace $d\sigma/dt$ by $\Delta\sigma/\Delta t$, where $\Delta t$ is the time to record a change in $\sigma$ of $-\Delta\sigma$ at a given temperature T. Therefore, combining Equations (43) and (44) one obtains

$$\ln \Delta t = - \ln \nu + \ln (\sigma/\Delta\sigma) + E_a/kT \qquad (45)$$

Since $10^{11} \leq \nu \leq 10^{13}$ an error of not more than 10% occurs by dropping the second term in the brackets, $\ln (\sigma/\Delta\sigma)$, provided measurements are not made near $\sigma = 0$. Plotting $\ln \Delta t$ vs $1/kT$ yields a linear curve with slope equal to the binding energy and an intercept identified with $-\ln \nu$. Note that because only work function changes are measured directly by field emission methods, knowledge of the dependence of $\phi$ upon $\sigma$ is required.

It should be realized that activation energy measurements frequently involve some sort of average. For immobile layers the average is weighted toward the regions of lowest binding energy within the coverage increment, wheras for mobile layers in two-dimensional equilibrium the activation energy of desorption is often weighted towards the regions of highest binding energy.

Most adsorbate-substrate systems amenable to field electron microscopy lend themselves to the measurement of desorption rates by the above methods. It is only those systems which show no work function change on adsorption that are not easily investigated by field electron microscopy. So far, few such systems are known to exist.

## Coadsorption

Field electron microscopy has recently been applied to the investigation of two-component adsorbate-substrate systems (coadsorption). The systems potassium-hydrogen,[47] cesium-fluorine[48] and cesium-oxygen[49] have been studied thus far. Of primary interest in these investigations was the effect of various amounts of the more strongly adsorbed electronegative component on the work function changes, surface diffusion and desorption rates of the alkali metal.

Although the results of utilizing field electron microscopy for the investigation of coadsorption are in the preliminary stages, it can be stated with some degree of confidence that this technique has great promise

for providing a detailed understanding of the specific interactions involved in these more complex systems.

## Field Effects

As mentioned earlier, the sometimes undesirable perturbation of the surface event under investigation by the high field required for field electron microscopy can be eliminated by the use of pulsed field electron microscopy. Moreover, the embodiment of the field electron microscope makes it uniquely suited for the intentional study of the field perturbations of various surface phenomena. The latter characteristic has been exploited recently[50] in order to investigate the effect of field on the surface kinetics and thermal dynamic stability of cesium on various refractory metals. In practice, the direct viewing of the surface event under study can be retained even with the application of dc fields of varying magnitude and polarity by superposition of the pulsed viewing voltage on the dc voltage through a suitable resistor-capacitor combination.

The temperature dependence of the surface diffusion rates of cesium on tungsten in the presence of an electric field has been measured[50] for two different but successive modes of surface diffusion with an initial cesium coverage of approximately 0.2 monolayer. Values of the field dependent activation energy of surface diffusion $E_d(F)$ for the two modes were determined by assuming a diffusion coefficient $D(F, T)$ of the form

$$D(F, T) = D_0 \exp\left[-E_d(F)/kT\right] = \frac{x^2}{t} \tag{46}$$

where $D_0$ is a constant, and x is the distance traversed by the adsorbed cesium in time t. The temperature dependence of the diffusion rates in the presence of an electric field was found to obey Equation (46), thus permitting the calculation $E_d(F)$ and $D_0$ as functions of applied field. These results could be fitted to a particular model involving the

interaction of the applied electric field with the dipole moment formed by the adatoms, thereby giving considerable insight as to the electronic structure of the adsorbate.

The effect of positive field on thermal desorption (better known as field desorption) has been investigated for a variety of systems[51, 52, 53] and recently treated theoretically[54] for various types of adsorption. It is only through field electron microscopy techniques that field strengths sufficient to initiate field desorption can be generated at reasonable voltages and their effect on adsorbed layers conveniently studied.

According to Gomer and Swanson,[54] there are two basic mechanisms for field desorption, depending on whether $V_I - \phi$ is large or relatively small. Both cases involve a deformation of the potential energy of the ionic adsorbed state such that, beyond a certain distance $x_c$ from the surface, the ionic state is both the ground state and a repulsive state. In general, the rate constant for field desorption is expressable as

$$\tau_F = \frac{\exp\left[E_a(F)/kT\right]}{\nu s} \tag{47}$$

where $\nu$ is a frequency factor ($\sim 10^{13}\ \text{sec}^{-1}$), s is a transition probability or entropy factor which generally decreases with F. The quantity $E_a(F)$ is the activation energy for desorption, which may be written generally as

$$E_a(F) = \sum_n V_{I_n} - n\phi + E_a - \Delta(F) \tag{48}$$

where $V_{I_n}$ is the nth ionization potential, $E_a$ the zero field binding energy, and $\Delta(F)$ is a field dependent correction factor, which is different for the various types of binding: Ionic, Metallic, and Covalent. The first two fall under the category of small $V_I - \phi$.

Case I. $V_I - \phi$ Small: Ionic Adsorption. - This situation is the simplest to consider for the field correction is easily computed by differentiating the total potential for an ion bound to the surface. The

correction factor is found to be given by

$$\Delta(F) = (ne)^{3/2} F^{1/2} - F\, en(x_o - \lambda) \tag{49}$$

where $\lambda$ is a Thomas-Fermi screening length and $x_o$ is the equilibrium distance of the ion from the surface.

Metallic Adsorption. - In the case of metallic binding, $V_I - \phi$ is still small and the atomic valence level, which becomes broadened as the atom approaches the surface, lies near the Fermi level. If this valence level lies only partly below the Fermi level

$$\Delta(F) = 3.8n^{3/2} F^{1/2} - \frac{1}{2} (\alpha_a - \alpha_i) F^2 - MF \tag{50}$$

Where $\alpha_a$ is the effective polarizability at $x = x_o$, $\alpha_i$ is the ionic polarizability, and M is the effective dipole moment at $x = x_o$.

On the other hand, if the valence level falls completely within the conduction band of the metal, as would be the case of a metal atom adsorbed on a surface of identical atoms, the last term above is not effective so that

$$\Delta(F) = 3.8n^{3/2} F^{1/2} - \frac{1}{2} (\alpha_a - \alpha_i) F^2. \tag{51}$$

Case II. $V_I - \phi$ Large: Covalent Bonding. - When $V_I - \phi$ is large,

$$\Delta(F) = \frac{(ne)^2}{4x_c} + F\, en\, x_c + \Delta(P) \tag{52}$$

where $x_c = x_o + \lambda$ and $\Delta(P)$ refer to various polarization effects which are discussed in greater detail elsewhere.[54] Field desorption measurements not only provide knowledge as to the types of field interactions with the electronic structure of the adsorbate, but also provide considerable insight as to the detailed bonding of the adsorbate to the substrate and, in some cases,[55] yield precise mapping of the one-dimensional potential energy curves of the adsorbate-substrate system.

Since field desorption is most conveniently studied by field electron microscopy techniques from an immobile layer, probe techniques can be used to great advantage to isolate the measurements to single crystallographic planes. This, coupled with the ability to determine indirectly zero field activation energies of desorption from the existing field desorption theory, allows one in principle to determine the variation of the zero field binding energy as a function of adsorbate coverage on a single crystallographic plane.

## Epitaxial Layers

Another recent application of field emission techniques has been the investigation of the nucleation and growth kinetics of epitaxial layers on various substrates. Results of this nature were first reported by Melmed,[56] who extended his earlier field emission work on vapor phase grown metallic whiskers[43] to a study of two-dimensional epitaxial layers. Investigations of this nature, now reported for a variety of adsorbate-substrate systems,[57] have provided considerable insight as to the detailed mechanisms involved in the nucleation process and the effect of substrate and surface contaminants on the epitaxial growth kinetics.

Melmed discovered that certain low melting adsorbates, such as copper, which are not readily amenable to the usual field electron microscopy techniques, can be grown epitaxially on a tungsten substrate. In some instances it was observed that the epitaxial layer consisted of a clean, perfect single crystal structure of the face-centered copper structure grown across a tungsten field emitter surface and could be used for subsequent adsorption studies by field electron microscopy techniques.

## Summary

Some of the recent applications of field electron microscopy to surface phenomena are as follows: (1) Work function-coverage relationships;

(2) Zero field surface migration; (3) Thermal desorption; (4) Coadsorption; (5) Field effects on surface kinetics; (6) Investigations of epitaxial growth; (7) Electron impact desorption; (8) Substrate surface rearrangement (e.g., self-migration and sputtering). It seems safe to conclude, therefore, that field electrom microscopy has made important contributions to the understanding of various phenomena which occur at metal and semiconductor surfaces and will continue to make significant contributions as its use becomes more widespread.

# 5 - FIELD ION MICROSCOPY

## Introduction

An ideal tool for acquiring the desired understanding of metal surfaces would be one permitting actual atomic scale visualization of events occurring there. Because of its ability to resolve single atoms, the field ion microscope very nearly achieves this ideal. Although similar to the field electron microscope, the field ion microscope image is formed with ions rather than electrons. Here advantage is taken of the shorter wavelengths of the ions and the fact that ions from a cooled emitter surface have smaller transverse energy, making it possible to distinguish adjacent atoms which have a separation of 2.74 $\mathring{A}$ or less.

The basic principle of the field ion microscope is that atoms can be ionized in a high electric field, an effect predicted by Oppenheimer[58] and verified experimentally by Müller.[59] In this process, known as field ionization, the potential energy curve of the atom becomes distorted in such a way that an electron can tunnel from the atom into the metal, with the formation of a positive ion as illustrated in Figure 23. In the field ion microscope, the tip is maintained at a sufficiently high electric field to ionize the impinging gas atoms which are present within the tube (usually helium at a pressure of approximately one micron). The electric field at the surface of the tip approaches 4 or 5 volt/$\mathring{A}$, and is highest in the vicinity of the atoms which protrude beyond the average surface because of the crystalline nature of the tip. The rate of impingement of the surrounding gas atoms is greater than expected on the basis of kinetic theory because of attractive field induced dipole forces. There is a critical distance, $x_c$, from the emitter surface within which field ionization cannot occur because the ground state of the imaging gas atom falls below the Fermi level of the emitter so that tunneling of an electron

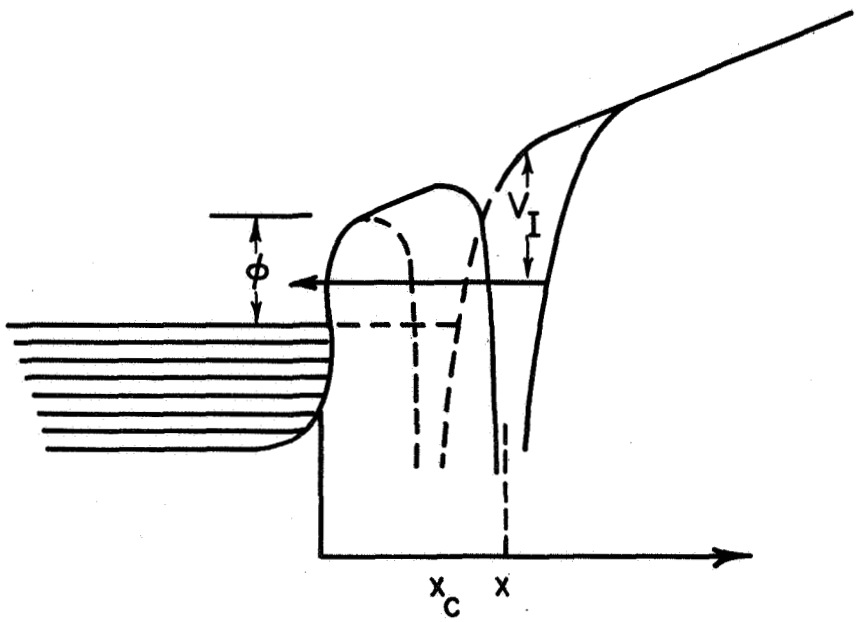


Figure 23. Potential energy diagram for field ionization.

is prohibited. Thus, best resolution is achieved by selecting a value of the electric field such that ionization occurs as near the critical distance as possible.

Most of the impinging gas atoms actually pass through the critical region without being ionized and as they collide with the surface they impart some of their kinetic energy to the substrate, being left with only enough energy to "hop" about on the surface. As they move about, they eventually hop over protruding surface atoms where the probability of ionization is greater because of the higher electric field and the ions thus formed are accelerated to the phosphor screen, creating an image of the surface as shown in Figure 24. Clearly, the resolution will be improved if the tangential velocity of the ions leaving the surface can be reduced. This is done by cooling the tip to liquid nitrogen or liquid hydrogen temperatures.

The field ion microscope has found application in the investigation of such phenomena as surface migration, adsorption, sputtering, field desorption, and surface structure, not to mention invaluable contributions made in the study of defects and related properties of the bulk crystal.[60,61] Despite the importance of these contributions, the field ion microscope is severely limited in its application to the examination of surfaces. The primary source of difficulty is, of course, the fact that the high electric field in which the studies must necessarily be made undoubtedly causes rearrangement or desorption of the adsorbate. In extreme cases, field evaporation of the substrate atoms themselves may occur. The occurrence of field evaporation, restricts use of the field ion microscope to metals whose melting points exceed roughly 1700°K. Exceptions are possible if one is willing to sacrifice resolution by working at lower than optimum fields. Another problem that has been encountered is that of etching of the emitter tip by field enhanced chemical reactions occurring between certain gases and the substrate.[62]

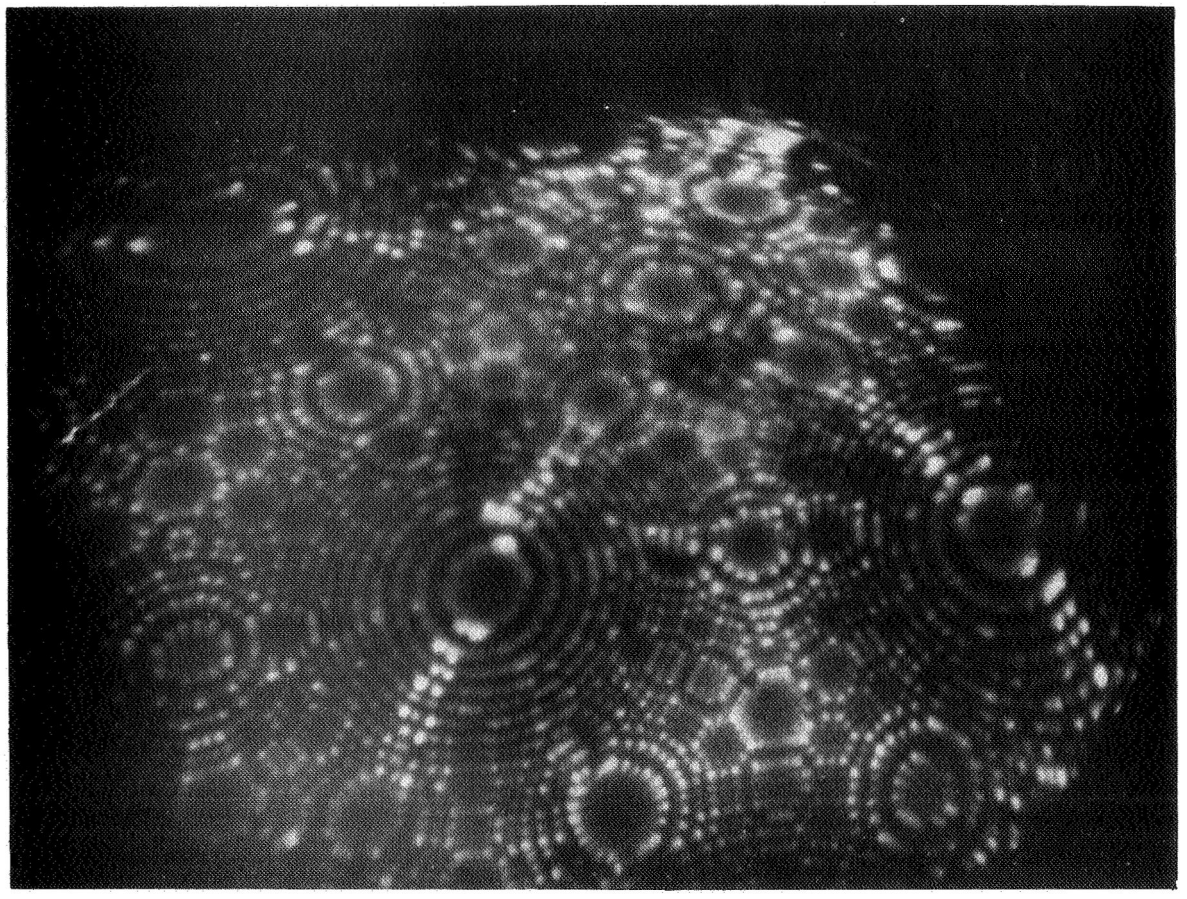

Figure 24. A field ion pattern of a tungsten surface illustrating the atomic resolution of the microscope.

Field ion microscopy does lend itself very well to the inspection of clean surfaces. Increasing the field slightly above that required for imaging of the surface[60] makes it possible to actually clean the tip by field evaporation of the substrate. Controlled removal of the surface layers allows one to investigate the depth of surface defects and other properties which lie a few atomic layers below the surface.

## Theory of Field Ion Emission

The mechanism of field ionization is also a quantum mechanical phenomenon, and is essentially field emission in reverse in that electrons tunnel from the gas phase molecules into the tip. Since there are no empty electronic levels in the metal below the Fermi energy, $E_F$, the applied field must raise the valence level of the atom to $E_F$, so that (neglecting polarization effects) the condition for field ionization is:

$$Fx_c = V_I - \phi - \frac{e^2}{4x_c} \tag{53}$$

where $V_I$ is the ionization potential of the molecule, $\phi$ is the work function, and $x_c$ is the minimum distance at which field ionization can occur; the last term of Equation (53) is due to the image potential.

As in the case of field emission, an expression for the field ion current is obtained by multiplying the rate of supply of molecules to the high field region near the tip by the probability of field ionization. The exact details of this calculation are complex and will not be reproduced here, except for the following approximate expression for the lifetime with respect to field ionization:

$$\tau_i = 10^{-16} \exp \frac{0.68\ V_I^{3/2}}{F} \tag{54}$$

where $V_I$ is in electron volts and F in volts per angstrom.

In view of the above, the mechanism of image formation in the field ion microscope becomes quite clear. Atoms or molecules approaching the tip are ionized in the vicinity of $x_c$, either on the way in or on the rebound; the ions are accelerated along the lines of force toward the negative screen so that a magnified image $\sim x/(k_t r)$ of the ionization zone is produced there, where x is the tip to screen distance in centimeters, r is the tip radius and $k_t \cong 1.5$ is an image compression factor.

According to Equation (54) the probability of ionization is a sensitive function of field, so that the ion image is a reproduction of the microscopic field distribution at the surface of the emitter. Since ionization occurs at $x_c$, any overlap of the equipotentials of the surface atoms will cause a certain amount of loss of structure. Also any distortion of the electronic structure at the surface due to the high fields required for image formation will also lead to image distortion.

The resolution of the field ion microscope depends on two factors: first, the transverse velocity of the image forming ions and second, the loss in detail in the field distribution at $x_c$. Diffraction effects, which must also be taken into account, are found to be negligible. As pointed out by Müller,[60] partial thermal accommodation on the tip reduces the incoming thermal and polarization velocity components of the image gas. Under these conditions the resolution limit due to transverse velocity components becomes

$$d = 4r\, k_t \left(\frac{kT}{eV}\right)^{1/2} \tag{55}$$

for $r = 10^{-5}$cm, $k_t = 1.5$, and $V = 10^4$ Volts, Equation (55) gives a resolution of 10 Å at 300°K.

The second factor which limits resolution is more difficult to assess, but an approximate calculation[41] shows the form of the functional dependence as

$$d \simeq 53\epsilon \frac{(V_I - \phi)}{V_I^{3/2}} \tag{56}$$

where $\epsilon$ is a numerical constant of the order of 0.5 to 1.0, d is in angstroms and $V_I$ and $\phi$ are in electron volts. It can be readily shown that d, as given by Equation (56), goes through a maximum $35\epsilon\ V_I^{-1/2}$ at:

$$V_I = 3\phi \tag{57}$$

which suggests that Equation (56) places the most severe limitations on the resolution for imaging gases whose ionization potential is nearly three times the substrate work function.

It has also been postulated[60] that the impinging molecule, after partial thermal accommodation, undergoes a series of hopping motions because of the attraction of the inhomogeneous field acting upon the induced dipole. The average hopping height h turns out to be

$$h = \frac{3kTr}{4\alpha F^2} \tag{58}$$

where $\alpha$ is the polarizability of the impinging molecule. It is further suggested that the most favorable resolution and highest image intensity are obtained when the hopping distance is slightly larger than $x_c$.

In order to realize best resolution and image intensity for the field ion image it will be necessary to optimize the conditions expressed in Equations (54) and (58) with respect to such variables as $V_I$, $\phi$, T, r and F. Also, the above considerations, which are derived for a degenerate metal, may not apply exactly in the case of a nonmetallic adsorbate. For instance, the equipotentials above an adsorbed molecule may not reproduce its atomic structure unless the molecule behaves as a conductor (i.e., does not tolerate internal electric fields); in addition, the overlap of metal and adsorbate orbitals must be sufficient to allow fast electron exchange in order to maintain a uniform surface charge on the adsorbate during field ionization.

## Summary

The field ion microscope is a unique tool for the investigation of surfaces because it permits single atom resolution of the surface. Consequently, field ion microscopy is a valuable tool for gaining information about the substrate. However, this technique is limited in its application to the investigation of surface-adsorbate interactions because of the effects of the extremely high electric fields present at the surface which can cause rearrangement or even desorption of the adsorbed molecules.

# 6 - WORK FUNCTION MEASUREMENTS

## Introduction

The presence of an adsorbate on the surface of a metal may alter the electron potential barrier of the metal and change the work function.[63] To understand how these changes occur, it is necessary first to acquire a qualitative understanding of the work function, which is simply the work required to remove an electron from a metal at $0^{\circ}K$. The origin of the potential barrier at the surface of the metal may be thought of in terms of the way in which the potentials for the constituent atoms interact with one another.

When a large number of atoms are brought together to form a crystal, the potential inside the solid assumes the periodicity of the lattice, a periodicity which is terminated at the surface, as shown in Figure 25. The height of the potential barrier above the Fermi level is the electronic work function, which is influenced by two factors.[64] The first, the chemical potential, is determined solely by the bulk properties of the solid and is independent of the surface. The second, the surface potential, is very sensitive to the properties of the surface and is related to the electrostatic potential energy at the surface of the metal. The latter effect decays slowly with distance away from the surface. Although there are undoubtedly many contributions to the surface potential, some of the principle ones that have been considered theoretically are the following: (1) Of primary importance is the penetration of the electrons beyond the surface of the conductor. This is a quantum effect which leads to the formation of a dipole layer (negative side outward) at the surface and an increase in the magnitude of the surface potential. (2) Accompanying this "spill-over" of electrons is the decrease in the surface potential due to the decrease in the density of electrons within the metal. This energy is called the correlation energy and is due to

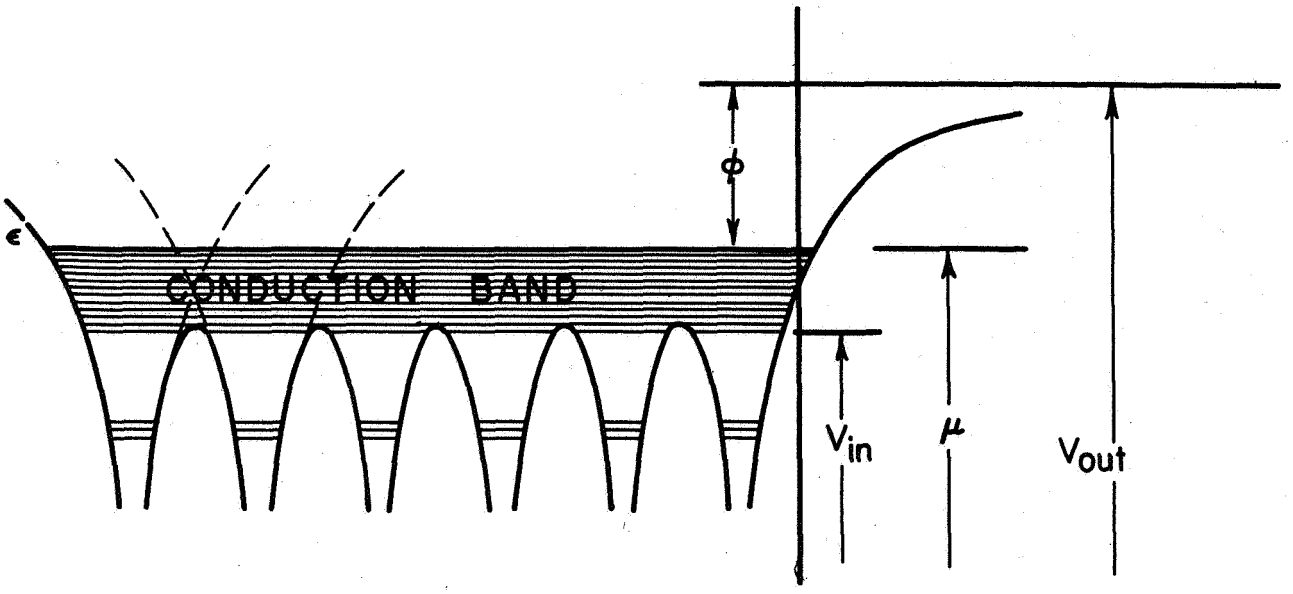


Figure 25. Potential energy diagram for a metal.

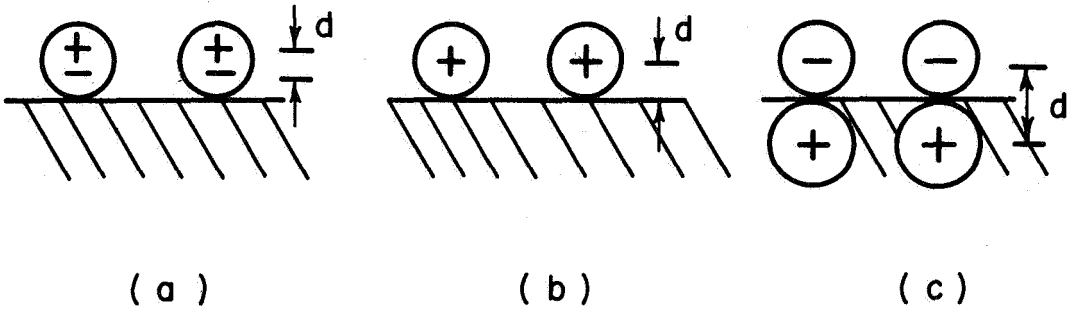


Figure 26. Pictorial representation of dipoles for (a) van der Waals, (b) ionic, (c) covalent adsorption.

the mutual repulsion of the electrons through Coulomb interactions and the Pauli exclusion principle. (3) Still another contribution to the surface potential is the energy of interaction between the ion cores themselves which will be different for different crystal planes. From what has been said, it is reasonable to expect that an adsorbed layer would alter the surface potential, especially if the adsorbed molecules exist in a charged or partially charged state on the surface.

As used here, the surface potential refers to the difference between the electrostatic potentials inside and outside the metal and will be written $\chi = V_{in} - V_{out}$. As implied above, the surface potential is a structure sensitive property of the surface.

The state of any solid, liquid or gaseous phase containing electrons may be described thermodynamically by the <u>electrochemical potential</u> $\bar{\mu}$, where for a solid of essentially fixed volume at constant temperature, $\bar{\mu}$ is defined by

$$\bar{\mu} = (\partial F/\partial n)_{T,v} \tag{59}$$

where $F = U - TS$ is the Helmholtz potential. The ambiguity associated with the way in which S depends upon the number of electrons n is removed by requiring that $(\partial S/\partial n)_{T,v} \longrightarrow 0$ as $T \longrightarrow 0$. This is equivalent to defining $\bar{\mu}$ as the work done in bringing an electron from infinity and adding it isothermally to a metal of fixed volume. Thus any change in the potential at the surface of the metal will alter the electrochemical potential $\bar{\mu}$.

Now it is seen readily from Figure 25 that the work function measured in electron volts can be written as

$$\phi = V_{out} - \bar{\mu}/e \tag{60}$$

If we define the <u>chemical potential</u> as

$$\mu = \bar{\mu} - eV_{in} \tag{61}$$

then

$$\phi = -\chi - \mu/e \qquad (62)$$

Defined as it is, $\mu$ is a quantity dependent solely upon temperature and the bulk properties of the material. Consequently, changes in $\phi$ due to adsorption are directly related to changes in the surface potential $\chi$. By considering the dipole layer at the surface as a parallel plate capacitor, the value of the surface potential may be shown to be

$$\chi = M_t/\epsilon_o$$

where $M_t$ is the total dipole moment per unit area and $\epsilon_o$ is the permittivity of free space. (MKS units are used)

The work function of a metal is changed as a result of the adsorption of gases on the surface.[63] That this is the case is not surprising if we think of the adsorbed gas as having a dipole moment which tends to modify the total dipole moment at the surface and consequently change the work function.

A dipole layer of $\sigma$ dipoles/area, all identically oriented normal to the surface, may be treated in first approximation as a parallel plate capacitor with plate separation d. The plates then have a uniform charge distribution $\sigma$ e and the product of d and the electric charge e is the effective dipole moment M. The external field of this layer is zero and the change in work function is equal to the change in surface potential. Thus,

$$\Delta\phi = -\Delta\chi = \pm \Delta M_t/\epsilon_o \qquad (63)$$

but $\Delta M_t = \sigma M$, so $\Delta\phi = \sigma M/\epsilon_o$.

Writing the coverage $\theta = \sigma/\sigma_o$ ($\sigma_o$ is the number of adsorption sites) then

$$\Delta\phi = \pm \sigma_o \theta M/\epsilon_o$$

or

$$M = \epsilon_o \Delta\phi / \sigma_o \theta \qquad (64)$$

We note immediately from this that the sign (+ sign for - ions) of M is dependent upon the charge of adsorbed molecules and the magnitude is given by the separation of the two charge layers. The three cases corresponding to van der Waals', ionic and covalent bonds are depicted in Figure 26.

## Experimental Methods

Over the years in which work function measurements have been made, a number of techniques have been developed[63, 65] and, since each method has found extensive use, each will be discussed separately. The measurements will be divided into three categories. The first deals with methods involving the cathode of an electron emission system and includes thermionic, photoelectric, and field emission techniques. The second category also involves electron emission, but the effects being investigated occur at the anode; these will be referred to as emission contact potential difference methods. Finally, consideration will be given to the capacitive contact potential difference method.

## Electron Emission Methods

Thermionic Emission. - In thermionic emission, electrons are emitted from a metal because the tail of the electron energy distribution within the metal extends above the vacuum level. The current density of electrons emitted from such a system is shown theoretically to be dependent upon the temperature of the cathode through the so-called Richardson equation:[64]

$$J = A T^2 \exp \left[ - e\phi / kT \right] \qquad (65)$$

where $\phi$ is the work function of the metal and A = 120 amp/cm$^2$-deg$^2$. Note that a graph (called a Richardson plot) of $J/T^2$ against $1/kT$ is a straight line with slope equal to $e\phi$. Thus, a change in the work function of the cathode will show up as a change in the slope of the Richardson plot.

Experimentally, Richardson plots are found generally to be straight lines, although the intercept is usually not equal to the theoretical constant and often $\phi$ is temperature dependent. Thus, an experiment designed to measure the work function changes occurring during adsorption must include careful temperature control and measurement, as well as emission current measurements. The Richardson equation is reasonably valid for single work function cathodes; but if patches of different work function are present on the surface, emission will arise predominantly from one patch or another leading to an average work function weighted toward the lowest value present. Additional difficulty arises in attempting to measure changes in work function due to adsorption because of the possibility of thermal desorption, an effect which is exaggerated if the adsorbate tends to increase the work function, because an even higher temperature is required to obtain emission. However, it is possible to measure the change in work function due to adsorption of alkali metals on refractory metals by this method because significant electron currents are emitted at relatively low temperatures.[66] Also, since the electric field must be uniform for the Richardson equation to be valid, precautions must be taken to provide a geometry amenable to this requirement.

Photoelectric Emission. - When electromagnetic radiation of sufficiently high frequency is directed upon a metal surface, electrons are emitted in a process known as photoelectric emission.[67] It is a rather easy matter to show that the threshold frequency for emission is related to the work function by the expression

$$\phi = \frac{h \nu_o}{e} \tag{66}$$

where $\nu_o$ is the threshold frequency for photoemission. Hence, changes in work function of the metal surface are given by

$$\Delta\phi = \frac{h}{e} (\nu - \nu_o) \tag{67}$$

Because of competition from thermal emission, the threshold for photoemission is not always easily determined, and it has been found useful to apply a method devised by Fowler to determine $\nu_o$. The basic equation in the Fowler analysis[68] is written

$$\log (I/T^2) = B + F(X) \tag{68}$$

where I is the photocurrent, B is a constant independent of the frequency, F (X) is a function having the same form for all metals, and

$$X = (h\nu - h\nu_o) / kT$$

Specifically,

$$F(X) = \log\left\{\frac{\pi^2}{6} + \frac{1}{2} X^2 - \left[\exp(-X) - \frac{\exp(-2X)}{2^2} + \frac{\exp(-3X)}{3^3} - \cdots\right]\right\} \quad X = 0$$

Thus, a graph of $\log (I/T^2)$ vs $h\nu/kT$ will yield a curve identical to the theoretical F(X) vs X curve except that it will be shifted in the vertical direction by an amount B and in the horizontal direction by an amount $h\nu_o/kT$. The latter shift is used to obtain $\nu_o$.

For measurements made on surfaces having more than one work function, the photoelectric measurements yield average values, weighted in favor of the lowest work functions present. Other difficulties which are common to the photoelectric method of measuring work function are: (1) in order to obtain a precise value for $\phi$, currents of the order $10^{-14}$A must be measured in the region of $\nu_o$; (2) for work functions of 5 volts or more, the threshold frequency is in the ultraviolet region which introduces numerous experimental difficulties.

Field Emission. - The reader is referred to the section of this report dealing with field emission microscopy for a detailed discussion of methods of measuring work function.

## Emission Contact Potential Difference Methods

Magnetron Method. - The magnetron method[69, 70] is not widely used as a means of measuring work functions and therefore will be given only brief mention here. Consider an axially symmetric thermionic diode system arranged as shown in Figure 27 and suppose that a solenoid is provided for producing an axial magnetic field. The potential of an electron relative to the anode as illustrated by Figure 28, is given by

$$V_e = V_a + \epsilon(T) + (\phi_c - \phi_a) \tag{69}$$

where $V_a$ is the applied potential, $\epsilon(T)$ is a temperature dependent term related to the distribution in the energies of the emitted electrons, and $\phi_c$ and $\phi_a$ are the work functions of the cathode and anode, respectively.

When current is passed through the solenoid, the anode current is reduced by the effect of the magnetic field. It can be shown that if the solenoid current is such as to reduce the emitted electron current to one-half its initial value,

$$V_e = KI^2_{1/2}$$

and hence,

$$\phi_a = \phi_c + \epsilon(T) + V_a - KI^2_{1/2} \tag{70}$$

where K is a constant depending upon the geometry of the system. Plotting $I^2_{1/2}$ against $V_a$ yields a linear graph with intercept equal to $\phi_c - \phi_a + \epsilon(T)$ so that $\phi_a$ may be calculated readily once $\phi_c$ and $\epsilon(T)$ are known. The quantity $\epsilon(T)$ is about 0.2 eV.

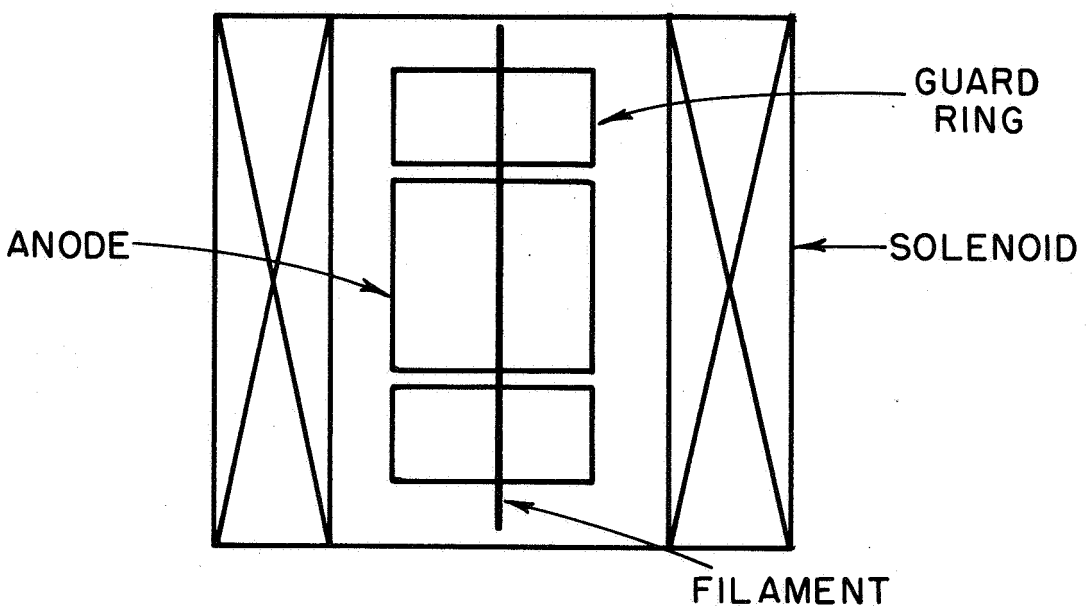


Figure 27. Magnetron system for measuring work function changes of the anode.

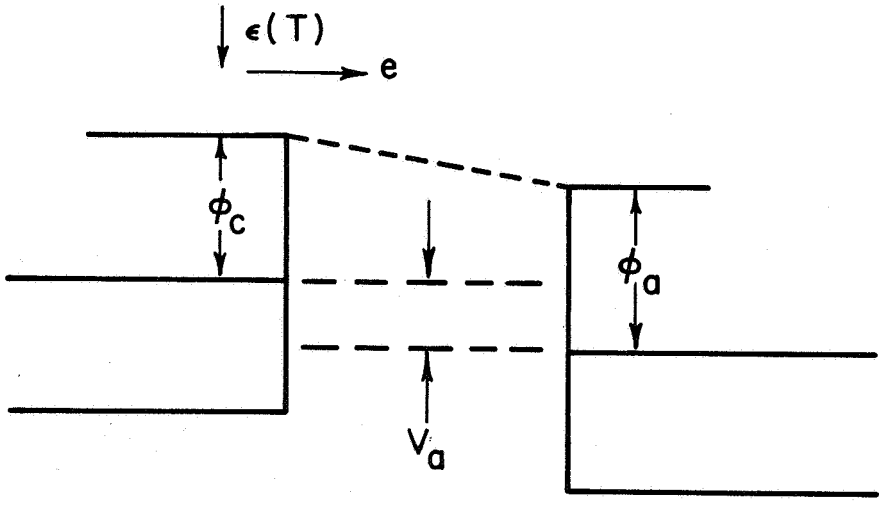


Figure 28. Potential energy diagram of an electron relative to the anode.

Space Charge Limited Diode. - The emission of electron current in a space charge limited thermionic diode is found to depend upon the three-halves power of the applied potential and the mean work function of the anode.[63] The dependence upon the anode work function is such that the current-voltage characteristic for the system is shifted toward higher or lower potentials depending upon whether the work function increases or decreases, as illustrated in Figure 29. Experimentally, a wide variety of geometrical configurations are possible and all types of surfaces including evaporated films have been used. This method is especially applicable to studies involving adsorption of both electronegative and electropositive species.

Thermionic Retarding Potential Method of Measuring Work Function. Consider a plane parallel, two electrode system consisting of a cathode and an anode with the cathode heated to a temperature T and possessing a uniform work function $\phi_c$, and the anode at a low temperature and having a uniform work function $\phi_a$. If a potential difference is applied to this system such that a small accelerating field exists at the cathode surface, the emission current density is given by the well-known Richardson equation (Equation 65). In this case the barrier to emission is simply the cathode work function $\phi_c$ (Figure 30 (a) ). However, if a negative potential V of sufficient magnitude is applied to the anode, the barrier to emission becomes, as shown in Figure 30 (b), $\phi_a - V$, and it can be readily shown[71] that the emission current density is given by

$$J_e = A T^2 \exp\left[e(-\phi_a + V)/kT\right] = J_o \exp\left[e(\phi_c - \phi_a + V)/kT\right] \quad (71)$$

(It should be mentioned that implicit in the derivation of Equation (71) is the conservation of the Maxwellian normal energy distribution). Thus, a

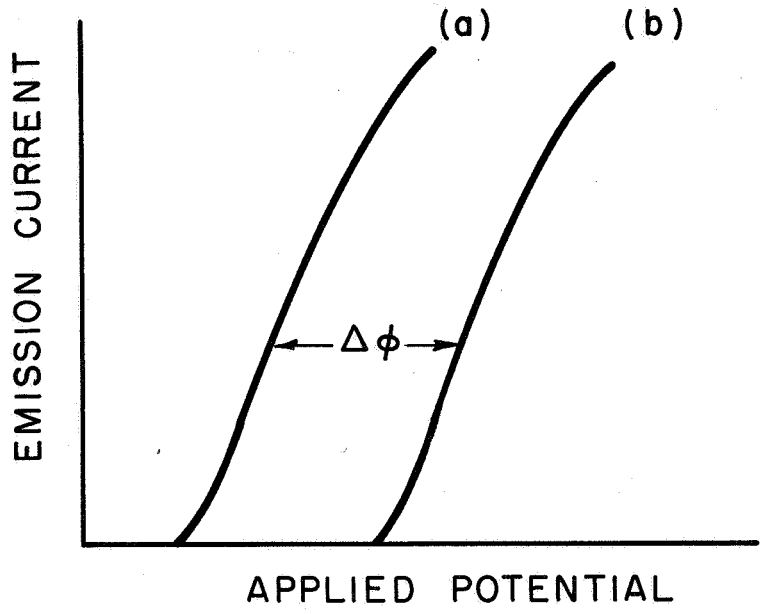


Figure 29. Current - voltage characteristics for (a) clean anode and (b) anode with increased work function.

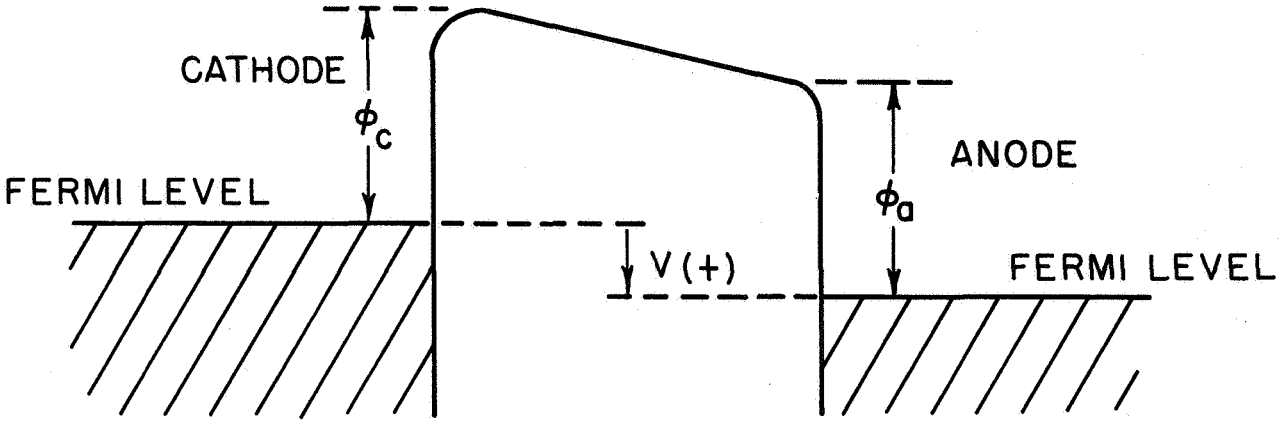


(a) $V \geq \phi_c - \phi_a$

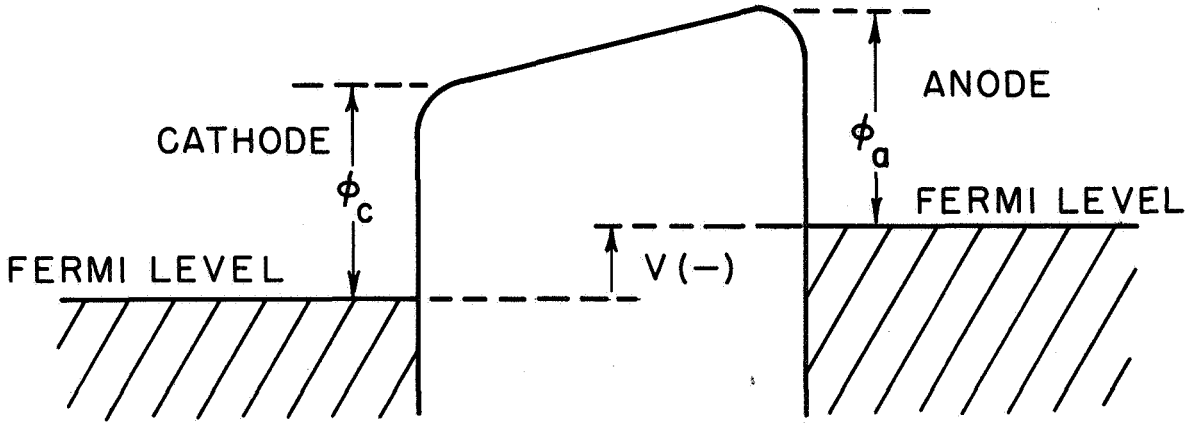


(b) $V \leq \phi_c - \phi_a$

Figure 30. Energy barrier to thermionic emission when the current is (a) cathode-limited, or (b) anode-limited.

plot of log $J_e$, or more conveniently log I, as a function of anode voltage V results (a) in a straight line independent of V for $V \geq \phi_a$, or (b) in a straight line with a slope 2.30/kT for $V \leq [\phi_c - \phi_a]$ (See Figure 31). The voltage at the point of intersection of these two straight lines, the so-called "knee" of the curve, is just equal to the difference in the work functions of the two surfaces (their contact potential). Increasing the temperature of the cathode increases the current at any value of V. Plotting the current as a function of temperature in the form of a Richardson plot (log $I/T^2$ versus $1/T$) permits determination of the work function of the cathode for case (a) and of the anode for case (b) from the slopes of the resulting straight lines.

The simple picture presented above is in practice complicated by a large number of effects, among which are space charge, the Schottky effect, nonuniform work functions, variation of work function with temperature, as well as others.[64, 72] For the plane parallel diode, space charge is a serious limitation; it can be shown[71] that space charge causes deviations in the expected I(V) curve for low values of V of either sign, and that the range of V affected increases with increasing $I_o$, the current corresponding to the saturation current density $J_o$. This limitation can be overcome by placing a third electrode with a small aperture in it between the cathode and the anode and with sufficient potential to reduce space charge to a negligible amount. In this case, however, the current collected at the anode passes through an aperture which has a divergent lens effect on the beam, and thus will affect the I(V) curve.[73] This effect can be reduced to a negligible amount by use of an axial magnetic field of sufficiently high strength such that the maximum possible radius $a_M$ of the helical path traveled by any electron is less that the radius of the aperture a:[73]

$$a_M = 3.37\ V_c^{1/2} / H < a \qquad (72)$$

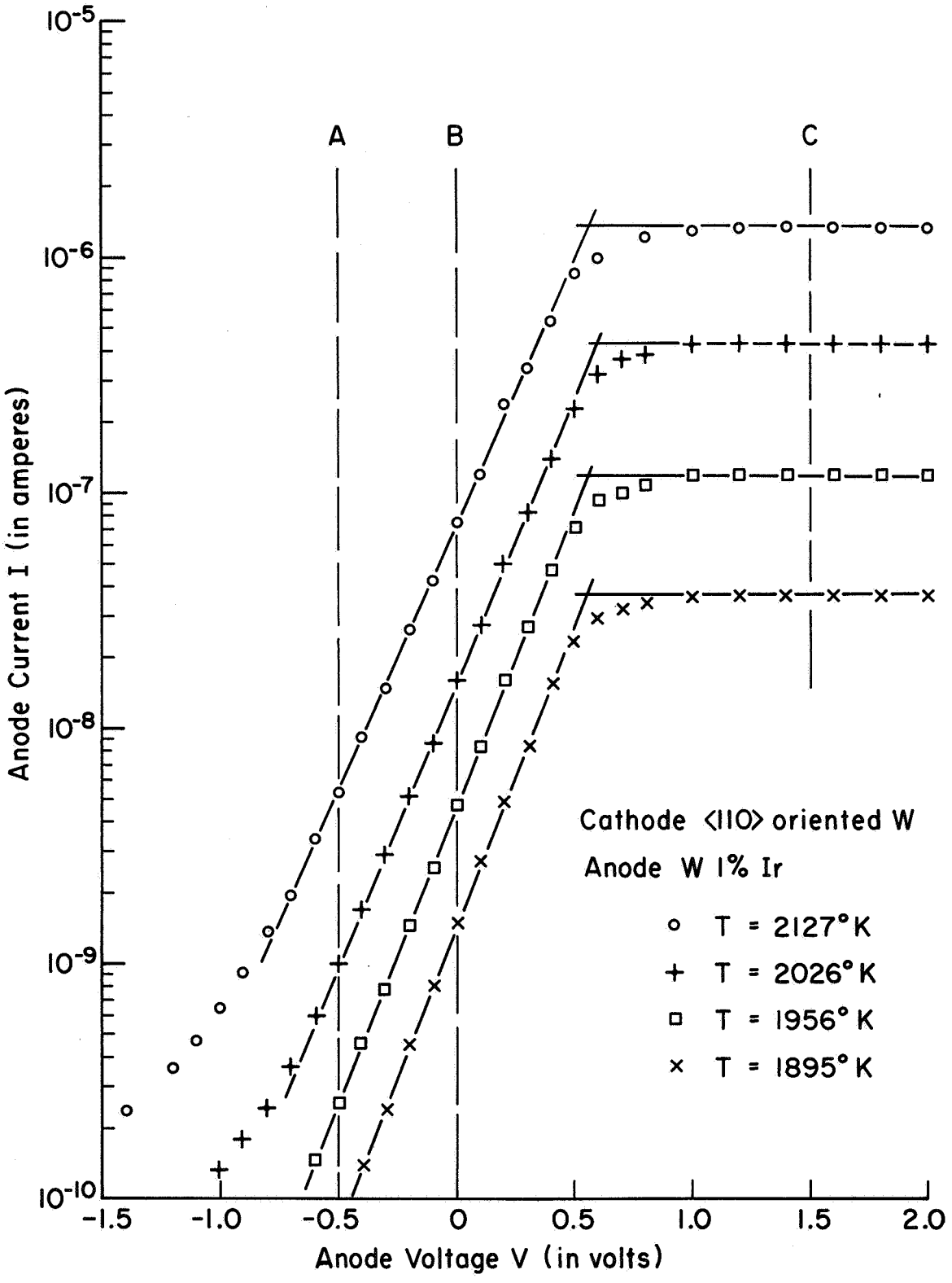


Figure 31. Typical plots of the anode current as a function of anode voltage for selected cathode temperatures. The temperatures are obtained from the slopes of the semilogarithmic portions of the curves.

where $a_M$ is in cm, $V_c$ is the voltage of the center electrode in volts, and H is the magnetic field in gauss.

Nonuniform work functions and deviations in geometry from the plane parallel case (i.e., effects which disturb the conservation of normal energy) affect the I(V) curve primarily by rounding the knee. The position of the knee under these circumstances may be obtained by extrapolation of the two straight lines of cases (a) and (b) until they intersect.

A variation of work function with temperature affects the I(V) curves in two ways: (1) the position of the knee is shifted with respect to the V axis; (2) the measured thermionic constants $A_r$ and $\phi_r$ for the heated cathode will differ from the constants A and $\phi$ in Equation (65). If we assume $\phi_c = \phi_{oc} + \alpha T$, then $\alpha = \Delta V/\Delta T$, where $\Delta V$ is the shift in the knee for a temperature change $\Delta T$. Also Equation (65) becomes

$$J_o = A T^2 \exp\left[-e(\phi_{oc} + \alpha T)/kT\right]$$
$$= A T^2 \exp(-e\alpha/k) \exp(-e\phi_{oc}/kT) \qquad (73)$$

assuming other complications such as reflection are negligible in comparison with the temperature effect. Thus, $\phi_r = \phi_{oc}$, and the temperature coefficient of the work function $\alpha$ may be obtained from

$$A_r = A \exp(-\alpha/k) \qquad (74)$$

Field Emission Retarding Potential Method. - A field emission retarding potential method for measuring work functions has been developed recently by Holscher.[74] It has been shown theoretically by Young[75] and verified experimentally by Young and Müller[76] that in field emission electrons are emitted with energies near the Fermi energy of the cathode with a total energy spread of only a few tenths of an electron volt. In an experimental tube consisting of a field emission cathode, an accelerating electrode, and a collector, the potential energy diagram for the system

may be represented by the graph shown in Figure 32. It may be seen from this figure that the threshold for collection of electrons emitted from the Fermi level will be just the work function of the collector. If electrons were emitted solely from the Fermi level, the collected current would depend upon the collector potential as shown in Curve(a) in Figure 33. Since, however, this is not the case, the collected current will follow Curve(b) in Figure 33.

Of all the methods of determining work function, this method appears to be the best. In the first place, it permits an absolute measurement of work function. And, because the electrons are emitted from the Fermi level with a relatively small spread in energy, there is little uncertainty associated with the experimental results.

A critical consideration in the design of a satisfactory field emission retarding potential analyzer is that of ensuring that the collected electrons arrive normal to the collector surface, because whether or not an electron with a given energy is collected depends strongly upon the momentum of the electron normal to the surface. When this condition is not fulfilled, the collected current curve will be spread over a wider retarding potential range as represented by Curve (c) in Figure 33 and, consequently, a loss in precision of the measured work function will result. This requires that special attention be given to the alignment of the electrodes in the tube as well as to making certain that the collector surface is smooth. An experimental tube similar to that used by Holscher is shown in Figure 34.

Capacitor Method. - The contact potential difference between two metals connected electrically is just equal to the difference in their respective work functions. The contact potential difference arises from the transfer of electrons from the metal of lowest work function to the second metal until their Fermi levels line up as illustrated in Figure 35. If the two metals are arranged as the two plates of a capacitor, then in

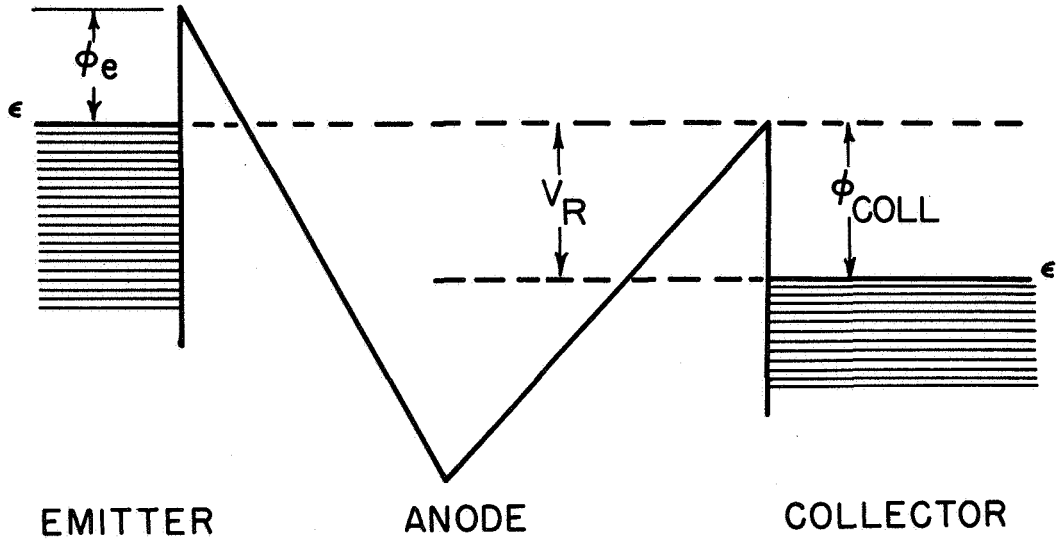


Figure 32. Potential energy diagram for field emission retarding potential method showing that the threshold potential for collection of electrons is equal to the work function of the collector.

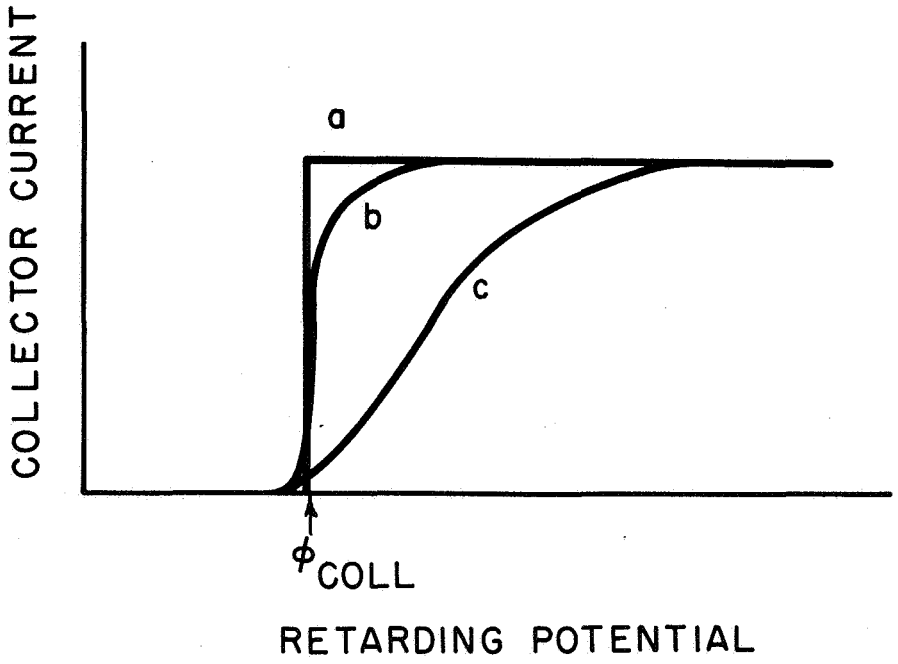


Figure 33. Retarding potential curves for (a) electrons emitted entirely from fermi level, (b) for real case of electrons emitted at 77° K with a spread of energy and a small thermal "tail" to left of curve (a) at threshold, and (c) electrons not collected with normal incidence.

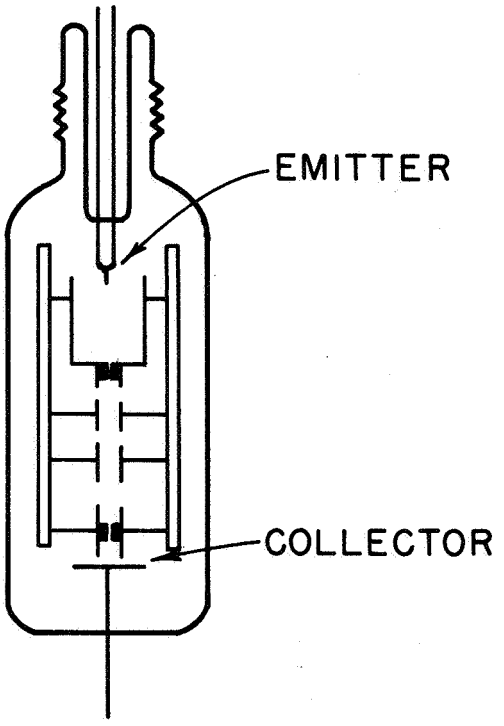


Figure 34. Field emission retarding potential tube similar to that used by Holscher.

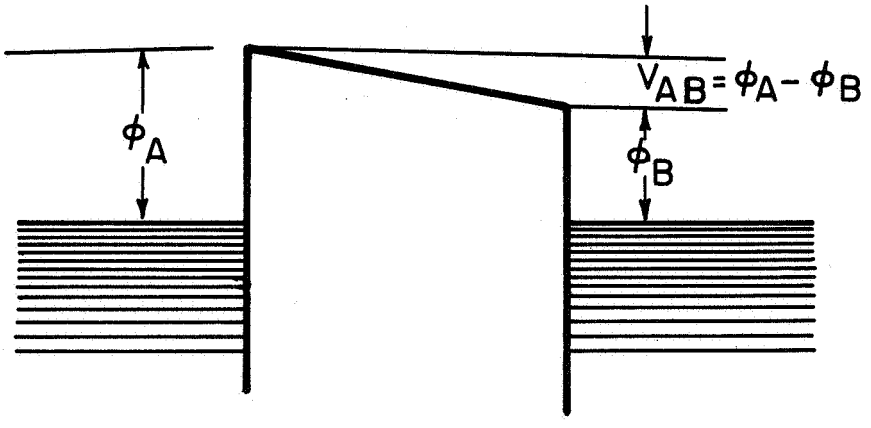


Figure 35. Potential energy diagram illustrating the relation of the contact potential difference $V_{AB}$ to the work functions of two dissimilar metals A and B.

the absence of an applied emf an electric field exists in the region between the plates by the application of a compensating potential, the field between the plates can be reduced to zero. In other words, the applied potential necessary to reduce the electric field between the plates to zero is just equal to the contact potential difference.

Experimentally, one of the plates of the capacitor is used as a reference electrode of known work function and then the work function of the second plate is determined by measuring the applied potential required to nullify the field between the plates. The actural zero field condition may be determined in two ways.[65] The first utilizes the fact that an alternating current will flow in an external circuit connecting the two plates of a vibrating capacitor. When the electric field between the plates is reduced to zero by the applied potential, the ac current likewise reduces to zero. In one such system, the experimental tube was shaped like a tuning fork with the reference electrode attached to one leg of the fork and adjacent to a fixed electrode, whose work function was to be determined. The tuning fork, and hence the reference electrode, was made to vibrate by means of an electromagnet coupled to the second leg of the tuning fork.

The second method for determining when the electric field between the plates is zero is by measuring directly the tendency for charge to flow as a result of changing the work function of one of the surfaces such as might occur during adsorption. In this static method, the tendency for charge to flow through the external circuit is detected electronically and used to very quickly establish the correct value for the compensating potential.

# 7 - MEASUREMENT OF THE BINDING ENERGY

## Introduction

An important contribution will be made toward an understanding of surface-adsorbate interactions when it is possible to determine the shape of the potential energy curve for an adsorbed molecule. Except for a few specialized systems, it has not yet been possible to theoretically compute the potential energy for a bound molecule with any degree of accuracy. In general, the quantum mechanical solution of the bonding forces is a difficult problem of which various aspects have been discussed in Volume II of this report.

Unfortunately, the determination of potential energy curves by experimental means is no less difficult and, except for a few scattered examples, the adsorbent-adsorbate potentials continue to be uncertain. In spite of the difficulty of measuring the potential energy for a bound molecule, it is possible to measure adsorption and desorption energies, which are quantities closely related to the potential energy curve, as demonstrated in Figure 36.

A distinction is made between the heat of adsorption and the heat of desorption for reasons best explained by the hypothetical potential energy curve shown in Figure 37 in which two overlapping binding states are shown. It is possible for a molecule to exist in one or the other of the two states separated by a potential energy hump. In the case of the particular surface-adsorbated system depicted in Figure 37, the heat of adsorption for the tightly bound state is seen to be q whereas the heat of desorption is $E_a$. Here, the heats of adsorption and desorption are related by

$$E' = E_a = q + \epsilon$$

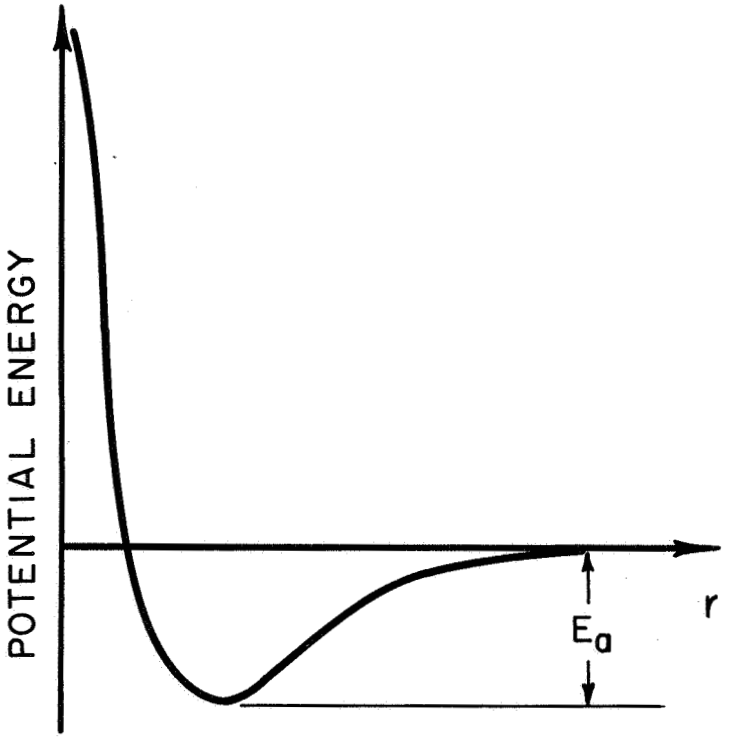


Figure 36. Potential energy curve for an adsorbed atom on a surface. The quantity $E_a$ is the binding energy identical, in this case, to the heat of adsorption and the activation energy of desorption.

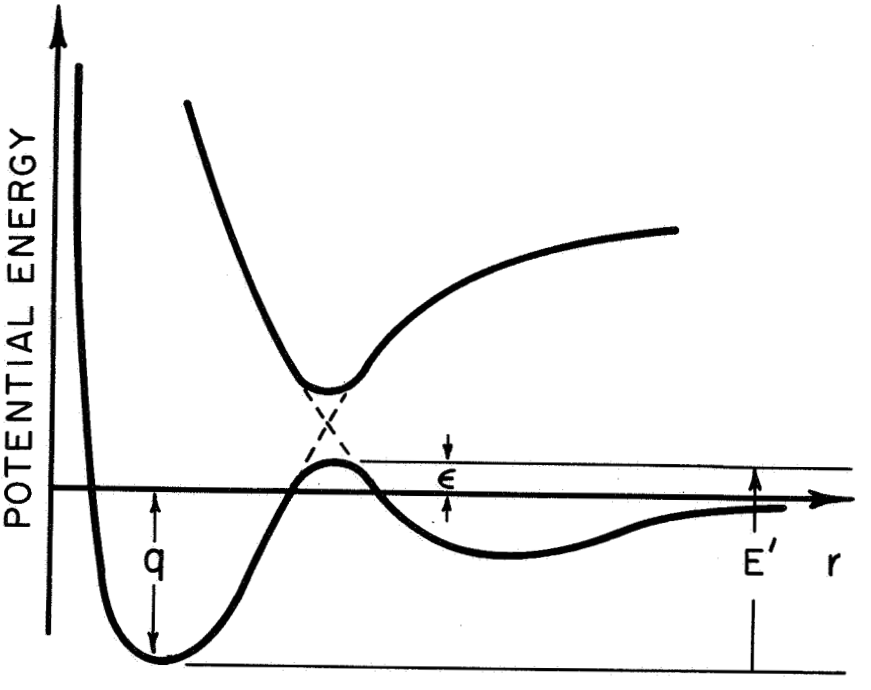


Figure 37. Overlapping potential curves for atom bound to a surface, indicating that in the tightly bound state the heat of adsorption q and the activation energy of desorption E′.

where $\epsilon$ is the activation energy for adsorption into the tightly bound state.

Since chemisorption is usually observed to occur without an energy of activation, the distinction between the two heats is unnecessary. However, a word of caution is needed when the mechanisms of adsorption and desorption are different as, for example, in the adsorption of diatomic molecules such as oxygen which dissociate upon adsorption.[65] Here the desorption of atoms results with an energy different from the heat evolved during adsorption.

## Experimental Methods

In general, there are three basic methods of measuring binding energies--they may be determined from adsorption isotherms, calorimetrically, or from desorption rates.[65] Although the first method is most common in the study of physical adsorption, there are examples in which chemisorption has been investigated by means of isotherms. Under the equilibrium conditions required of thermodynamic measurements, isothermal data yield heats of adsorption. Heats of adsorption determined from isothermal data depend strongly upon a thermodynamic interpretation of the data and, therefore, care must be exercised in formulating the thermodynamic relationships.[77] Calorimetric heats of adsorption may be measured either isothermally or under adiabatic conditions. Strictly speaking, the activation energy for desorption is measured by rate processes such as flashfilament desorption experiments.

## Isothermal Heats of Adsorption

If the surface coverage can be expressed as a function of temperature and pressure, say $\sigma = \sigma(p, T)$, then it is possible to graph $\sigma$ vs pressure at constant temperature (Figure 38-a). The heat of adsorption may be derived from a proper analysis of these adsorption isotherms.

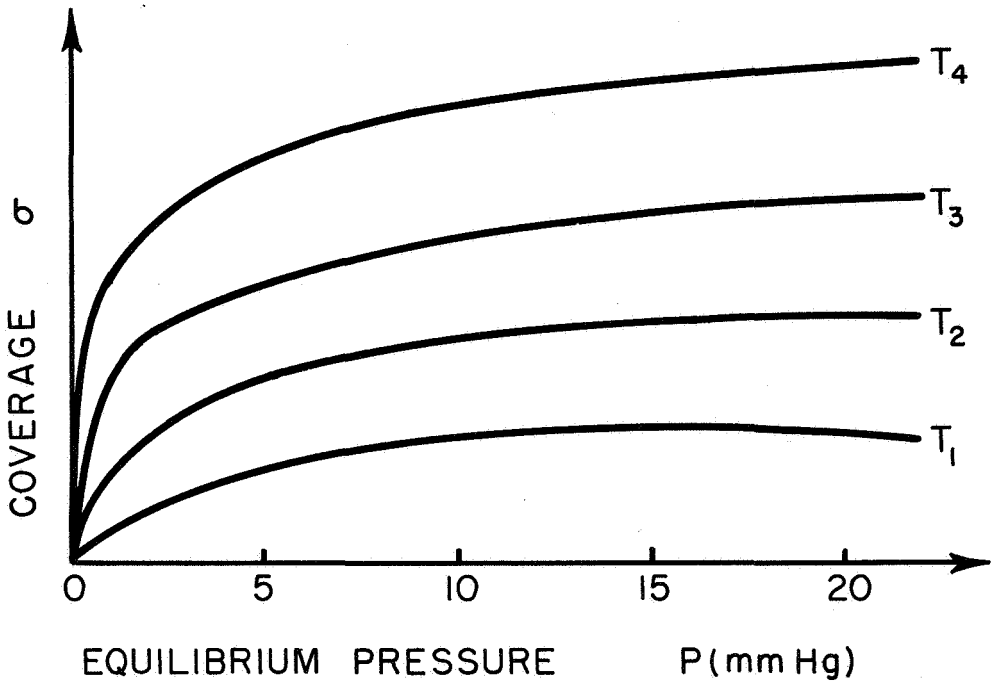


Figure 38a. Adsorption isotherms typical of gases adsorbed on metal surfaces.

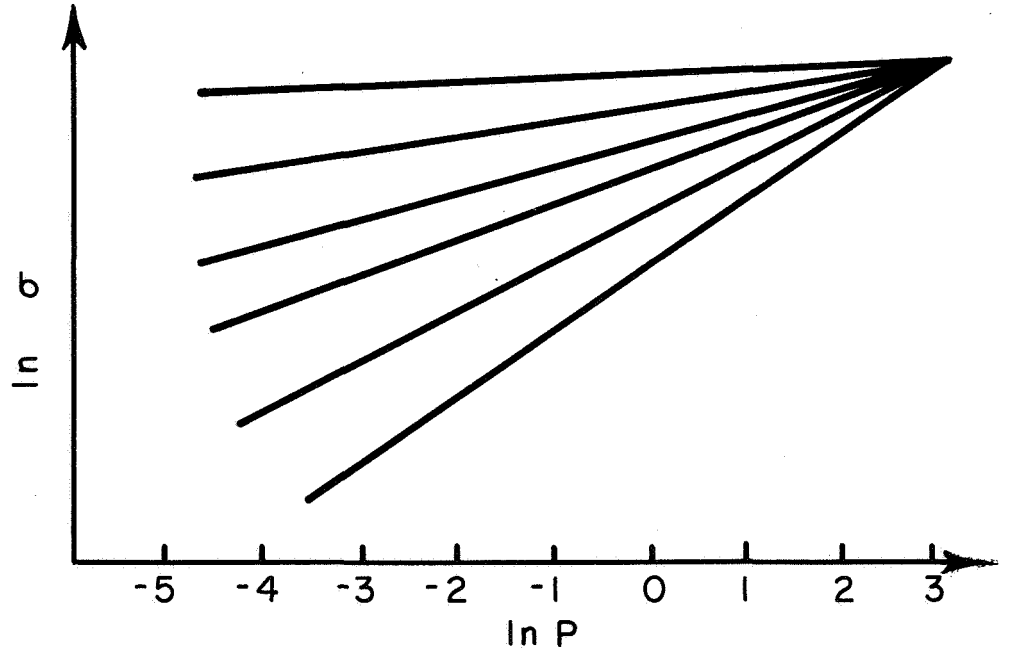


Figure 38b. Log-log adsorption isotherms for a typical gas-metal system.

There is a certain amount of ambiguity when it comes to defining the correct thermodynamic system for the analysis of adsorption.[77] The simplest choice is to regard the adsorbed gas as a single component system in equilibrium with the unadsorbed gas. Depending upon whether one chooses the spreading pressure $\pi$ or the area A as one of the independent variables, one is led to integral or differential heats and entropies of adsorption.

At constant coverage the isoteric heat of adsortpion $q_{iso}$ is given by

$$q_{iso} = RT^2 \left(\partial \ln p/\partial T\right)_{\sigma} \tag{80}$$

It can be shown that $q_{iso}$ is related to the differential heat of adsorption $q_d$ as follows

$$q_d = q_{iso} - RT$$

Since in general RT is small the two heats are nearly identical.

Another heat of adsorption which is an integral or equilibrium heat of adsorption is often desired and is given by

$$\Delta H = RT^2 \left(\partial \ln p/\partial T\right)_{\pi} \tag{81}$$

The value of this heat lies in its direct application to statistical mechanical expressions of adsorption. Unfortunately, the measurement of $\pi$ as a function of pressure is impractical since it requires the use of a "surface piston" which delivers an amount of heat $\pi dA$ to the surroundings during the adsorption of $dn_a$ moles of gas. Nevertheless, $\pi$ can be determined from adsorption isotherms through the Gibbs equation:

$$\pi = RT \int_0^p \frac{n_a}{A} \, d(\ln p), \quad T = \text{const.} \tag{82}$$

It is important to note that $\Delta H$ is related to $q_{iso}$ by the following expression:

$$\Delta H = q_{iso} - \frac{TA}{n_a} \left(\frac{\partial \pi}{\partial T}\right)_{p,\sigma} \tag{83}$$

Isotherms may be determined experimentally be measuring the volume or weight of gas adsorbed. It should be noted that in these measurements, knowledge of the actual surface coverage $\sigma$ is <u>not</u> required provided the area of the adsorbent remains constant.

Volumetric measurements have been made for both films and filaments.[65] A typical evaporated film is shown schematically in Figure 39. A known amount of gas is admitted to reservoir $R_2$ and a small amount of adsorbate is transferred from $R_1$ to $R_2$ by first trapping the gas in the small dead volume between valves $V_1$ and $V_2$. Similarly, a fraction of the gas in $R_2$ is admitted to the evaporation vessel and allowed to adsorb on a freshly deposited film. The pressure difference between the case of no film present and the case with a film is related to the volume of gas adsorbed. Plotting this quantity vs the equilibrium pressure at constant temperature yields the desired isotherm. With a system such as the one depicted in Figure 39, measurements are possible over a pressure range of several magnitudes.

Quantitative measurement of the weight of gas adsorbed relies directly upon the use of a very sensitive ultra-high vacuum micro-balance. Balances have been constructed with sensitivities of the order of $0.05 \times 10^{-6}$ g, which allow measurements of adsorption on surfaces as small as 10 $cm^2$.

## Calorimetric Heats of Adsorption

The energy released during adsorption may be measured calorimetrically in two ways, isothermally and adiabatically. In the former, the heat liberated is adsorbed in a liquid or a solid undergoing an isothermal

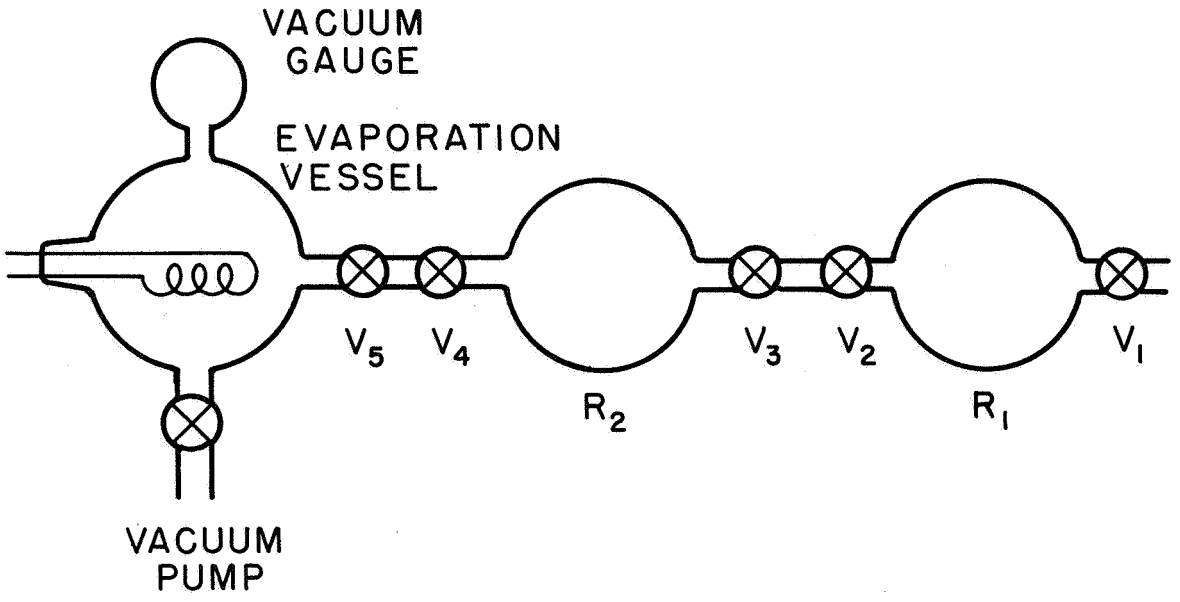


Figure 39. Apparatus for measuring isothermal heat of absorption.

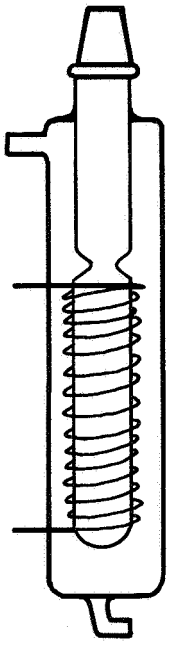

Figure 40. Calorimeter used for measuring heats of adsorption on evaporated films.

change. The total heat of adsorption is then proportional to the volume change in the surrounding substance. In many cases the amount of substance converted from one phase to another due to the heat evolved is too small to be measurable, so that isothermal methods are inadequate. This is especially true in experiments in which fractions of a monolayer are adsorbed or in which the sample is small as, for example, a ribbon filament. Under these conditions, adiabatic methods may be used to a decided advantage.

In adiabatic measurements the surface being investigated is thermally isolated so that there is no heat exchanged between the surface and its surroundings during adsorption. Actually, this is an idealization, never actually realized in practice, but by applying the appropriate corrections, errors due to heat loss may be reduced to a minimum.[78] Basically, the heat of adsorption is obtained from an expression of the form

$$q_a = C \left(\frac{\partial T}{\partial n_a}\right)_{\text{adiabatic}} \tag{84}$$

where C is the total heat capacity of the calorimeter as well as adsorbed and unadsorbed gases.

A calorimeter which appears to be quite successful in the determination of heats of adsorption of evaporated films is shown is Figure 40.[78,65] The metal film is evaporated on the inner walls of a very thin-walled glass tube surrounded by a jacket. The walls of the tube were thinned to a final thickness of 0.3 mm by etching in an HF solution. Water is passed through the jacket during evaporation in order to prevent the walls of the calorimeter from collapsing due to thermal heating, and it is evacuated for thermal isolation during adsorption. Temperature changes were detected by means of a platinum resistance thermometer wound about the calorimeter. The sensitivity of one such instrument, in which readings were taken from a ballistic galvanometer was reported to be roughly $3.4 \times 10^{-2}$ meter/ degree.

Determination of the heat capacity was carried out using a known amount of heat generated when current was passed through a film deposited on the inside of the calorimeter.

Although the most frequent applications of calorimetric measurements are to investigations of evaporated films, it is possible to determine heats calorimetrically for adsorption on ribbon filaments.

Through the use of rather sophisticated electronics, Kisliuk [79] was able to record changes in temperature occuring during the adsorption of nitrogen on a tungsten ribbon filament. Temperature changes of the ribbon (total area was 4 $cm^2$) were measured by an ac bridge operated at 450 cycles/sec with a minimum observable temperature change of $2 \times 10^{-4}\,^{o}C$. The number adsorbed could be determined by flashing the filament and noting the corresponding pressure increase.

## Rate Determination

The rate at which an adsorbed species evaporates from a surface is found to depend very strongly upon the binding energy of the species. Thus, measurements involving the rate of desorption offer a sensitive means of determining binding energy, which accounts, in part, for the fact that rate measurements are the most common method for determining binding energies of chemisorption. There are variations in the experimental procedures for obtaining these binding energies, and, although they all depend upon the assumption that the desorption obeys an Arrhenius equation of the form

$$\tau = \tau_o \exp\left[E/kT\right], \tag{85}$$

each method has been treated separately in the following discussion in order to emphasize their differences. The four major techniques are referred to as the flash filament, the Langmuir diode, the porous plug and the pulsed beam techniques.

## Flash Filament Technique

This technique has been discussed in detail in an earlier section and essentially consists of observing the rate of desorption of an adsorbate from a filament surface that is heated in a controlled manner. The shape of the pressure vs time curve is significant and may be interpreted in terms of the heat of adsorption.

## Langmuir Diode

The diode method of measuring heats of desorption of ions was first used by Taylor and Langmuir[80] and consists of a straight wire filament placed axially within a guarded ion collector. Adsorbate vapor is allowed to fill the otherwise evacuated cell to some desired pressure and after a monolayer of the vapor has adsorbed, the filament is flashed to some prescribed temperature and the ions thus formed are collected. The decay in ion current is assumed to follow the law

$$I^+ = I_o^+ \exp\left[-t/\tau\right] \tag{86}$$

and by measuring $\tau$ at various temperatures, the binding energy may be found from Equation (85).

## Porous Plug

The most recent of all the methods outlined here, the porous plug technique appears to have received only limited application. Basically, the experiment consists of a hollow cylindrical cavity, which may be heated, with one end enclosed by a sintered porous metal plug. The cavity is filled with the adsorbate capable of being surface ionized and allowed to diffuse through the porous plug which, upon reaching the outer surface, is thermally desorbed. As used by Husmann[81] (Figure 41), a

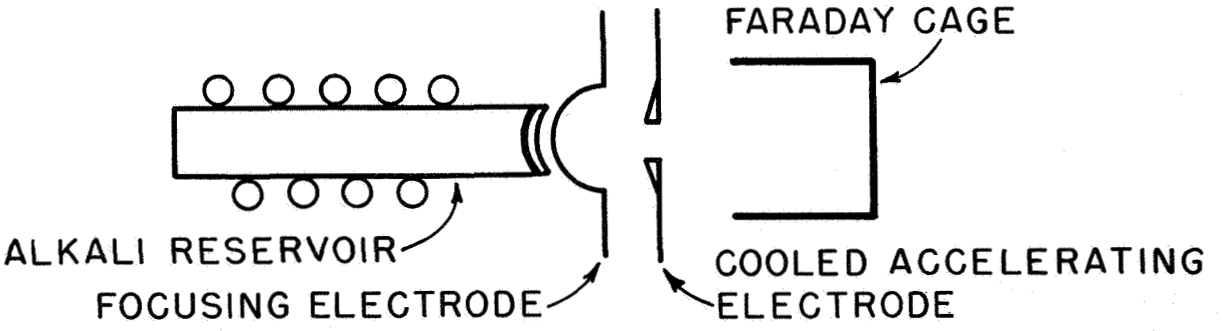


Figure 41. Porous plug system used by Husmann for determining the desorption energy of alkali-ions.

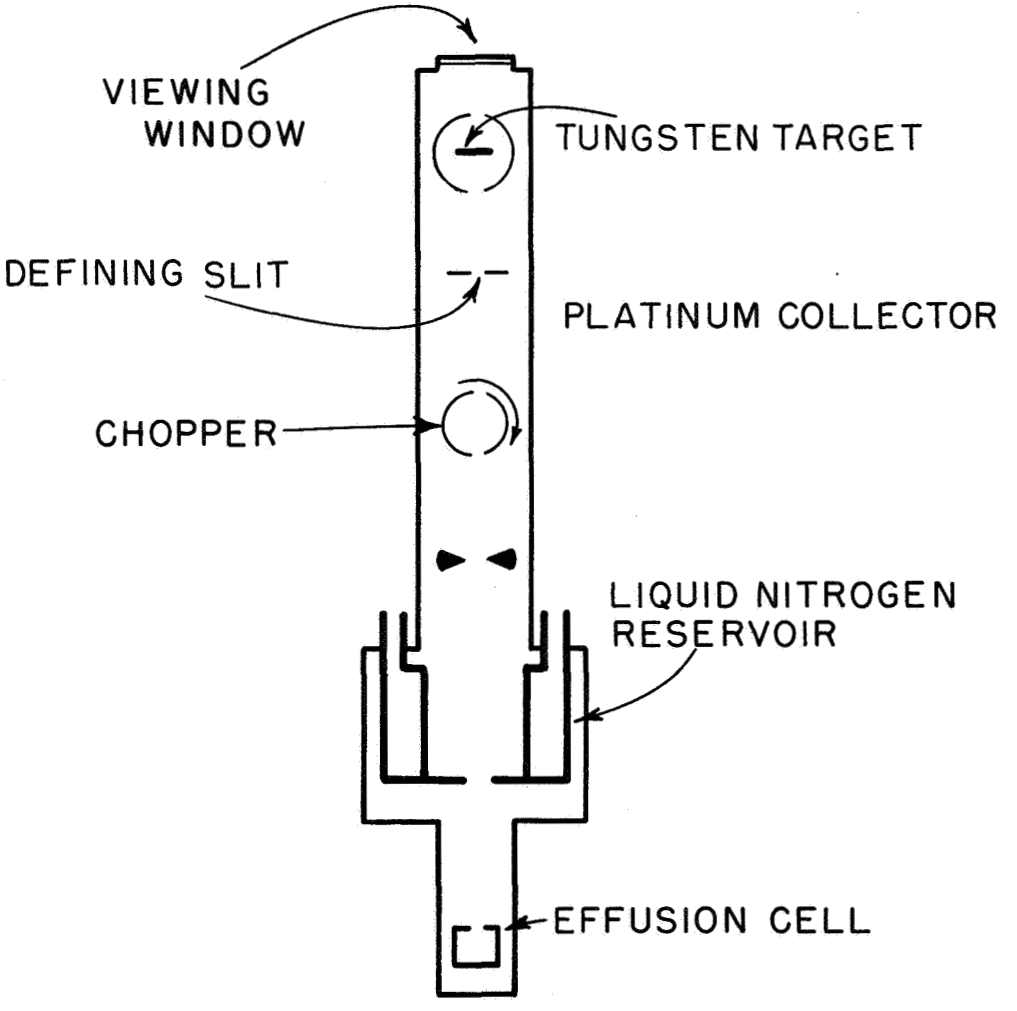


Figure 42. Schematic representation of pulsed beam apparatus used by Scheer and Fine to determine ion desorption energies.

biased control electrode prevented alkali ions from leaving the surface until an equilibrium concentration had built up from diffusion. When equilibrium had been established, the control electrode polarity was reversed, drawing the positive ions away from the surface so that they could be collected at a Faraday collector. The decay in the ion current was observed to be exponential and was assumed to follow Equation (86). Measurement of $\tau$ for a number of different temperatures permitted one to determine the heat of desorption from Equation (85).

## Pulsed Beam Technique

If a beam of atoms or ions is allowed to fall incident upon a heated surface (See Figure 42), a certain number of these particles are desorbed at a rate which depends upon the binding energy and temperature. Now, if the beam is pulsed in the form of square pulse, the decay of the desorbed pulse will look something like the curve (b) in Figure 43. The decay obeys Equation (86) and, again, measurements at different temperatures allow one to determine the heat of desorption from Equation (85). This method has been used extensively by Scheer and Fine[82] to determine the heats of desorption for various alkali ions.

## Field Emission

### Field Electron Microscopy

Field electron microscopy has been used rather extensively to determine the binding energy of an adsorbate. The procedures used have been discussed in some detail in the earlier section on field emission microscopy. In short, field electron microscopy permits one to determine the rate of coverage change from the rate of change of work function as a function of heating temperature, and from this, one is able to compute the heat of adsorption.

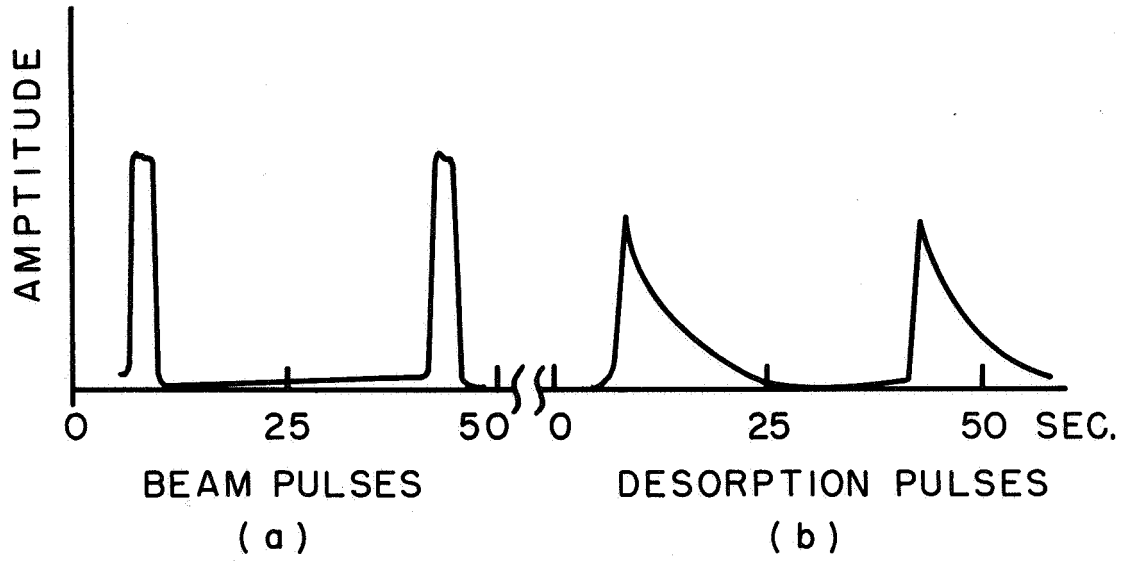


Figure 43. Representative oscillographs comparing the beam pulse on the left and the desorbed pulse on the right. The amplitudes in each case are not in the same units.

# 8 - SURFACE COVERAGE

The surface coverage is an important parameter in adsorption phenomena and, because of the nature of most real surfaces, is often difficult to ascertain. In order to establish an absolute adsorbate density, the surface area of the substrate must be established. As it is now well-known that equilibrium shapes of macroscopic surfaces often are not smooth and planar, the surface roughness factor must be critically examined before the true surface area can be established. For surfaces with extremely large surface-to-volume ratios, such as field emission tips, the dominant surface tension forces assure a nearly atomically smooth surface. Unless, otherwise specified, adsorbate surface density must be obtained indirectly by assuming a surface roughness factor or a monolayer coverage density. A variety of methods, including volumetric and gravimetric measurements, can be employed to obtain the total amounts adsorbed. Flash filament methods establish total amounts adsorbed by noting the pressure change and thereby the amount adsorbed on flashing a filament. Atomic or molecular beams of predetermined flux density impinging on a surface constitutes another method of determining the amount adsorbed provided sticking coefficients are known. Most of these methods can also be used to establish relative coverage.

Upon establishing work function-coverage relationships, the measurement of work function can be employed to establish adsorbate coverage. When adsorbate coverages are measured relative to monolayer coverage, it is important to establish an unambiguous definition of the monolayer coverage. This is not only difficult theoretically but also practically, especially when polycrystalline surfaces are employed.

## SECTION B-COMPILATION OF EXPERIMENTAL DATA

In this section, we summarize the pertinent adsorbate-substrate parameter, eg, energies, activation energies for diffusion, work function changes due to adsorption and adsorbate density, for a variety of metal substrates. Some quantitative information on dipole moments and sticking coefficients is also given. The philosophy of data selection has been discussed and adhered to in this compilation. Obviously, in reviewing such a large body of data some important results will have inadvertently been omitted.

The quantitative data have been summarized and categorized alphabetically according to substrate. For each substrate, the adsorbates have been categorized alphabetically. Cross-tabulation of the data according to experimental parameters have been given at the end of this section.

Reference to the experimental methods used is given in the text by the set of initials following the author's name and the date. The following Table of Techniques gives the techniques to which the initials apply. Most of these techniques have been described in Section A. The bibliography of authors referenced in Section B is presented at the end of the section.

### TABLE OF TECHNIQUES

CP - Contact Potential refers to any one of a variety of techniques in which the difference of potential between a reference electrode and an electrode of unknown work function is measured.

EID - Electron Impact Desorption is discussed in detail in Section A and refers to desorption of atoms from a surface by electron bombardment.

FD - Field Desorption refers to techniques involving desorption due to high fields at the surface of a field emitter tip.

FEM - Field Electron Microscopy refers to tunneling of electrons through a thin potential barrier surrounding a needle-shaped tip and subsequent radial expansion of the electron beam to a phosphor screen. Effects of adsorbates on the potential barrier may be studied.

FF - Flash Filament refers to a variety of techniques discussed in Section A where experimental parameters are measured from the kinetics and thermodynamics of interaction of a gas with a macroscopic surface area.

FIM - Field Ion Microscopy is a technique where ions which come within a high field region close to a sharp tip are ionized and travel radially outward to a phosphor screen where they form a pattern which specifies positions of atoms of the tip.

LEED - Low Energy Electron Diffraction refers to the bombardment of a single crystal surface with low energy electrons. Owing to their wave nature, the electrons are diffracted as they interact with the lattice and produce a regular array of spots on a screen behind the source. The array is altered by the presence of adsorbates and gives information on the arrangement of adsorbates on single crystal planes.

LD - Langmuir Diode refers to a technique used for measuring alkali desorption rates by intercepting a fraction of desorbing species and ionizing them on a hot tungsten filament. The rate of neutral or ionic desorption can be determined by application of appropriate potentials.

MS - Techniques where a mass spectrometer is employed to analyze desorption products.

PB - Pulsed Beam is a method of determining adsorption lifetimes on a heated surface by use of a pulsed beam of adsorbate and observing the decay of adsorbate ion currents between pulses.

PP - a heated porous plug of metal is used to surface ionize the adsorbate.

RT - Radiotracer Techniques refers to the use of radioactive isotopes of adsorbates to determine surface concentrations.

TE - Thermionic Emission refers to a general body of techniques where experimental parameters are determined from thermionically measured work function variations from a heated substrate.

TFC - Thin Film Calorimetry refers to a technique in which gas is adsorbed onto a thin film of metal and the actual temperature change of the film due to adsorbate-substrate interaction is measured.

TFCP - Thin Film Contact Potential refers to surface potential measurements applied to thin films.

## EXPERIMENTAL RESULTS

### ALUMINUM

Oxygen. - An integral heat of adsorption of 9.2 eV was measured for oxygen on aluminum thin films. (Brennan, et al, 1960, TFC). On exposure to dry oxygen, the work function of aluminum was observed to decrease with increasing fractional monolayer coverage reaching a minimum value about 0.05 eV below the fresh surface value at monolayer coverage before increasing with further oxygen exposure. This unusual insensitivity of the work function to oxygen coverage was explained on the

basis of a two-site chemi-sorption model involving dissociation of the $O_2$ on adjoining sites and a place exchange of one of the oxygen atoms with an underlying aluminum atom (Huber and Kirk, 1966, CP). Employing FEM techniques, the first effect of exposure to $O_2$ was a decrease in emission, most notably on the vicinals of the cube face. The planes least affected by oxygen exposure were the most closely-packed (111) planes. The oxide exhibited no regular structure itself, nor did it seem to form a cohesive film in the earlier stages of oxidation. In later stages, it was sometimes noted that the patterns became less irregular, almost as if a cohesive and smooth film were forming (Melmed and Gomer, 1961).

Water and Oxygen. - Water vapor lowers the work function of both the fresh surface and an oxygen exposed surface about 1 eV. This is consistent with the polar nature of water, assuming either $H_2O$ or OH groups chemisorbed on the metal oxide surface with the hydrogen outward. Microbalance and work function data indicate that water initially reacts with a fresh metal surface to produce a monolayer of oxide before forming the hydrogen outward dipole layer (Huber and Kirk, 1966, CP).

## BERYLLIUM

Cesium. - The vacuum thermionic work function for polycrystalline beryllium was 3.67 eV (Wilson, 1966a, LD). Adsorption of cesium yielded a work function of 1.94 eV with no apparent minimum (Wilson, 1966b, LD).

## CHROMIUM

Carbon Dioxide. - The average integral heat of adsorption was given as 3.5 eV (Brennan and Hayward, 1965, TFC).

Carbon Monoxide. - The initial sticking probability was determined to be 0.2 (Haque and Farnsworth, 1964, LEED).

Cesium. - The vacuum thermionic work function for polycrystalline chromium was reported as 3.90 eV (Wilson, 1966a, LD). Adsorption of

cesium yielded a minimum work function of 1.71 eV and 1.94 eV for a saturated surface (Wilson, 1966b, LD).

Nitrogen. - An initial sticking probability of 0.03 was determined for nitrogen on chromium (Haque and Farnsworth, 1964, LEED).

Oxygen. - A maximum work function increase of 2.1 eV was determined upon adsorbing oxygen at 78°K (Quinn and Roberts, 1964, TFCP). The mean integral heat of adsorption was reported as 7.05 eV (Brennan, et al., 1960, TFC). An initial sticking probability of 0.3 was measured (Haque and Farnsworth, 1964, LEED).

## COBALT

Carbon Dioxide. - The initial heat of adsorption was given as 1.6 eV (Brennan and Hayward, 1965, TFC).

Carbon Monoxide. - The initial heat of adsorption was given as 2.0 eV (Brennan and Hayward, 1965, TFC).

Oxygen. - The initial heat of adsorption was given as 4.3 eV (Brennan et al., 1960, TFC).

## COPPER

Barium Oxide. - Adsorption of barium oxide onto a thin film of copper caused the work function to decrease from 4.3 to 2.1 eV (Ptushinskii, 1960, TFCP).

Carbon Monoxide. - Carbon monoxide adsorbed on a thin film of copper deposited at 90°K produced a work function decrease of 0.315 eV (Pritchard, 1962, TFCP).

Cesium. - The vacuum thermionic work function for polycrystalline copper was measured at 4.42 eV (Wilson, 1966a, LD). Adsorption of cesium yielded a work function of 1.64 eV and with no apparent minimum

(Wilson, 1966, LD).

Hydrogen. - Adsorption of hydrogen on copper films deposited and kept at 90°K resulted in a work function increase of 0.35 eV. The activation energy for desorption at low coverage was found to be 0.74 eV. (Pritchard, 1962, TFCP). Hydrogen adsorption caused no change in the work function on the (100) face of a copper single crystal (Lee and Farnsworth, 1965, LEED).

Nickel. - Nickel was evaporated one monolayer at a time on a clean (111) copper single crystal substrate and studied by LEED techniques. The condensed layers formed an ordered structure at 200°C with the same orientation as the substrate but with the lattice spacing of nickel. The successive monolayers grew epitaxially with respect to the preceding layer, always maintaining the lattice spacing of nickel. A maximum of 5 monolayers was evaporated. The first three layers of (111) nickel contribute essentially all of the diffracted intensity up to 250 V and the first two monolayers were similarly effective below about 150 V. One monolayer coverage produced a large change in the intensity distributions from copper (Haque and Farnsworth, 1966, LEED).

Nitrogen. - Ground state nitrogen did not adsorb on a Cu (100) surface. Adsorption of both molecular and atomic nitrogen occurred when the gas was subjected to electron impact during exposure (Lee and Farnsworth, 1965, LEED).

Oxygen. - A surface oxygen net, having oblique symmetry, was formed on the Cu (100) plane by oxygen exposures of $1 \times 10^{-5}$ torr/min at room temperature. Exposures greater than $3 \times 10^{-5}$ torr/min produced a three-dimensional structure providing a surface described by Cu (100) $2 \times 4\text{-}45^{\circ}\text{-}0$ (Lee and Farnsworth, 1965, LEED). The addition of a large single dose of oxygen to a clean copper film at 298°K caused the work function to increase by 1.46 eV (Quinn and Roberts, 1964, TFCP).

## GOLD

Carbon Monoxide. - Carbon monoxide adsorbed on a gold film at 90°K caused the work function to decrease by 0.805 eV (Pritchard, 1962, TFCP).

Hydrogen. - Hydrogen adsorbed onto a gold film deposited and kept at 90°K resulted in a work function increase of 0.193 eV (Pritchard, 1962, TFCP). It was shown that exposure of gold whiskers to $10^{-5}$ torr of $H_2$ produced no observable pattern or work function changes (Melmed and Gomer, 1961, FEM).

Mercury. - A value of 4.89 $\pm$ 0.06 eV was obtained for the minimum work function of mercury on gold (Lawson and Carter, 1966, CP). It was shown that mercury is extremely reactive toward gold, adsorbing on its surface with a high sticking coefficient, and lowering the work function of gold by about 0.5 eV. The value for the work function of gold was found to be 5.22 $\pm$ 0.05 eV. It was pointed out that several previous measurements of the work function of gold are incorrect due to the high reactivity of mercury with gold which can occur in bakeable vacuum systems utilizing mercury diffusion pumps (Huber, 1966, CP).

Oxygen. - Exposures of gold to $10^{-5}$ torr of $O_2$ produced no observable pattern changes but decreased electron emission by 40% (Melmed and Gomer, 1961, FEM).

## IRIDIUM

Acetylene, Ethane, Ethylene, and Hydrogen. - The qualitative character of field electron emission patterns indicated a rather uniform covering of the high index faces of iridium by all species studied in the temperature range 70-300°K. Hydrocarbon species, once chemisorbed, are substantially immobile at temperatures below 700°K; above 700°K an increase in electron emission, probably due to carbonization, occurs around the edges

of the (111) planes. Iridium surfaces containing adsorbed species were flash heated for controlled periods of time to controlled temperatures; characteristic changes in work function resulted which were both time and temperature dependent. These experiments indicated that hydrogen is readily desorbed from iridium above 400°K, and that a large portion of the adsorbed ethane is readily desorbed at 100°K; but a residue from adsorbed ethane is not desorbed below 1000°K. For a given heating time, curves representing work function as a function of temperature for adsorbed ethylene and acetylene showed characteristic differences below 450°K. Results were interpreted as indicating chemisorbed acetylene and chemisorbed hydrogen, desorption of chemisorbed hydrogen, dehydrogenation of chemisorbed acetylene and finally, crystallization of carbon residue (Arthur and Hansen, 1962, FEM).

Carbon Monoxide. - Two types of adsorption sites were observed in the field ion microscope when carbon monoxide was adsorbed on iridium. The adsorption sites can be distinguished by the position of the adsorbate over either one or two surface atoms. The first type was considered to be a single adsorbed atom, the second, an adsorbed molecule. Field desorption of carbon monoxide from iridium caused corrosion of the substrate which was attributed to oxygen dissociated from the molecule by electron impact desorbtion (Mulson and Müller, 1963, FIM).

Cesium. - The vacuum thermionic work function for polycrystalline iridium was measured at 5.27 eV (Wilson, 1966c, LD). Adsorption of cesium yielded a minimum work function of 1.79 eV and 1.86 eV for a saturated surface (Wilson, 1966d, LD).

Hydrogen. - An atomically bound state found for samples dosed at 300°K exhibited an initial activation energy for desorption, $E_o$ = 1.0 eV and desorbed at higher coverages according to $E(\sigma) = E_o - g\sigma$ where g is 0.6 $\pm$ 0.1 eV $(10^{15}$ molec/cm$^2)^{-1}$. The desorption spectrum for samples

dosed at 100°K contained two peaks, $\alpha$ and $\beta$. The distribution of the isotopes in the desorbed phase formed from coadsorbing $H_2$ and $D_2$ indicates that both states are atomically bound (Mimeault and Hansen, 1966, FF-MS).

Nitrogen. - Two types of adsorption sites were observed in the field ion microscope with nitrogen adsorbed on iridium similar to carbon monoxide adsorption. Field desorption of a nitrogen atom from a single site also removed the underlying iridium atom but desorption of a nitrogen molecule did not corrode the iridium substrate (Mulson and Müller, 1963, FIM).

## IRON

Carbon Dioxide. - The initial heat of adsorption of carbon dioxide was measuredat 3.0 eV (Brennan and Hayward, 1965, TFC).

Carbon Monoxide. - The initial heat of adsorption of carbon monoxide is given as 2.0 eV (Brennan and Hayward, 1965, TFC).

Cesium. - The vacuum thermionic work function of iron was measured to be 4.2 to 4.6 eV (Wilson, 1966a, LD). Adsorption of cesium yielded a minimum work function of 1.82 eV and 1.84 eV for a saturated surface (Wilson, 1966b, LD).

Nitrogen. - Nitrogen adsorbed on aniron film caused the work function to decrease by 0.27 eV up to a coverage of $1 \times 10^{15}$ mdec/cm$^2$ (Suhrmann, et al, 1963, TFCP).

Oxygen. - Successive oxygen doses resulted in a work function increase of 1.55 eV for a film at 78°K. Subsequent warming of the film to 193°K reduced the work function increase to 0.5 eV (Quinn and Roberts, 1964, TFCP). The initial heat of adsorption of oxygen was measured to be 5.9 eV (Brennan, et al, 1960, TFC).

## MANGANESE

Carbon Monoxide. - The initial heat of adsorption of carbon monoxide was measured as 3.4 eV (Brennan and Hayward, 1965, TFC).

Oxygen. - A value of 6.5 eV was measured for the initial heat of adsorption of oxygen (Brennan and Hayward, 1965, TFC).

## MOLYBDENUM

Barium. - The work function was measured thermionically by the Richardson method for three faces of single crystal molybdenum: $\phi_{110} = 5.10 \pm 0.05$ eV, $\phi_{100} = 4.40 \pm 0.05$ eV, $\phi_{111} = 4.15 \pm 0.05$ eV, using an arrangement employing both spherical and plane electrodes. In the case of a spherical specimen a lower value of 4.8 to 4.9 eV was obtained for $\phi_{110}$. Evaporation of barium on the (111) face lowered the work function to $2.3 \pm 0.1$ eV. The mean heat of adsorption of barium on the (111) face of the molybdenum crystal was determined from adsorption curves as $H_{111} = 3.90 - 4.00$ eV (Azizov, et al, 1966, FEM-TE).

Carbon Monoxide. - The initial heat of adsorption on a thin film was measured as 3.2 eV (Brennan and Hayward, 1965, TFC). $O^+$ ion yield from a fully covered surface demonstrated a maximum value of $3 \times 10^{-7}$ ions/electron at an incident energy of 100 eV for electron impact desorption (Redhead, 1964b, EID). Cross sections are given for electron impact desorption of $O^+$ from CO covered molybdenum of $3 \times 10^{-21}$ $cm^2$ for $\beta$ phase. The threshold for ionization was found at 20 eV. This suggests that the electron interaction with surface CO may not be significantly different from the gas phase electron-CO interaction. The mechansim theorized was of a CO molecule ionized to $CO^+$ which will not itself desorb. If it is raised, however, to a repulsive excited state, it may fragment and desorb an $O^+$ ion. The smaller desorption cross section for $O^+$ from $\beta$ CO is explained by its smaller distance from the surface

(Lichtman et al, 1966, EID-FF).

Cesium. - A minimum work function of 1.5 eV was determined by field electron emission techniques yielding a maximum work function change of 2.70 eV. The work function-coverage curves agree closely with existing ones measured by thermionic methods. A study of the temperature effect on work function for cesium on molybdenum showed a negative temperature coefficient of approximately $1.3 \times 10^{-4}$ eV/deg (Swanson, et al, 1964a, FEM). The activation energy for surface diffusion was measured by field electron emission techniques to $0.43 \pm 0.1$ eV (Bennette, et al, 1966, FEM). Field effects were found to be the same as for tungsten. The heat of desorption of $Cs^+$ from molybdenum was given as 1.72 eV with a pre-exponential factor $\tau_o = 12.3 \times 10^{-13}$ sec (Husmann, 1965, PP). The vacuum thermionic work function of molybdenum was measured to be 4.0 to 4.3 eV (Wilson, 1966c, LD). Adsorption of cesium yielded a minimum work function of 1.61 eV and 1.77 eV for a saturated surface. (Wilson, 1966d, LD).

Gold. - The heat of desorption was found to be $4.2 \pm 0.2$ eV and the pre-exponential factor was $0.5 \times 10^{-13}$ sec (Von Goeler and Luscher, 1963, RT).

Hydrogen. - The initial heat of adsorption is given as 1.74 eV (Cerny, et al, 1966, TFC). The sticking probability of hydrogen was found to be 0.35 for polycrystalline filaments, and a surface coverage of $8.2 \times 10^{14}$ atoms/cm$^2$ was reported at 295°K. Saturation surface coverages were independent of pressure for the range ($10^{-8}$ - $10^{-5}$ torr) studied, but strongly temperature dependent from 225 to 500°K. Adsorbed hydrogen was readily displaced by other gases. The sticking probability versus coverage is shown in Figure 44 at several temperatures (Pasternak and Wiesendanger, 1961, FF). Hydrogen is readily desorbed at ~ 900°K. CO is much more tenaciously bound than $H_2$ (Moore and Unterwald, 1964, FF).

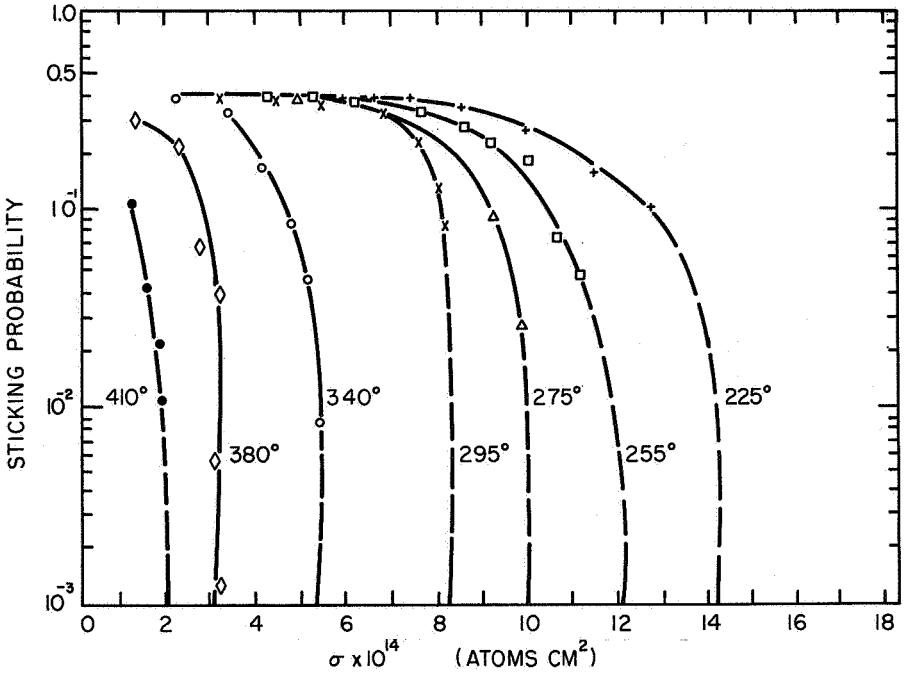


Figure 44. Sticking probability vs surface coverage for hydrogen on molybdenum. The temperatures are in degrees Kelvin. From Pasternak and Wiesendanger, J. Chem. Phys., 34, 2062 (1961).

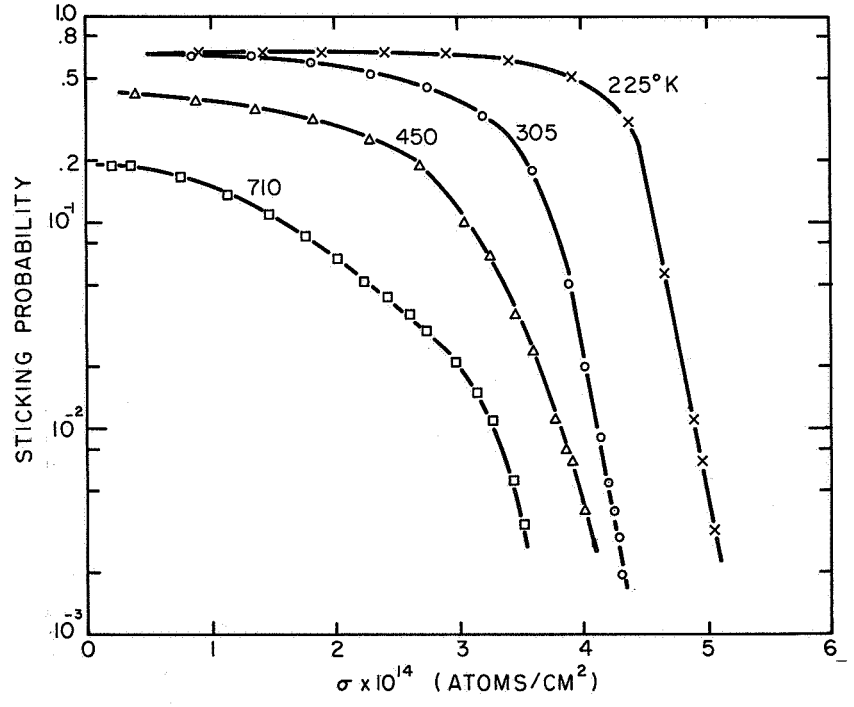


Figure 45. Sticking probability vs surface coverage for nitrogen on molybdenum. From Pasternak and Wiesendanger, J. Chem. Phys. 34, 2062 (1961).

Mercury. - The terminal coverage heat of desorption was measured to be 1.82 $\pm$ 0.15 eV with a pre-exponential factor of $1.6 \times 10^{14}$ sec. Increasing coverage caused the work function to increase by 0.40 eV at $\theta \sim 0.4$ to a maximum of 4.6 eV, then decrease (Swanson, 1967, FEM).

Nickel. - Nickel was found to adsorb "coherently" on molybdenum and preferentially on the (111) planes of the substrate. For coverages of about 1/5 of a monolayer, the activation energy of surface migration was measured at 1.48 $\pm$ 0.06 eV. The desorption energy measured was 2.10 $\pm$ 0.05 eV and did not vary with degree of coverage. Multilayers of nickel were also investigated (McIrvine and Bradley, 1957, FEM).

Nitrogen. - In the adsorption of nitrogen on molybdenum polycrystalline filaments, the saturation surface coverage decreased about 30% as the temperature was raised from 222°K to 710°K, and the initial sticking probability decreased from 0.7 to 0.2 as the higher temperature was approached. At room temperature, the initial sticking probability of 0.7 was found and a surface coverage of $4.4 \times 10^{14}$ at / $cm^2$ measured. A plot of sticking probabilities versus surface coverage is shown in Figure 45 at various temperatures for nitrogen on molybdenum filaments (Pasternak and Wiesendanger, 1961, FF). The initial sticking probability for nitrogen on molybdenum films was found to be 0.6 at room temperature, but the shape of the sticking probability versus coverage curve did not agree with those obtained from flash filament work (Pasternak, et al, 1966a, TF).

Oxygen. - The maximum work function change for oxygen adsorbed on molybdenum films was 1.65 eV. No distinction between values of the work function obtained at 77°K and 298°K could be made. Addition of hydrogen to an oxidized film at 25°K produced no change, but at about 423°K the work function decreased as hydrogen was slowly adsorbed (Quinn and Roberts, 1964, TFCP). Flash filament studies showed two desorption peaks. These could be resolved by heating the filament to 1300°K in about 1 sec. The peaks occurred in the ranges 300-600°K and 800-1000°K

(Gasser and Schuftan, 1963, FF). The initial heat of adsorption was measured as 7.5 eV (Brennan, et al, 1960, TFC). Observations by Redhead show that oxygen is adsorbed in two states at room temperature from electron impact desorption with approximate heats of adsorption of 2.6 and 4.8 eV. Neutral desorption cross sections were found to be $7.8 \times 10^{-22}$ $cm^2$ and $1.3 \times 10^{-18}$ $cm^2$ respectively for the two states and ion desorption cross sections were $1.4 \times 10^{-23}$ $cm^2$ and $2.6 \times 10^{20}$ $cm^2$ respectively at an electron energy of 100 eV. The ion formation threshold energy was found to be 17.6 $\pm$ 0.2 eV. (Redhead, 1964a, EID). The LEED structures observed as oxygen adsorbs on Mo (110) were found to be similar to those for W (110) (Hass and Jackson, 1966, LEED).

Silver. - The desorption energy of silver was measured as 1.9 $\pm$ 0.3 eV (Von Goeler and Peacock, 1963, RT).

## NICKEL

Barium. - Adsorption of barium resulted in a maximum work function decrease of 2.2 eV. Barium oxide adsorption decreased the work function 2.9 eV (Ptushinskii, 1961, TFCP).

Carbon Monoxide. - Carbon monoxide was found to adsorb on nickel in three states with desorption energies at 0.15, 0.28, and 2.28 eV. The differential activation entropies calculated from the experimental data for these states were -44.5, -42.2 and 8.4 cal/mole-deg (Degras, 1965, FF). The initial heat of adsorption has been measured as 1.83 eV (Brennan and Hayward, 1965, TFC). Exposure of a clean (110) nickel surface to CO pressures in the range $10^{-6}$ to $10^{-7}$ torr does not yield any new diffraction orders. However, the intensity of the diffraction beam changes markedly. The photoelectric work function increased by 0.3 eV (Park and Farnsworth, 1964b, LEED).

Cesium. - A layer of cesium resulted in a work function decrease of 2.9 eV (Ptushinskii, 1961, TFCP). The vacuum thermionic work

function of nickel was measured to be 4.4 to 4.86 eV (Wilson, 1966a, LD). Adsorption of cesium yielded a work function minimum of 1.6 to 2.4 eV and a work function of 1.6 to 2.4 eV for a saturated surface (Wilson, 1966b, LD). Field electron emission techniques yielded values of 3.1 $\pm$ 0.2 eV for desorption of cesium atoms and 2.2 $\pm$ 0.2 eV for desorption of cesium ions. The work function minimum was found to be 1.38 eV resulting in a work function decrease of 3.62 eV (Bennette, C. J. et al, 1967, FEM).

Hydrogen. - It was found that boundary-free migration occurs at coverages up to $\theta \sim 1$ with an activation energy of 0.30 $\pm$ 0.04 eV by field electron emission studies. For $\theta > 1$ spreading occurs near 4°K, as with hydrogen on tungsten. The activation energy of desorption of $H_2$ from nickel was measured to be 2.0 $\pm$ 0.13 eV for $\theta \ll 0.1$ from the temperature variation of the desorption rates. The failure to observe on nickel the intermediate coverage boundary spreading found on tungsten by field emission techniques is believed to result from the fact that nickel is much more closely packed, so that all portions of the nickel surface seem "smooth" to H atoms. Evidence in favor of this argument is found in the fact that the ratio of the diffusion to adsorption activation energy is approximately unity for nickel. This ratio corresponds to that found for radial boundary diffusion on tungsten (Wortman, et al, 1957, FEM). A field dependent transformation in the adsorbed film was found between 2° and 4°K and interpreted as a shift in the equilibrium between adsorbed $H_2$ molecules and the terminal fraction of adsorbed H atoms. The implications of this result for the mechanism of $H_2$-$D_2$ exchange can be considered (Wortman, et al, 1957, FEM). An isoteric heat of adsorption of 1.2 eV was measured for hydrogen adsorbed on a (110) surface of a nickel single crystal(Germer and MacRae, 1962a, LEED). The average integral heat of adsorption was given as 0.95 eV (Brennan and Hayes, 1964, TFC).

Oxygen. - The maximum work function change on a nickel thin film was 1.4 eV for a deposit formed and held at 78°K. (Quinn and Roberts, 1964, TFC). The initial heat of adsorption of oxygen on nickel was 4.6 eV (Brennan, et al, 1960, TFC). When oxygen is adsorbed on the (110) surface of nickel at room temperature, the substrate is separated from the oxide by distinct strata representing increasing oxygen content. The atoms in these strata are regularly arranged in substitutional sites to form structures related to those of nickel until the composition NiO is reached. A similar oxidation process is observed for the (111) and (100) faces. From indirect evidence involving oxygen sorption on a surface previously covered with CO, the $Ni_3O$ structure is estimated to be at least 10 atomic layers thick (Park and Farnsworth, 1964a, LEED).

Silver. - The heat of desorption of silver from nickel was determined to be 1.6 $\pm$ 0.3 eV (Von Goeler and Peacock, 1963, RT).

## NIOBIUM

Carbon Monoxide. - There are at least two chemisorbed binding states, the weaker one being desorbed above 150°K. The field electron emission patterns resulting from heating to 600°K and above indicate a decomposition of the CO held on the surface in the more strongly bound state. Heating a CO covered surface in the region of 150°K lead to a characteristic mottling of the field electron emission pattern ascribed to surface clustering. Evidence that adsorption and desorption are irreversible was given. The work function increase due to CO adsorption was found to be 0.7 eV (Klein and Little, 1964, FEM).

Cesium. - The vacuum thermionic work function of niobium was measured to be 4.19 eV (Wilson, 1966a, LD). Adsorption of cesium yielded a work function minimum of 1.44 eV and 1.63 eV for a saturated surface. (Wilson, 1966d, LD).

Nitrogen. - Nitrogen adsorbs onto niobium with an initial sticking probability of about 0.4 at 298°K and a surface coverage of $7 \times 10^{14}$ atoms/$cm^2$. Above 400°K nitrogen diffuses into the bulk (Pasternak, 1965, FFD). The heat of desorption was determined to be 2.4 eV (Pasternak, et al, 1966b, FF).

Oxygen. - The initial heat of adsorption measured was 9.0 eV. (Brennan, et al, 1960, TFC). For a well outgassed sample, the room temperature sticking probability measured initially at 0.8 drops linearly with coverage to zero at a coverage of $6.5 \times 10^{14}$ molecules/$cm^2$. At temperatures above approximately 500°K sorption continues beyond an amount which would be equivalent to a monolayer. At high temperatures, oxidation and solution take place in a fashion which indicates two adsorption states on the surface. When the sample is heated at high temperatures, no molecular oxygen is evolved; and the oxygen is desorbed as oxide and possibly some atomic oxygen (Pasternak and Evans, 1967, FF).

## OSMIUM

Cesium. - The vacuum thermionic work function of osmium was measured to be 4.83 eV (Wilson, 1966c, LD). Adsorption of cesium resulted in a work function of 1.44 eV for a saturated surface with no apparent minimum (Wilson, 1966d, LD).

## PALLADIUM

Carbon Monoxide. - The initial heat of adsorption of carbon monoxide was found to be 1.9 eV (Brennan and Hayward, 1965, TFC).

Oxygen. - An initial heat of adsorption of 3.0 eV was measured for oxygen on palladium (Brennan, et al, 1960, TFC).

## PLATINUM

Carbon Monoxide. - The initial heat of adsorption was measured at

2.1 eV (Brennan and Hayward, 1965, TFC). Two structures form on the (100) plane of platinum corresponding to high and low coverage. The low coverage phase has a structure 1 x 3 times the Pt (10) spacing with major axes parallel to the Pt (10) directions. The high coverage phase has a structure 2 x 4 times the Pt (11) spacing with major axes parallel to the Pt (12) directions (Tucker, 1964a, LEED).

Cesium. - The vacuum thermionic work function was measured to be 5.6 to 5.8 eV (Wilson, 1966a, LD). Adsorption of cesium yielded a work function minimum of 1.59 eV and 1.66 eV for a saturated surface (Wilson, 1966b, LD).

Hydrogen. - Hydrogen chemisorption at 300°K to a maximum coverage of about 0.2 monolayer was attained at a rate corresponding to a sticking probability of 0.001. The heat of desorption was found to be 1.13 eV (Wiesendanger, 1963, FF).

Nitrogen. - No chemisorption of nitrogen occurs on platinum at 300°K and at pressures below $10^{-7}$ torr (Wiesendanger, 1963, FF).

Oxygen. - It was found that under certain circumstances heavy oxygen contamination of platinum was nearly impossible to remove, and there appeared to be a definite interaction of the oxygen with the platinum field emission tips (Melmed, 1965a, FEM). The initial heat of adsorption measured was 3.0 eV (Brennan, et al, 1960, TFC). From diffraction pattern observations, it is concluded that adsorption of oxygen on the (110) face leads to rearrangement of the top layer of platinum atoms (Tucker, 1964b, LEED).

## RHENIUM

Barium. - The heat of desorption and pre-exponential factor of $Ba^+$ are given as $4.74 \pm 0.21$ eV and $(0.6 \pm 0.4) \times 10^{-13}$ seconds respectively (Scheer and Fine, 1963a, PB).

Cesium. - The heat of desorption and pre-exponential factor of $Cs^+$ have been determined by three different techniques and are listed in the following table:

| | $\tau_o$(sec) | $E_p$(eV) | Worker |
|---|---|---|---|
| $Cs^+$ | $1.93 \times 10^{-13}$ | 1.96 | (Taylor, 1964a, LD) |
| $Cs^+$ | $11.4 \times 10^{-13}$ | 2.2 | (Husmann, 1965, PP) |
| $Cs^+$ | $(1.9 \pm 0.9) \times 10^{-13}$ | $2.04 \pm 0.04$ | (Scheer and Fine, 1963a, PB) |

The vacuum thermionic work function of rhenium was measured to be 4.96 eV (Wilson, 1966a, LD). Adsorption of cesium yielded a work function minimum of 1.51 eV and 1.56 eV for a saturated surface (Wilson, 1966d, LD). Using field emission techniques adsorption of cesium on rhenium gave a work function minimum of $1.45 \pm 0.05$ eV and a work function of $1.80 \pm 0.03$ for a saturated surface (Swanson, et al, 1964a, FEM). Swanson, et al, also determined activation energies for desorption of cesium atoms and ions and measured 3.8 eV and $2.0 \pm 0.1$ eV respectively. The activation energy of surface diffusion was measured in the range of 0.33 to 0.39 eV (Swanson, L. W., et al, 1963b, FEM).

Nitrogen. - Using a polycrystalline sample cleaned by heating to $2000^{\circ}K$, the following sticking probabilities and surface coverages were found (Scheer and McKinley, 1966, FF):

| $T^{\circ}K$ | s | $\sigma$(molec/cm$^2$) |
|---|---|---|
| 205 | 0.060 | $8 \times 10^{13}$ |
| 300 | 0.009 | $7 \times 10^{13}$ |
| 373 | 0.007 | $6 \times 10^{13}$ |

Adsorption of nitrogen on rhenium lowers the Fowler-Nordheim work function from its clean value of 4.9 eV to a value of 4.5 eV for a saturated surface in the pseudo clean configuration. Migration was not observable because it requires higher temperatures than desorption (Klein and Little, 1967, FEM).

Potassium. - The heat of desorption and pre-exponential factors of $K^+$ are given as 2.33 ± 0.03 eV and (1.0 ± 0.3) x $10^{-13}$ seconds respectively (Scheer and Fine, 1963b, PB).

Rubidium. - The heat of desorption and pre-exponential factor of $Rb^+$ were measured 2.28 ± 0.03 eV and (0.8 ± 0.3) x $10^{-13}$ seconds respectively (Scheer and Fine, 1963b, PB).

Sodium. - The heat of desorption and pre-exponential factor of $Na^+$ are given as 2.75 ± 0.03 eV and (0.2 ± 0.1) x $10^{-13}$ seconds respectively (Scheer and Fine, 1963b, PB).

Thorium. - The Richardson constants for rhenium were found to be $\phi$ = 4.85 eV, and $A_r$ = 66 A/$cm^2$-$deg^2$. As thorium is adsorbed, the work function decreases to a minimum of 3.15 eV at a coverage of 4.2 x $10^{-14}$ atoms/$cm^2$ and then rises to a constant value of 3.3 eV at a coverage of 8 x $10^{14}$ atoms/$cm^2$. A comparison with the tungsten system gives the same respective coverages. The activation energy for desorption was 8.30 ± 0.15 eV at low coverages (Anderson, et al, FF-TE).

## RHODIUM

Carbon Monoxide. - The initial heat of adsorption of 2.0 eV was measured for carbon monoxide on rhodium (Brennan and Hayward, 1965, TFC).

Hydrogen. - Hydrogen adsorption is atomic at 300°K and obeys second order kinetics with an activation energy of $E(\sigma) = E_o - g\sigma$ where $E_o$ = 0.78 eV and g = 1.0 ± 0.1 eV ($10^{15}$ molec/$cm^2$)$^{-1}$. The desorption spectrum of hydrogen desorbed from rhodium dosed at 100°K contains two peaks, $\alpha$ and $\beta$. The distribution of the isotopes in the desorbed phase formed by coadsorbing $H_2$ and $D_2$ indicate that the $\alpha$ and $\beta$ phases are both atomic (Mimeault and Hansen, 1966, FF).

Oxygen. - The initial heat of adsorption measured for oxygen was 4.45 eV (Brennan, et al, 1960, TFC).

## TANTALUM

Carbon. - Carbon, once deposited on tantalum, cannot be removed by high-temperature treatment alone as in the case of tungsten. From field electron microscopy techniques, low-carbon contamination causes (334) planes to appear as high work function areas, just as for carbon on tungsten. At temperatures in the region of 950°K, platelets, presumably TaC, form and migrate to the (111) zones of the emitter single-crystal tip. The activation energy of this surface migration process was 2.3 eV (Klein and Leder, 1963, FEM).

Carbon Monoxide. - Adsorbed carbon monoxide shows three states of binding on tantalum. The weakest of these was desorbed at temperatures above 125°K with no observable surface migration; bonding with the surface was of the van der Waals type. This is in contrast with the second state, which was desorbed above 650°K. The third state was dissociated before desorption to give the oxygen-on-tantalum field electron emission pattern. Surface migration involving the second adsorbed state occurs with an activation energy of 1.7 eV. The work function of a carbon monoxide covered tantalum surface, obtained by spreading the carbon monoxide on a shadowed tip at 40°K, was 0.8 eV greater than that of the corresponding clean tantalum. The first state of desorption yielded a value of 0.17 eV for the desorption energy which was considerably higher than the heat of vaporization of carbon monoxide, 0.06 eV, so that some interaction with the tantalum must occur (Klein and Leder, 1963, FEM). The initial heat of adsorption of carbon monoxide on tantalum measured by Brennan and Hayward was 5.85 eV (Brennan and Hayward, 1965, TFC).

Cesium. - The heat of desorption and pre-exponential factor of $Cs^+$

are given as 1.65 eV and 1.8 x $10^{-9}$ sec respectively (Husmann, 1965, PP). The minimum work function of Cs on Ta was found to be 1.6 eV (Gorbatyi and Rysbchenko, 1965, FEM). The vacuum thermionic work function of tantalum was measured to be 4.25 eV (Wilson, 1966c, LD). Adsorption of cesium resulted in a work function minimum of 1.69 eV and 1.70 eV for a saturated surface (Wilson, 1966d, LD).

Oxygen. - Brennan, et al, measured the initial heat of adsorption of oxygen on tantalum at 9.2 eV (Brennan, et al, 1960, TFC). The work function of the clean (110) plane was measured as 4.74 $\pm$ 0.02 eV, and the activation energy for oxide growth was estimated to be 0.24 $\pm$ 0.04 eV (Boggio and Farnsworth, 1964, LEED).

Potassium. - The heat of desorption and pre-exponential factor of $K^{+}$ were given as 2.05 eV and 41.6 x $10^{-13}$ seconds respectively (Husmann, 1965, PP).

Rubidium. - The heat of desorption and pre-exponential factor were given as 1.81 eV and 2.36 x $10^{-13}$ seconds respectively. (Husmann, 1965, PP).

## TITANIUM

Cesium. - The vacuum thermionic work function was measured to be 3.65 to 4.3 eV (Wilson, 1966a, LD). Adsorption of Cs yielded a minimum work function of 1.33 eV and 1.44 eV for a saturated surface (Wilson, 1966b, LD). Bennette, et al, found the maximum work function decrease for the $(10\bar{1}0)$ plane to be 2.92 eV (Bennette, et al, 1967, CP).

## TUNGSTEN

Argon. - It was found that a work function decrease of 0.80 eV occurs for a saturated monolayer when measured at 4.2°K. The work function change is most pronounced near the (100) face. Multilayer

adsorption also occurs. It appears that dipole-dipole repulsions suffice to make the first layers gaslike (Gomer, 1958b, FEM).

Adsorption of Ar on tungsten lowers the work function by 0.87 eV at 20°K. Binding to the surface is structure sensitive--it is strongest around the (100) poles, in the vicinity of the (116) and (130) planes, and weakest at the (111), as observed in field electron emission patterns. This sequence of binding energies corresponds to that calculated for different lattice sites on the assumption of dispersion forces. The lowering of the work function caused by adsorption was interpreted as a polarization of the gas atoms by the dipole layer of the metal surface; formally, the interactions at a metal resemble those of the rare gases adsorbed on ionic crystals. Interaction of polarized adatoms and the anti-parallel field applied for field electron emission increases the free energy of the adlayer, bringing about rearrangements particularly important for adsorbed argon. Observations of changes in field electron emission with temperature yield a value of 0.04 eV for the diffusion activation energy of argon over the (310) toward the (100) (Ehrlich and Hudda, 1959, FEM).

Barium. - The initial heat of adsorption was given as 3.6 eV (Moore and Allison, 1955, RT), 4.68 eV (Zingerman, et al., 1961, TE), and 4.7 eV (Gavrilyuk and Medvedev, 1963, CP-FF). Upon adsorption of barium, the work function decrease at room temperature was 2.5 eV and then increased with further coverage to a final decrease of 1.9 eV (Zingerman, et al., 1961, TE). The work function of a saturated surface of barium on tungsten was found to be 2.1 eV with no apparent minimum (Zubenko and Sokolo'skaya, 1961, FEM).

Field desorption of barium occurs at about 100 MV/cm (Muller, 1956, FEM-FD). It was found that adsorption seems to be polar but not ionic and that desorption of $Ba^+$ occurs under the conditions of field desorption experiments. If this interpretation is correct, $\alpha = 60\text{Å}$ for the polarizability of adsorbed Ba which is close to the value for the

free atom. It was found that positive fields have more effect on the activation energy and pre-exponential term of the diffusion coefficient than negative fields. While a $1/2\ \alpha\ F^2$ dependence of the activation energy is compatible with the limited data for negative fields, no simple behavior was found for positive values. The activation energy goes through a minimum of zero with increasing positive field accompanied by a drastic reduction in the pre-exponential term. Values for the zero heat of adsorption were obtained over a wide coverage interval and agree well with those of Moore and Allison (above), where overlap occurs (Utsugi and Gomer, 1962a, FEM-FD).

The electron desorption cross section for barium on tungsten was found to be $< 2 \times 10^{-22}$ cm$^2$ (Menzel and Gomer, 1964a, FEM-EID).

Barium Oxide. - Field desorption of BaO occurs as $BaO^+$ within the 80-400°K range and as $BaO^{++}$ within the 500-1000°K range. Barium is field-desorbed from W in the form of singly-charged ions over the 80-300°K and 1000-1200°K regions, and as doubly-charged ions at 300-1000°K (Naumovets, 1963, FEM-FD).

Beryllium. - The adsorption of beryllium does not affect the work function of tungsten; presumably, because it has the same work function as tungsten (Zingerman, et al, 1961, TE).

Bromine. - At low bromine coverages, the work function decreases to 4.1 $\pm$ 0.1 eV corresponding to a decrease of 0.4 eV, accompanied by a 60 times reduction in apparent field electron emitting area. This effect is ascribed to the penetration of bromine atoms below the effective surface plane. Extended exposure to bromine ($5 \times 10^{-9}$ torr) vapor produced a work function increase of 1.0 eV with respect to clean tungsten (Duell and Moss, 1965, FEM).

Calcium. - Adsorption of calcium lowered the work function by 1.9 eV at $5 \times 10^{14}$ atoms/cm$^2$ and 1.7 eV at a saturated coverage of

$8 \times 10^{14}$ atoms/cm$^2$ (Zingerman, et al, 1961, TE).

Carbon Monoxide. - Adsorption of carbon monoxide has been studied using a variety of techniques. The more recent data has employed ultra-high vacuum techniques. A summary of the data is given in the following table:

| $\Delta\phi$ (eV) | $s_{300^\circ K}$ | $\sigma \times 10^{-14}$ molec/cm$^2$ (at 300°K) | Desorption Energies (eV) | | | | Worker |
|---|---|---|---|---|---|---|---|
| | | | $\alpha$ | $\beta_1$ | $\beta_2$ | $\beta_3$ | |
| | | | | 2.3 | | | (Klein, 1959, FEM) |
| 0.85 | 0.2 | 7.4 | | | | | (Eisinger, 1957, FF) |
| | 0.49 | 9.5 | 1.26 | 2.56 | 3.02 | 3.28 | (Redhead, 1961, FF) |
| | 0.5 | 4.5 | 0.87 | | 3.26 | 4.35 | (Ehrlich, 1961b, FF) |
| | | | | 2.3 | 3.3 | 4.3 | (Ehrlich, 1962, FEM) |
| | | | 0.87 | 2.26 | 3.04 | 4.35 | (Rootsaert, et al, 1962, FEM) |
| 0.85 | 0.48 | 5.8 | 0.91 | 2.70 | | 4.00 | (Gavrilyuk and Medvedev, 1963, FF) |
| | | | 1.0 | 2.74 | 3.35 | 3.9 | (Rigby, 1964, FF) |
| | | | 1.0 | 2.6 | | | (May and Germer, 1966, LEED) |
| | 0.27 | 10.1 | | | | | (Ricca, et al, 1962, FF) |

The desorption kinetics indicate that adsorption is nondissociative and can be quite complex. At room temperature, transfer takes place between the $\alpha$ phase and the $\beta$ phase (Rigby, 1964, FF).

When $C^{12}O^{18}$ and $C^{13}O^{16}$ were adsorbed together on tungsten, rapid isotopic mixing to form $C^{12}O^{16}$ and $C^{13}O^{18}$ occurred at temperatures above 850°K. No evidence was found for dissociation of CO into mobile adsorbed C and O atoms. A four-center bimolecular exchange was postulated which involves surface bonding through both carbon and oxygen. The rate constant

for the bimolecular surface exchange reaction was $1.9 \times 10^{-10}$ exp(-30,000/RT) (Madey, et al., 1965b, FF). Room temperature studies of the surface potential variation with CO dose for the W (211) plane are explained by assuming a random occurrence of pairs and clusters (Armstrong, 1965, FF-CP). Further complexities involve the β state which is a composite of at least three states, each with different desorption energies. The $\beta_1$ state occurs on (411), (310) and (210) faces, the $\beta_2$ state occurs on (111) and other faces and the $\beta_3$ occurs on the (111) zones (Rootsaert, et al., 1962, FEM). The complexities of the system are even more pronounced at low temperatures, with the appearance of a nonreversible state called the "virgin layer". This state was found upon adsorption at low temperature (20°K) and increased the work function to 5.6 eV, indicating a negative dipole moment. The layer appeared to desorb and convert to the recognized *a* and β states upon heating above 170°K, but further readsorption of CO at 20°K did not restore the previously obtained high work function. This characteristic was interpreted by recognizing the fact that the *a* state has a positive dipole moment while the β states are characterized by negative dipole moments. After heating the "virgin layer" to 170°K, further adsorption cannot restore the initial conditions represented by the negative dipole but instead is the result of depositing more of the *a* CO over a β layer (Swanson and Gomer, 1963a, FEM-FD). The relative abundance, relative dipole moments, and absolute sticking coefficients of virgin, *a* and β CO adsorbed on tungsten have been determined by a combination of work function versus coverage measurements with step-desorption spectra and sticking coefficient measurements. The dipole ratios were $M_a/M_{virgin} = 0.68$; $M_\beta/M_{virgin} = 0.68$ for the initial, and $M_\beta/M_{virgin} = 1.10$ for the terminal portion of the β layer. The relative abundances were total β/total virgin = 0.55; (virgin converted to β)/(β from virgin conversion) = 2.1; *a*/total β = 1.2. Initial sticking coefficients are close to unity up to 700°K and decrease rapidly at coverages

(relative to the maximum amount of adsorbate retained at that temperature) of 0.6 - 0.4 (Bell and Gomer, 1966, FEM-FF). It was found that the binding modes of CO could be distinguished and confirmed by their differing electron impact desorption cross sections which were $Q_{virgin} = 3 \times 10^{-19}$ cm$^2$, $Q_{virgin\ to\ \beta} = 10^{-19}$ cm$^2$ and $Q_\alpha = 3 \times 10^{-18}$ cm$^2$ for 80 volt electrons. Evidence for thermal conversion of virgin states to both $\beta$ and $\alpha$ states was obtained. Electron bombardment also seemed to convert virgin to $\beta$ states. In addition to desorption, dissociation with carbon formation occurred. The ratio of dissociation to desorption was estimated to be between 0.5 and 0.1, and seems to be least for $\alpha$ and greatest for $\beta$ desorption. The results on carbon formation indicated that a large fraction of CO in the $\alpha$ and virgin modes is adsorbed with the C end of the molecule bonded to the substrate (Menzel and Gomer, 1964b, FEM-EID). General agreement with the theory of field desorption seems to hold for the CO-W system and could be confirmed, in particular, for the energetics of desorption and for adsorbate tunneling. The general reasonableness of the potential curves and that of the CO-W spacings obtained indicates that the ion-metal interaction can be expressed by an image potential to distances of the order of 2 Å (Swanson and Gomer, 1963, FEM-FD). Field desorption of carbon monoxide adsorbed on tungsten was found to remove tungsten atoms at the same time (Mulson and Müller, 1963, FIM). Plots of the coverage dependence of sticking probability, work function and desorption heat are shown in Figure 46 (Gavriliyuk and Medvedev, 1963, FF).

Carbon Monoxide and Nitrogen (coadsorption). - The maximum coverage found for adsorption of CO and $N_2$ on tungsten were $10.1 \times 10^{14}$ and $4.5 \times 10^{14}$ molec/cm$^2$ respectively. The initial values of the sticking probability were 0.27 for CO and 0.10 for $N_2$. The effects of preadsorption of the two gases on each other is shown in the following two tables:

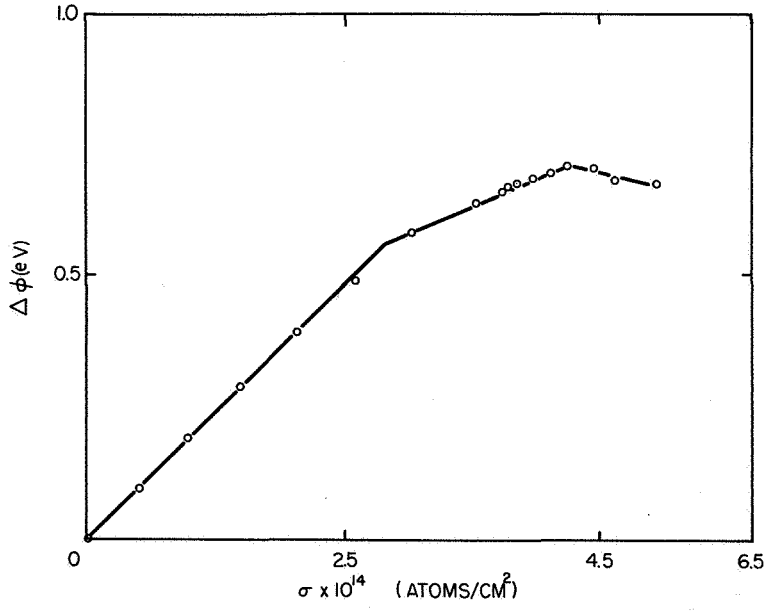


(a)

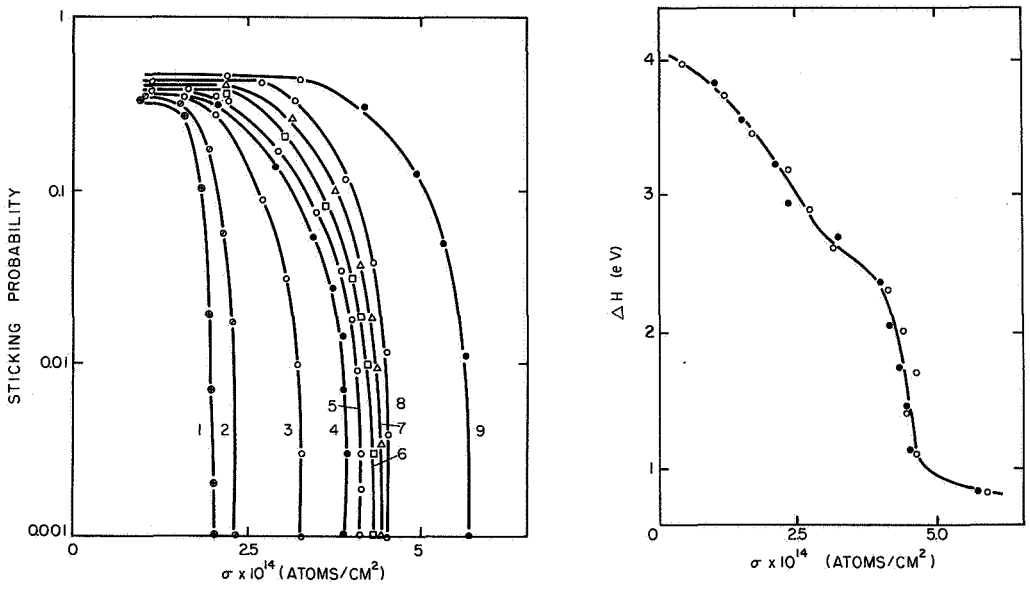


**Substrate temperature (°K). 1) 1100; 2) 1000; 3) 900; 4) 800; 5) 700; 6) 600; 7) 500; 8) 400; 9) 300.**

(b) (c)

Figure 46. Coverage dependence of various experimental parameters for CO on W. (a) Work function vs coverage. (b) Sticking probability vs coverage at various temperatures. (c) Heat of adsorption vs coverage. From Gavrilyuk and Medvedev, Soviet Physics-Solid State, 4, 1737 (1963).

Maximum Adsorbed Quantities for Room-Temperature Adsorption of CO on a Tungsten Surface Partially Covered with $N_2$ (molecules/$cm^2$) x $10^{-14}$

| | | | | | |
|---|---|---|---|---|---|
| Preadsorbed $N_2$ | | 1.10 | 2.20 | 3.30 | 4.50 |
| Maximum CO | 10.10 | 8.90 | 7.75 | 6.80 | 5.65 |
| Total $N_2$ and CO | 10.10 | 10.00 | 9.95 | 10.10 | 10.15 |

Maximum Adsorbed Quantities for Room-Temperature Adsorption of $N_2$ on a Tungsten Surface Partially Covered with CO (molecules/$cm^2$) x $10^{-14}$

| | | | | | |
|---|---|---|---|---|---|
| Preadsorbed CO | | 1.00 | 2.00 | 3.00 | 4.00 |
| Maximum $N_2$ | 4.50 | 3.64 | 2.70 | 1.70 | 1.30 |
| Total $N_2$ and CO | 4.50 | 4.65 | 4.70 | 4.70 | 5.30 |

(Ricca, et al, J. Catalysis 1,458 (1962) ).

Later coadsorption work with CO and $N_2$ showed that nitrogen replaces $\alpha$ CO and in doing so lowers the energy of the $\beta$ phases of CO (Rigby, 1964, FF-MS). In this case, the adsorption of the nitrogen was on identical sites vacated by the carbon monoxide with a large interaction between the unreplaced and replacing atoms (Rigby, 1965b, FF-MS).

Carbon Monoxide and Hydrogen. (coadsorption). - In the replacement of hydrogen by CO, the adsorption of the carbon monoxide was on sites which were not occupied by the hydrogen with subsequent desorption of the hydrogen from the adjacent sites (Rigby, 1965b, FF-MS).

Carbon Dioxide. - Heating of a field electron emission tip partly covered with $CO_2$ to 400-600°K resulted in the surface diffusion of oxygen onto the initially clean portions of the emitter. Further heating to 750°K resulted in the diffusion of another substance with an activation energy of 2.18 $\pm$ 0.22 eV. The temperature change and pattern appearance made it very probable that this was CO. These results suggested that $CO_2$ is dissociated into CO and O on a tungsten surface. The fractional oxygen

monolayer coverage before diffusion could be estimated as 0.15 from the change in work function of the initially clean portion of the emitter after oxygen diffusion. It was felt that dissociation is almost complete at, or possibly below, 600°K since the maximum $CO_2$ uptake on evaporated W films at 300°K corresponds to a monolayer coverage of 0.19. There was an indication that a small fraction of undissociated, loosely chemisorbed $CO_2$ exists at high coverage and low temperature, (below 600°K). Some desorption of the dissociation products, presumably CO, occurs near 1000°K. Heating above 1000°K leads to the formation of the typical oxide field electron emission patterns which result from heating W emitters dosed with small initial oxygen deposits. When large doses of $CO_2$ were deposited on a cold emitter, migration occurred with a sharp moving boundary, at 60-70°K. This corresponds to the diffusion of physically adsorbed gas on top of the first chemisorbed layer with precipitation at the edge. The activation energy of diffusion of physically adsorbed $CO_2$ was estimated as 0.10 eV from the rate of this process. The heat of binding in this layer was found to be 0.24 eV from the maximum diffusion distance of constant $CO_2$ doses at various temperatures. The work function increase at maximum chemisorption coverage was 1.0 eV. The presence of a second, physically adsorbed layer decreases this by 0.4-0.5 eV (Hayward and Gomer, 1959, FEM).

Cesium. - The initial heat of desorption and the respective pre-exponential factor for cesium ions from tungsten has been determined by several workers. The results are given as follows:

| $E_p$(eV) | $\tau_o$(secs) | Worker |
|---|---|---|
| 1.91 | | (Taylor and Langmuir, 1933, FF) |
| 2.04 | $1.1 \times 10^{-12}$ | (Scheer and Fine, 1962b, PB) |
| 2.73 | $2.4 \times 10^{-15}$ | (Taylor, 1964a, LD) |
| 1.95 | $1.77 \times 10^{-12}$ | (Husmann, 1965, PP) |

The minimum work function of cesium on tungsten was found to be 1.70 eV (Taylor and Langmuir, 1933, FF), and 1.5 eV (Swanson, et al, 1964a, FEM). Shapes of the work function-coverage curves measured by field electron emission techniques agree closely with existing ones measured by thermionic methods. Field electron emission probe techniques were used to compare the work function-coverage relationship on the (100) and (110) planes of tungsten with the corresponding average work function relationship. The work function minimum was found to occur at 1.47 eV on the (110) plane and 1.60 eV on the (100) plane (Swanson, et al, 1964a, FEM). The vacuum thermionic work function of tungsten was measured to be 4.52 eV (Wilson, 1966c, LD). Adsorption of cesium yielded a work function minimum of 1.60 eV and 1.64 eV for a saturated surface (Wilson, 1966d, LD). Langmuir and Taylor determined heats of metal and ion desorption to be 1.91 and 2.98 eV respectively (Taylor and Langmuir, 1933, FF). The field electron emission results for neutral desorption agree extremely well with the data of Taylor and Langmuir in the coverage range 0 to $1.4 \times 10^{14}$ atoms/cm$^2$, but fall below the heats of these authors at higher coverages. The combination of neutral and ionic heats yields a value of $\phi = 5.3$ eV for the zero coverage work function of the regions from which ionic desorption occurs. The phenomenon of phase segregation observed by Taylor and Langmuir at very low coverages under steady-state conditions can be shown to be a kinetic rather than a thermodynamic effect (Schmidt and Gomer, 1965c, FEM). Strayer, et al, found agreement with Taylor and Langmuir's desorption data at low coverage but disagreement at high coverages. Values of 2.4 $\pm$ 0.1 and 3.0 $\pm$ 0.1 are given for ionic and neutral heats of desorption (Strayer, et al, 1962, FEM).

The activation energy for diffusion was found to be 0.48 for the (110) plane and 0.76 for the (123) plane (Strayer, et al, 1962, FEM). The zero field activation energy for surface diffusion measured using field

electron emission techniques was found to take place in two modes at $\theta$ = 0.2. Migration took place around the (110) plane along close packed (110) type ledges with an activation energy of 0.43 eV. In the second mode diffusion was into the (110) plane over (110) ledges with an activation energy of 0.50 eV (Swanson, et al, 1964b, FEM-FD). The activation energy of migration of cesium on tungsten was measured by another method to be 0.61 eV (Langmuir and Taylor, 1932, LD).

At low coverage the field desorption of Cs from tungsten can best be explained on the basis of a covalent ground state which suggests that an electronic transition is involved in the desorption process. On this basis, the polarizability of adsorbed Cs is found to be close to that of the free atom. The results were much the same as those found for Ba (Utsugi and Gomer, 1962b, FEM-FD). Field dependent variations of both the pre-exponential factor and activation energy of the surface diffusion coefficient written as $D = D_o \exp ( -E_d^F /kT)$ were found. At temperatures sufficient to induce mobility, an increase or decrease in cesium coverage in the high field region of the emitter occurs with both positive and negative fields; positive fields, on the other hand, produce large variations in desorption rates dueto field desorption. Most of the field effects can be analyzed in terms of MF and $1/2\ \alpha\ F^2$ interactions (Swanson, et al, 1964b, FEM-FD).

Cesium-Fluorine. - The effects of preadsorption of fluorine on cesium adsorption kinetics have been studied by deposition of CsF on a heated field electron emission tip. The CsF dissociates on the tip and the components migrate separately at different temperatures. The cesium can be desorbed above $\sim$1000°K to leave a fluorine layer. Deposition of Cs on the fluorine results in work function minima as low as 1.0 eV. In contrast to oxygen, the minima occurs at the same coverage on a fluorine-tungsten layer as on clean tungsten. The fluorine increases the activation energy for migration of cesium (Swanson, et al, 1966, FEM).

Cesium-Oxygen. - Preadsorbed oxygen lowers the work function minimum to 1.13 eV and shifts the minimum found with cesium on clean tungsten to lower cesium coverages. Preadsorbed oxygen also increases the activation energy of migration (Swanson, et al, 1964c, FEM).

Copper. - The binding energy of copper on tungsten was 3.5 $\pm$ 0.5 eV (Godwin and Luscher, 1965, FF). Small amounts of copper form a layer on the surface of tungsten field electron emission tips which raise the work function from 4.52 to 4.83 eV and can be desorbed thermally with an activation energy of 4.12 eV. This has been termed type I adsorption and is believed to form the first monolayer of copper in which all adatoms are bonded directly to the tungsten substrate and are therefore polarized negatively outward, giving rise to the observed increase in work function. Copper adsorbed upon the type I layer forms type II, which lowers the work function to 4.2 eV, diffuses over the tip surface with an activation energy of 0.87 eV, and is desorbed thermally with an activation energy of 3.05 eV. It is believed to comprise a layer 2 atoms thick which forms a copper lattice strained to conform to the substrate structure. Further adsorbtion of copper leads to a type III layer that is desorbed with an activation energy of 2.76 eV and diffuses over the field electron emission tip surface with an activation energy of 0.52 eV. A measured increase in work function from 4.2 to 4.3 eV is thought to be due to a change in the shape of the tip surface instead of a real work function change. Further adsorption of copper over the three atom layers produces nuclei which are thought to be crystallites having a true copper lattice structure (Jones, 1964, FEM). Adsorption of one to ten atomic layers of Cu was studied from changes in the field electron emission pattern and average work function of a coated W field emitter. Surface diffusion was investigated for single-, double-, and triple-layer diffusion, and for successive diffusion of one layer of Cu on others up to four layers. The negative electric field used in some of the measurements was found to decrease

the apparent activation energy and the pre-exponential factor of the diffusion equation. The activation energy for diffusion varied over the tungsten surface and increased with atomic roughness; it also varied with coverage, decreasing rapidly at first and then less rapidly with increasing coverage as shown in the following table:

| Diffusion Type | Region of Surface | $E_d$ (eV) (zero field) | Temperature range, (°K) | $D_o$ ($cm^2$/sec) (zero field) |
|---|---|---|---|---|
| Single layer | Average | 0.74± 0.09 | 548-673 | $6 \times 10^{-5}$ |
| Double layer | Average | 0.56± 0.04 | 533-653 | $6 \times 10^{-6}$ |
| Triple layer | Average | 0.43± 0.04 | 488-653 | $6 \times 10^{-7}$ |
| Second layer | Average | 0.48± 0.04 | 553-673 | $2 \times 10^{-8}$ |
| Third layer | Average | 0.43± 0.04 | 553-673 | $2 \times 10^{-6}$ |
| Fourth layer | Average | 0.39± 0.04 | 553-673 | $1 \times 10^{-6}$ |
| Single layer | (011)-(112) | 0.48± 0.04 | 473-573 | $7 \times 10^{-7}$ |
| Single layer | (001)-vicinal | 0.95± 0.09 | 523-673 | $1 \times 10^{-3}$ |
| Single layer | (011) | 0.35 | 289-313 | |

(Melmed, 1965b, FEM).

Bennette, et al, determined the heat of desorption as 3.17 eV, the activation energy for surface diffusion as 1.15 eV and the maximum work function as 4.75 eV (Bennette, et al, 1966, FEM).

The effect of adsorbed oxygen and nitrogen on the mobility of copper on tungsten depends on the relative amounts of gas and copper and on the local substrate crystallography. Generally stated, they increase the activation energy for surface diffusion. The zero field activation energies for surface diffusion of Cu/W, Cu/O/W, and $Cu/N_2/W$ are as follows: 0.87 eV, 1.21 eV, and 1.17 eV respectively (Melmed, 1966, FEM).

Germanium. - At least two types of migration have been observed. Low-temperature migration which occurs starting at room temperature, with an activation energy of 0.2 eV is related to a mechanism in which

the only mobile atoms are those in the second, physically adsorbed layer. Migration of the second type which occurs starting at T = 800°K, with energies of 1.24 and 1.7 eV is participated in by the atoms in the chemisorbed layer. An analysis of the volt-ampere characteristics of the field electron emission current, the emission patterns, and the nature of the migration, led to the conclusion that low-temperature migration produced germanium layers having semiconducting properties, while the layers resulting from high-temperature migration were not continuous, and the electron-emitting surfaces were spots of pure tungsten (Sokol'-skaya and Mileshkina, 1964, FEM).

Gold. - The observed binding energy of gold on tungsten was 3.6 ± 0.5 eV (Godwin and Luscher, 1965, FFD).

Hydrogen. - Hydrogen adsorbs on tungsten with an initial sticking probability of approximately 0.2 and the work function rose to 5.0 eV as the surface concentration reached a room temperature maximum of 7.5 ± 1.0 x $10^{14}$ molec/$cm^2$. Two adsorption peaks were found at 1100°K and 1800°K with an energy difference of 0.5 (Eisinger, 1958b, FF).

A sticking probability of 0.1 was found by Hickmott and two distinct states were isolated. At a coverage of less than 3 x $10^{13}$ molec/$cm^2$, a β state was observed which obeyed second order kinetics and has an activation energy for desorption of 1.35 eV. At higher coverages the energy lowers, probably due to the formation of a molecular α state. The concentration in the α state was proportional to pressure. Above 1100°K, atoms evaporate with an activation energy of 2.9 eV (Hickmott, 1960, FF).

Russian workers have found two β states which obey second order kinetics with activation energies for desorption of 0.61 eV ± 0.06 and 1.48 eV ± 0.07 (Ageev, et al, 1965, FF).

Ricca, et al, reported three pairs of states from desorption spectra. Of the six observed peaks, two ($\gamma_1 + \gamma_2$) occur in the temperature range

77-90°K. The $\alpha$ states ($\alpha_1$ and $\alpha_2$) occur between 190 and 300°K, and the $\beta$ states ($\beta_1$ and $\beta_2$) occur in the region 300 to 600°K. The $\beta_2$ state appears to be practically filled before the $\beta_1$ state is significantly populated (Ricca, et al., 1965, FF).

Rigby reported two $\beta$ states obeying first order kinetics with activation energies of desorption of 1.10 eV and 1.26 eV and a third $\beta$ state with an activation energy for desorption of 1.22 eV which obeyed second order kinetics (Rigby, 1965b, FF).

Four chemisorbed complexes were identified for hydrogen by Rootsaert, et al. The bond strengths on individual sites correlated with the number of surface atoms contacted simultaneously and with their degree of unsaturation. At low over-all coverage the adsorbate was concentrated on the faces with the highest heat of adsorption: these faces became populated mainly by surface migration from less attractive crystal faces. Only at very low temperature, where surface migration was severely restricted, did a uniform distribution of the adsorbate over the crystal faces result. The heat of adsorption on the (211) faces was found to be 2.0 eV. On the overall field electron emission tip four states of adsorption were found which desorbed in the following temperature range:

| T°K | E | |
|---|---|---|
| 280 | 0.87 - 2.0 eV | increase in work function |
| 220-280 | 0.65 - 0.87 eV | decrease in work function |
| 120-200 | 0.35 - 0.61 eV | increase in work function |
| 120 | 0.26 - 0.43 eV | physisorbed state |

(Rootsaert, et al., 1962, FEM)

It was found by Gomer, et al, that spreading of hydrogen on tungsten occurs in three distinct phases. At very high initial coverages a moving boundary migration occurred below 20°K, corresponding to migration of physically adsorbed $H_2$ on top of the chemisorbed layer. Precipitation at its edge, and further migration over the newly-covered region.

For initial deposits corresponding to ~1 monolayer, spreading set in at ~ 180°K with a boundary moving radially outward from the close-packed (110) faces. The activation energy measured for the process was 0.26 eV and corresponded to migration over the smooth (close-packed) regions of the tip followed by precipitation of chemisorbate at trap sites on the rough regions. At coverages too low to permit saturation of traps, diffusion out of the latter became rate controlling so that boundary-free diffusion with $E_d$~ 0.41 eV and at even lower coverages with $E_d$~ 0.69 eV was observed. The heat of adsorption of $H_2$ at extremely low coverage was found to be 2.78 eV but dropped rapidly with increasing coverage. These results led to the conclusion that surface heterogeneity was largely the result of surface topography and was inherent on all but the close-packed faces of W. The activation energies for diffusion were found to be 10 to 20% of the binding energy, depending on the nature of the sites. It was also seen from the low-temperature spreading that ~ 75% of the chemisorbed layer could be formed below 20°K with effectively zero activation energy (Gomer et al, 1957, FEM).

Electron induced desorption cross sections Q were determined from work function and Fowler-Nordheim pre-exponential changes and were significantly smaller than would be expected for comparable molecular processes. $Q = 3.5 \times 10^{-20} cm^2$ and $5 \times 10^{-21} cm^2$ for processes tentatively interpreted as the dissociation of molecularly adsorbed $H_2$ and desorption of H, respectively. These results were interpreted in terms of transitions from the adsorbed ground state to repulsive portion of excited states, followed by de-exciting transitions which prevent desorption. It was argued that the excitation cross sections should be essentially "normal" i.e., $10^{-16}$ to $10^{-17} cm^2$, and that much smaller overall cross sections observed were due to high transition probabilities to the ground state, estimated as $10^{14}$ to $10^{15}$ $sec^{-1}$ (Menzel and Gomer, 1964a, FEM-EID).

Single crystal studies of sticking probabilities and work function as hydrogen adsorbs on tungsten were studied (Armstrong, 1966, LEED) and are given in the following table:

| Plane | W(100) | W(211) | W(111) | W(110) |
|---|---|---|---|---|
| $\Delta\phi_m$ | 0.88 | 0.65 | 0.15 | ----- |
| $S_o$ | 0.1 | 0.3 | 0.01 | $10^{-3}$ |

Single crystal studies of hydrogen on tungsten by other workers gave the following work function changes for various planes (Hopkins and Pender, 1966b, FF-MS-CP):

| Plane | W(100) | W(113) | W(111) | W(110) | Polycrystalline foil |
|---|---|---|---|---|---|
| $\Delta\phi$ | 0.54 | 0.43 | 0.30 | -0.14 | 0.63 |

Desorption of hydrogen was found to be a second order process for samples dosed at 300°K. The desorption energy was represented by $E = E_o - g\sigma$ where $E_o$ = 1.5 eV and g = 1.2 $\pm$ 0.1 eV $(10^{15}\text{molec/cm}^2)^{-1}$. The desorption spectrum for a sample dosed at 100°K yields two peaks, $\alpha$ and $\beta$. From the isotopic distribution the $\alpha$ peak was found to be molecular (Mimeault and Hansen, 1966, FF-MS).

As hydrogen was adsorbed on W(100) at room temperature a sequence of LEED patterns were observed consisting of the formation of 1/2 x 1/2 spots, splitting and eventually disappearing with simultaneous formation of 1/4 order spots and finally, at saturation, all extra diffraction features disappeared. The work function increases with coverage to 0.9 eV at saturation (Estrup and Anderson, 1966, LEED).

Hydrogen and Nitrogen (coadsorption). - Nitrogen adsorption on preadsorbed hydrogen. The adsorption of nitrogen is believed to be on identical sites vacated by the replaced hydrogen with a strong interaction

between the unreplaced and the replacing atoms. If the adsorption sites for the replaced hydrogen and nitrogen are identical, sites for the nitrogen are only produced when a weakly-adsorbed phase is thermally desorbed (Rigby, 1965b, FF-MS).

Iodine. - It is believed from field electron emission experiments that the "triangular" sites which occur on the (111) planes are favorable for iodine adsorption (Moss and Kimball, 1960, FEM). Extended exposure to iodine ($5 \times 10^{-9}$ torr) vapor produced a constant work function increase of 0.4 eV with respect to clean tungsten. Iodine adsorption-desorption was sensitive to surface topography, adsorbing on the (133), (122), (233) planes and in the region of the (124) planes on heating (Duell and Moss, 1965, FEM).

Krypton. - Adsorption of Kr lowers the work function of clean tungsten by 1.18 eV at 20°K. Binding to the surface appeared structure sensitive and resembled argon. Observations of changes in field electron emission with temperature yield an activation energy for surface diffusion of Kr over the (310) toward the (100) of 0.048 eV (Ehrlich and Hudda, 1959, FEM).

Lithium. - Field electron emission studies on tungsten yielded the clean work functions and the work function minimum and saturated surface values for adsorption of lithium on individual crystal planes as tabulated below (Gavrilyuk and Medvedev, 1966, FEM).

| Plane | $\phi_o$(eV) | $\phi_{min}$(eV) | $\phi_{sat}$(eV) |
|---|---|---|---|
| (112) | 4.6 | 2.65 | 2.75 |
| (110) | 5.2 | 2.2 | 2.75 |
| (111) | | 2.7 | 2.7 |

Magnesium. - Adsorption of magnesium lowered the work function by 0.9 eV at $7 \times 10^{14}$ atoms/cm$^2$ and further adsorption to $12 \times 10^{14}$ atoms/cm$^2$ caused work function to decrease by 0.75 eV (Zingerman, et al, 1961, TE).

Mercury. - Field electron emission studies of surface diffusion and desorption yielded a terminal coverage heat of desorption of 1.92 $\pm$ 0.18 eV for mercury on tungsten. The surface diffusion activation energies determined were 0.51, 0.40, and 1.0 eV for the (111), (123), and (100) planes respectively. Increasing coverage of Hg caused the work function of the substrate to first increase by 0.40 eV at $\theta_m = 0.4$ and then decrease (Swanson, 1967, FEM).

Neon. - It was found that a work function decrease of 0.15 eV occurred for saturated monolayers of neon on tungsten when measured at 4.2°K. It is believed that dipole-dipole repulsions are very small and do not necessarily make the first layers gas-like (Gomer, 1958b, FEM).

Nitric Oxide. - Nitric oxide chemisorbs nondissociatively at room temperature. Dissociation occurred at elevated temperature with an activation energy of about 2.0 eV. Heating of an NO shadowed field electron emission tip above 700°K resulted in the formation of a receding boundary which remained sharp during the entire course of its backward motion over the initially covered region. This is consistent with a model involving dissociation of NO at the boundary where empty sites are available. For a monolayer of NO ($1.4 \times 10^{15}$ molec/cm$^2$) on polycrystalline tungsten, a work function increase of 1.85 $\pm$ 0.01 eV was measured with respect to clean tungsten; this corresponds to an average surface dipole moment of 0.35 Debye per chemisorbed NO molecule at full coverage. Coadsorption of $N_2$ and $O_2$ indicated that saturation with oxygen poisons the surface against further nitrogen adsorption (Yates and Madey, 1966, FF-FEM-MS).

Nitrogen. - Three states of adsorption were observed by 1961, a $\gamma$ state with a desorption energy of 0.39 eV , an $\alpha$ state with a desorption energy of 0.87 eV and a $\beta$ state with a desorption energy of 3.5 eV. A plot is shown in Figure 47 of sticking probability versus surface coverage of the various phases of nitrogen on tungsten (Ehrlich, 1961a, FF), (Ehrlich and Hudda, 1961, FEM), (Ehrlich, et al, 1958a, FEM-FF).

The $\beta$ state was found to obey second order kinetics at low coverages. At high coverages, the $\beta_2$ appeared to split and a second peak, $\beta_1$ was found which obeyed first order kinetics and had an activation energy for desorption slightly lower than the $\beta_2$ peak. The $\beta$ states are believed to be atomically bound; but at higher coverages, it may be difficult to distinguish the desorption of two adjacent atomically bound atoms from molecular desorption using the kinetic behavior alone. Mass spectrometric evidence using isotopes showed that the small $\alpha$ phase was molecular and the $\beta$ phase atomic. Figure 48 is a plot of the distribution in the various phases versus coverage (Rigby, 1965a, FF). Isotopic studies show that no exchange takes place between the gas phase and the adsorbed phase (Rigby, 1964, FF). The results of Rigby were simultaneously confirmed and the $\gamma$ state was shown to be molecular from isotopic exchange studies. A plot of equilibrium surface coverage versus temperature is shown in Figure 49. (Yates and Madey, 1965, FF). Nitrogen adsorption raised the work function in all states except the $\gamma$ state which lowered the work function (Ehrlich and Hudda, 1961, FEM). This effect was substantiated by Hill and Pethica using flash filament techniques (Hill and Pethica, 1962, FF-FEM).

A study by Delchar and Ehrlich combining flash filament techniques with contact potential measurements on macroscopic planes cut from single crystal tungsten provided information on the relationship between binding states and crystal face. An atomically bound $\beta$ state forms on the (100) plane which lowers the work function by 0.4 eV.

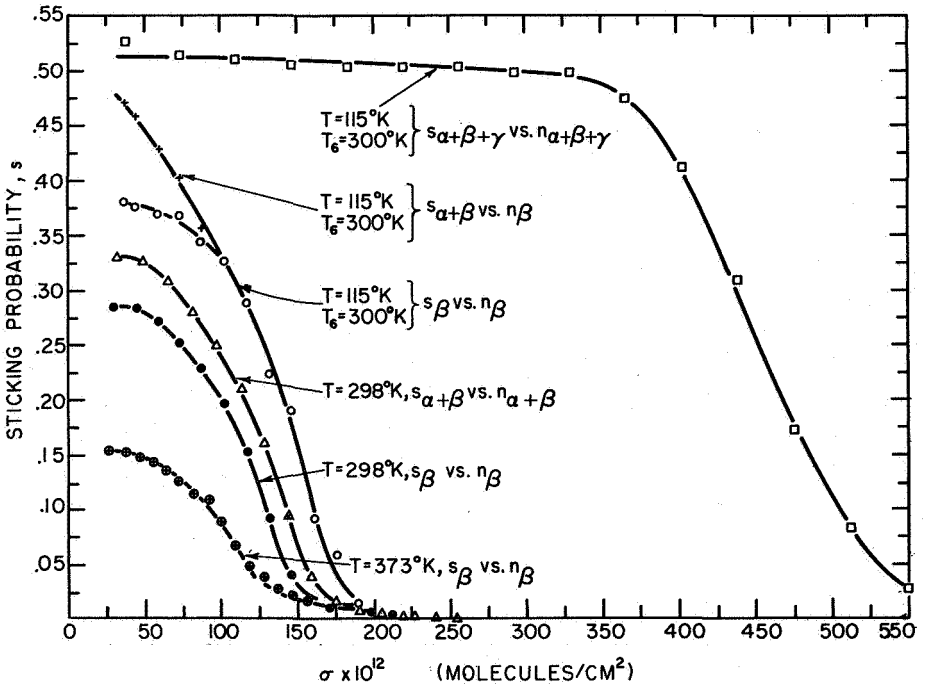


Figure 47. Sticking probabilities of nitrogen on a polycrystalline tungsten filament. T = surface temperature, $T_g$ = gas temperature. From Ehrlich, J. Chem. Phys. 34, 29 (1961).

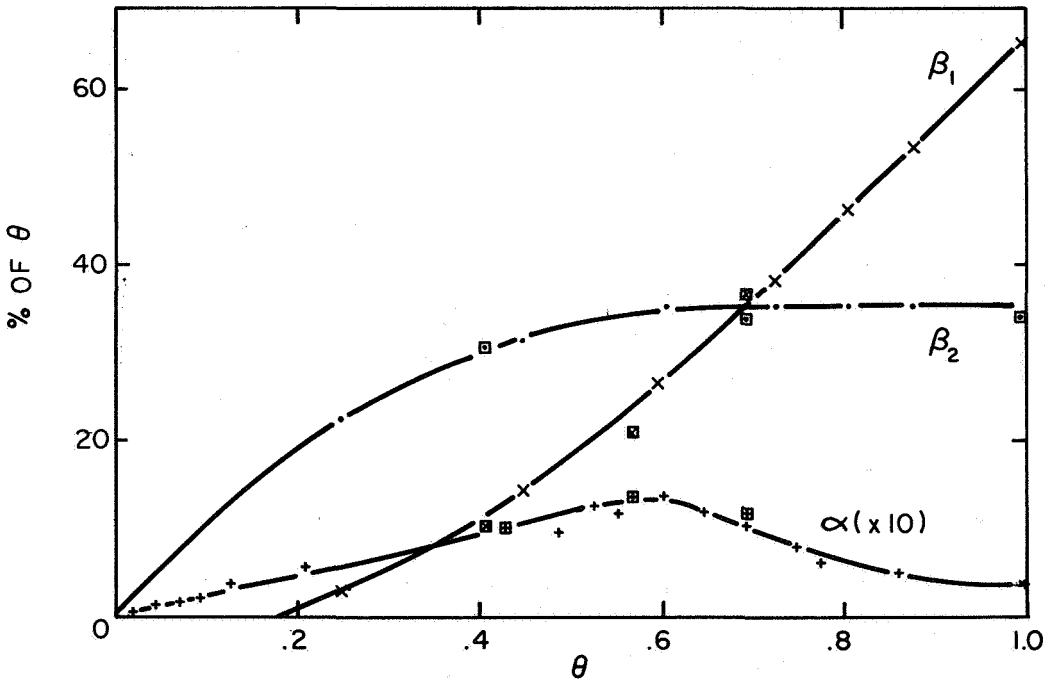


Figure 48. The amount of each phase desorbed vs the total amount desorbed. From Rigby, Canadian J. of Phys. 43, 532, (1965).

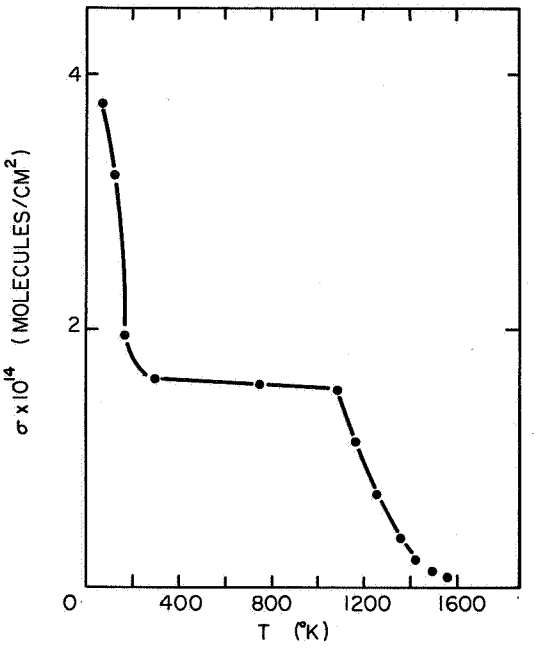


Figure 49. $N_2$ saturation coverage as a function of tungsten sample temperature at $1.8 \times 10^{-6}$ torr. From Yates and Madey, J. Chem. Phys. 43, 1055, (1965).

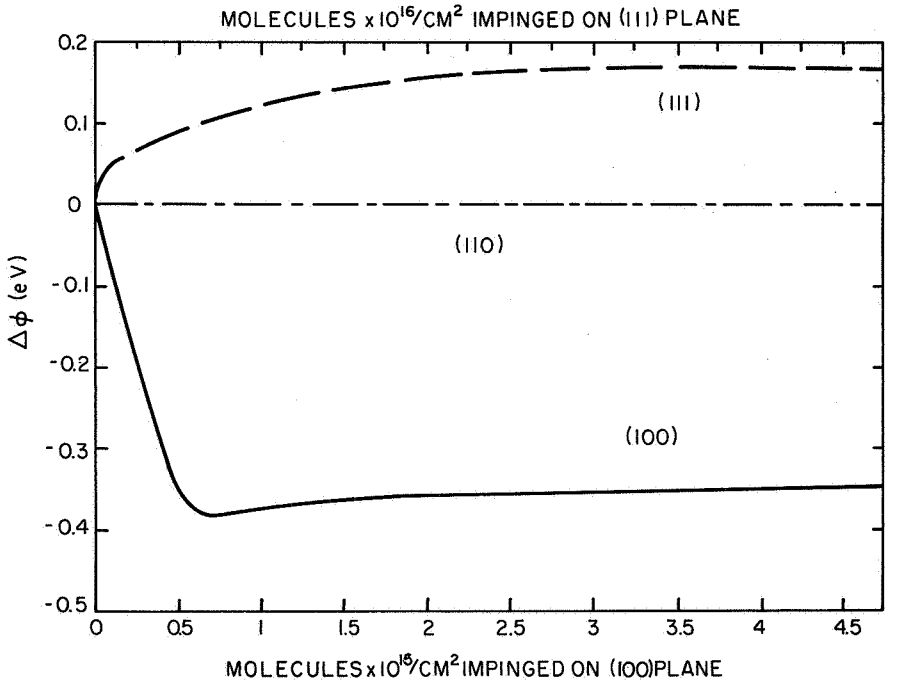


Figure 50. Work-function changes of tungsten single-crystal planes after nitrogen adsorption at 300°K. From Delchar and Ehrlich, J. Chem. Phys. 42, 2686 (1965).

Two states, a molecular $\alpha$ state and a $\beta$ state, form on the (111) plane and raise the work function 0.15 eV. At high concentrations, a second $\beta$ state was observed on the (111) plane. The (110) was inactive except at low temperatures where it formed a $\gamma$ state which was atomic and lowered the work function. A summary of these results is given in the following table (Delchar and Ehrlich, 1965, FF), (Ehrlich, 1962, FEM-FIM):

Nitrogen Adsorption on Individual W Planes

| Plane | T ($^{o}$K) | State | E(eV) | Association | Dipole Moment (Debye) |
|---|---|---|---|---|---|
| (110) | 110 | $\gamma$ | 0.39 | Atoms | $>+0.04$ |
| (100) | 110 | $\gamma^{+}$ | 0.44 | ? | $> 0$ |
| | | $\gamma^{-}$ | 0.48 | ? | $< 0$ |
| | 300 | $\beta$ | 3.26 | Atoms | +0.4 |
| (111) | 110 | $\gamma$ | 0.39 | ? | $> 0.1$ |
| | 220 | $\alpha$ | 0.70 | Molecules | $<-1$ |
| | $\sim$ 300 | $\beta$ | 3.26 | Atoms | -0.2 |

This work provides evidence of the sensitivity of adsorption to structure and the multiplicity of states on single crystal planes. A plot of $\Delta\phi$ versus molecules impinged is given in Figure 50.

It was shown that individual nitrogen adatoms are visible in the field ion microscope and demonstrated that adsorption fails to perturb the lattice permanently. In probing the room temperature distribution of adsorbed nitrogen, the closely-packed (110) plane was found to remain clean even when exposed to nitrogen at a pressure of $2 \times 10^{-6}$ torr for

2 hours. All other planes, with the possible exception of the (100) and (310), were irreversibly covered. Nitrogen, presumably in the form of atoms, was bound on the (110) plane only at temperatures below 190°K. Adsorption on this plane at higher temperatures was limited not by an activation barrier but rather by thermodynamics; the binding energy on the (110) was only 5.1 eV, compared with 6.7 eV elsewhere on the surface (Ehrlich and Hudda, 1962, FIM). Field desorption of nitrogen adsorbed on tungsten was found to be the same as field desorption of nitrogen on iridium(Mulson and Muller, 1963, FIM). Using field electron emission probe tube techniques on a field electron emission tip saturated with nitrogen at 300°K, the following work functions were found for single crystal planes (Holscher, 1964, FEM):

| Crystal Face | $\phi_o$ (eV) | $\Delta\phi_m$(eV) |
|---|---|---|
| (311) | 4.50 | 0.26 |
| (611) | 4.30 | 0.29 |
| (110) zone | 4.40 | -0.13 |
| (100) | 5.2 | -0.9 |
| (310) | 4.35 | 0.39 |
| (111) | 4.40 | 0.30 |
| total surface | 4.50 | -0.18 |

The sticking probability and the room temperature coverage measured by various workers is given in the following table along with heats of desorption for various states.

| $\Delta\phi$ (eV) | s | $\sigma$ (molec/cm$^2$) | E(eV) | Worker |
|---|---|---|---|---|
| 0.44 | 0.33 | $5.6 \times 10^{14}$ | | Eisinger, 1958a, FF |
| | 0.35 | 1.72 | 5.0 | Kisliuk, 1959, FF |
| | 0.33 | 2.8 | 0.39, 0.87<br>3.5 | Ehrlich, 1961a, FF |
| | | | 3.18, 3.26 | Rigby, 1965a, FF |
| | 0.33 | 1.2 | 2.4 , 6.5 | Ustinov and Ionov 1966, FF |
| | 0.10 | 4.5 | | Ricca, et al, 1962, FF |

The variation in these parameters could be due in part to experimental uncertainty and partly to the variations in the specific nature of the surface used.

Oxygen. - Becker and Brandes observed oxygen adsorption on tungsten in the field electron microscope and detected three stages of adsorption. The heats of adsorption were found to be about 5 and 2.5 eV for two of the stages and the third stage consisted of molecular complexes with the substrate (Becker and Brandes, 1956, FEM). Gomer and Hulm examined low temperature diffusion and desorption of oxygen on tungsten and found three types of migration. At 27°K diffusion occurred with a sharp boundary and an activation energy of ~ 0.04 eV, which was believed to be migration of physically adsorbed $O_2$ over the chemisorbed layer, with precipitation on the clean tungsten surfaces. A study yielded an estimate of 0.1 eV for the heat of adsorption in the physisorbed layer. At 400-500°K and high coverages activation energies of diffusion of 1.0 - 1.08 eV were determined. It was found that 80% of the chemisorbed layer could be formed without appreciable activation at 27°K (Gomer and Hulm, 1957, FEM). An initial heat of adsorption of 8.4 eV has been given for oxygen on tungsten thin films (Brennan, et al., 1960, TFC). Evidence has been presented for the chemisorption of a monolayer of gas with a sticking coefficient of unity and the adsorption of a second, initially mobile layer of oxygen, also with a sticking coefficient of unity when the substrate temperature was 20°K. The results appear independent of the degree of surface order over the range considered. The second adsorbed layer was not observed at substrate temperatures of 300°K, and the use of the Langmuir postulate that only the clean surface contributes to the adsorption allows the definition of a constant sticking coefficient of 0.8 for oxygen on tungsten at 300°K (George and Stier, 1962, FEM-FIM). Kinetic rate studies of desorbed species using an in-line mass spectrometer indicate that oxygen adsorbs on tungsten in two states whose

desorption energies were 6.25 and 4.95 eV. Occupation of the lower state begins after the upper state is filled (Schissel and Trulson, 1965, FF). Electron impact desorption cross sections were found to be $4.5 \times 10^{-19} cm^2$ for the loosely bound state and $2 \times 10^{-21} cm^2$ for all other states (Menzel and Gomer, 1964a, FEM-EID).

Recent work by Ptushinskii and Chuikov show good agreement with the results of Schissell and Trulson. Two states of atomic adsorption were formed; one was associated with low temperature oxide desorption and the other was associated with high temperature atomic oxygen desorption. The desorption heats of the oxides and atomic oxygen were determined to be 4.2 eV and $\sim$ 6 eV respectively. The work function increases 1.9 eV as oxygen is adsorbed. The increase from zero to 0.8 is associated with the formation of oxides. (Ptushinskii and Chuikov, 1967, FF-MS).

In a recent study, a tungsten ribbon was exposed at room temperature to oxygen for varying times such that fractions of monolayers adsorbed. The mass peaks observed upon flash desorption using a line-of-sight mass spectrometer showed the desorption products to be atomic oxygen and the monotungstic oxides WO, $WO_2$, and $WO_3$. Neither molecular oxygen nor the polytungstic oxides were ever observed from a ribbon flashed after room temperature exposure to oxygen. However, impinging oxygen on tungsten at surface temperatures $> 1400^{\circ}K$ did produce the polytungstic oxides. An estimate of the adlayer composition showed that the composition of a saturated layer consisted of approximately a monolayer of atomic oxygen and a few tenths percent of monotungstic oxides. The measured heat of desorption was found to be 5.6 eV for atomic oxygen and $\sim$4.4 eV for the monotungstic oxides (McCarroll, 1967, FF-MS).

Single crystal studies showed only one state to be present on the (100) crystal face of tungsten with a binding energy between the metal and atom of 4.8 eV. (Zingerman and Ischuk, 1966, EID). Studies of work function change with exposure of W(110) single crystals to oxygen show that a number of structures or phases of the adsorbed film were

formed, some of which can reduce the work function owing to penetration of oxygen (Zingerman and Ischuk, 1967, CP-EID). Similar measurements of the work function change of (110) and (100) oriented crystals gave clean work work functions of 5.11 $\pm$ 0.02 eV for the (110) and 4.65 $\pm$ 0.04 eV for the (100). It was found, in agreement with Zingerman, et al., that both the (110) and (100) crystals have the same final work functions of 6.25 eV after long exposure to oxygen. Preliminary measurements indicated that it might also be true for the (113) orientation. A pronounced dip in the work function versus oxygen exposure curve for the (110) plane was explained by partial inversion of the tungsten oxygen dipole (Hopkins and Pender, 1966a, CP).

The clean W(111) surface was found to be unchanged after heating to temperatures as high as 2650°K. After an oxygen exposure of $5 \times 10^{-6}$ torr/sec, heating to 800°K brings about the rapid development of (211) planes with a hill and valley structure which is stable up to 1800°K. The clean (111) surface is restored by heating to 1900°K for several minutes or 2100°K for several seconds. Other structures, all based on arrangements of (211) surfaces are observed on increased exposure (Taylor, 1964b, LEED).

Oxygen adsorption on the various planes of a field electron emitter has been studied with a field emission probe tube and yielded maximum work function changes of 1.9, 2.2, 1.6 and 1.8 eV for the (110), (211), (100) and (111) planes respectively at 77°K. In a heating sequence involving oxygen desorption, the work functions of the (112) and the (110) planes exhibited a maximum of $\sim$ 7.6 eV (Swanson, et al., 1966, FEM).

Potassium. - The adsorption of potassium produced a minimum work function of 1.78 eV at a coverage of $3.2 \times 10^{14}$ atom/cm$^2$ which also coinicided with the minimum work function on the (110) planes. At approximately 2.3 monolayers the work function approached that of potassium. Distinct minima also occurred for other close-packed planes,

like the (211). At $\sigma = 3.9 \times 10^{14}$ atom/cm$^2$, the field electron emission pattern is indistinguishable from that of clean tungsten. The average charge per K atom varied from 0.27 at low coverage to 0.20 electron charges at $\theta = 0.8$. The value of the average charge per K atom on the close-packed W planes at low coverage may be considerably higher. The activation energy of neutral desorption varied from 2.67 to 2.4 eV over the interval $0 < \theta < 0.4$ and fell rapidly at higher coverage, approaching the heat of sublimation of K, 1.0 eV, at $\theta = 1.0$. The activation energy of ionic desorption was measured over the interval $0 < \theta < 0.07$, and indicated that ionic desorption occurred from regions with a work function of 5.3 eV. On these regions $d\phi/d\theta$ was very high, suggesting that the K-atom density exceeded the average by a factor of 3 or more, and that adsorption on these regions may be nearly ionic at low $\theta$. The activation energy of surface diffusion and the pre-exponential term of the diffusion coefficient increased with coverage from 0.3 eV at $\theta = 0$ to 0.8 eV at $\theta = 0.6$. This was tentatively explained in terms of activated hopping into the almost empty second layer, followed by rapid diffusion, terminated by recombination of the excited atom with a hole in the first layer. At $\theta = 0.8$ to 1.0, $E_d$ fell sharply, corresponding to diffusion in the second layer. It was suggested that K adsorption sites were relatively weakly structure dependent, so that a displacement of atoms from the initially occupied, optimal sites occurred at $\theta > 0.4$ in order to accommodate more adsorbate in direct contact with the substrate. The experimental results were shown to be consistent with a model based on delocalized bonding, i.e., metallic adsorption (Schmidt and Gomer, 1965a, FEM). More recent studies by Schmidt and Gomer compared the effects of equilibrated with unequilibrated doses of potassium on single crystal planes. The minima observed in work function versus coverage curves was replaced by points of inflection when the potassium was immobiley adsorbed. The summary data for four planes is shown in Figure 43. The work function versus coverage curves for immobilely adsorbed layers could be fitted remarkably well up to the

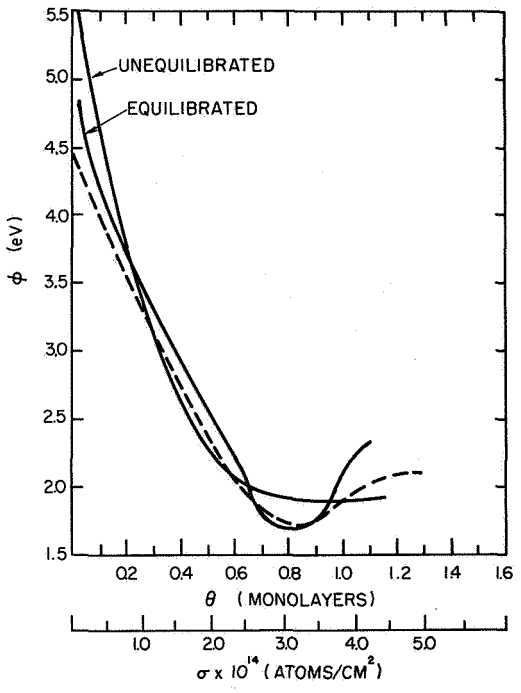


(a). (110) plane

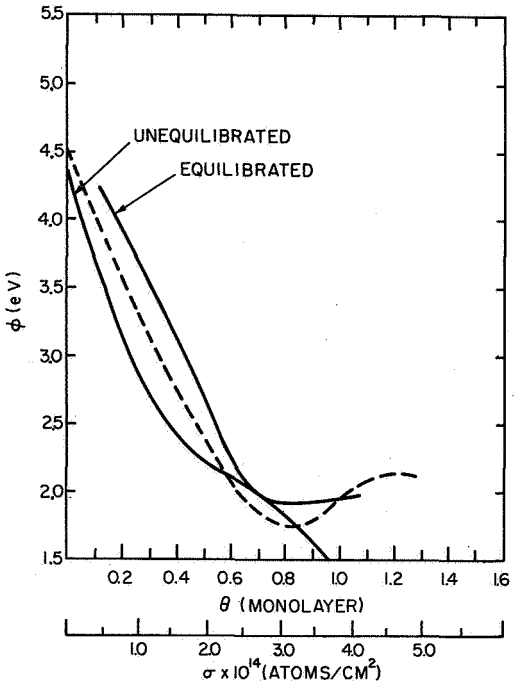


(b). (111) plane

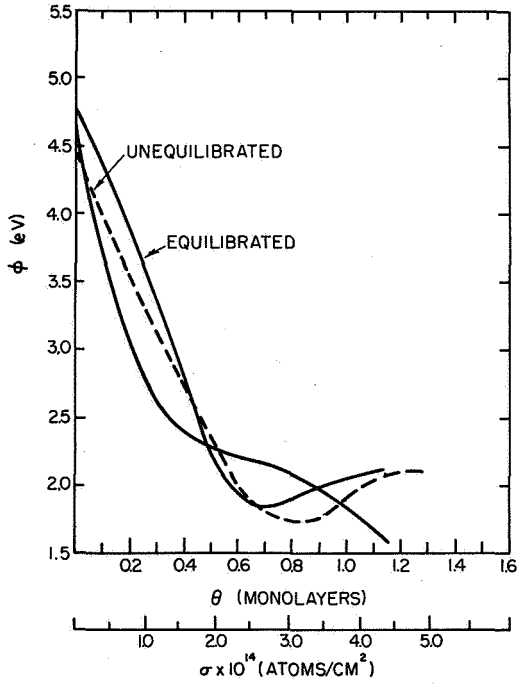


(c). (211) plane

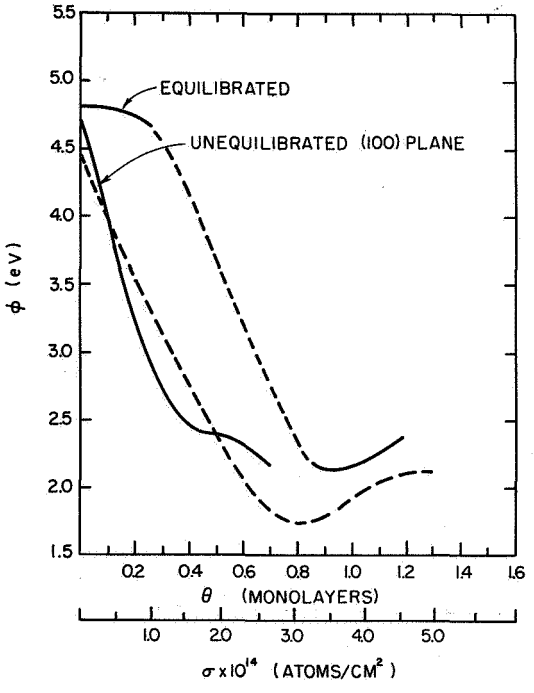


(d). (100) plane

Figure 51. Summary of equilibrated and unequilibrated work function results for potassium adsorption on various planes. The abscissae refer in the first case to $\bar{\theta}$ and $\bar{n}$ and in the second to $\theta$ and n. The $\bar{\phi}$ - vs - $\bar{n}$ curve obtained from total emission is also shown by the dashed heavy line. From Schmidt and Gomer, J. Chem. Phys. 45, 1605 (1966).

inflection points by the point dipole depolarization model based on the Topping formula. The work function change is given by

$$\Delta\phi = 2\pi M_o \sigma / (1 + 9 \alpha \sigma^{3/2})$$

where $M_o$ is the dipole moment at zero coverage and $\alpha$, the polarizability. A summary of the depolarization model results from plots of $\sigma/\Delta\phi$ vs $\sigma^{3/2}$ and is given in the following table:

| Plane | $\alpha$ ($\AA^3$) | $M_o$(Debye) |
|---|---|---|
| 110 | 26 | 15.8 |
| 211 | 42 | 16 |
| 111 | 29 | 10 |
| 100 | 35 | 11.5 |

The comparison of immobilely and mobilely adsorbed K showed that coverage anisotropies exist under equilibrium conditions (Schmidt and Gomer, 1966, FEM).

The binding energy of K on tungsten was found to be 2.22 eV and the pre-exponential factor $2.3 \times 10^{-13}$ sec (Husman, 1965, PP). The results of experiments on field desorption of potassium from tungsten with no migration may be reasonably interpreted on the basis of the theory that the ions evaporate over a Schottky barrier, which at zero field yields $E_p = 2.6$ eV; $\nu \sim 10^{12}$ $sec^{-1}$. The linearity observed experimentally in the $F_d = f(T)$ curve indicates that the forces binding the potassium ion with the (110) face of W may be regarded as electrostatic image forces up to a distance from the surface given by $x = 1/2 \sqrt{e/F} \sim 3\AA$. The surface diffusion rate of K atoms over W was very strongly dependent on the magnitude and direction of the electric field. The dipole moment between adsorbed K atoms and tungsten, which showed up as a reduction in work function at constant coverage, was strongest at (110) faces. (Naumovets, 1964, FEM).

Potassium Chloride. - Thermal activation of potassium chloride on tungsten at approximately 500°K resulted in the desorption of potassium leaving a tungsten chloride ($WCl_x$) layer which was stable to about 1100°K. Data were interpreted as showing that potassium chloride in the presence of tungsten at room temperature formed a WClK complex with the K-Cl bond being the weakest. It was shown by field electron emission techniques that potassium chloride on tungsten and chlorine on tungsten demonstrate identical properties in the temperature range 1100°-1900°K. Limiting processes above 1100°K were believed to be the formation and subsequent desorption of tungsten chloride and atomic chlorine. The heats of desorption and work function were found as follows: In the range of 475-600°K, E = 0.43 to 3.09 eV and $\phi$ = 2.3 to 5.3 eV; in the range 1100°-1400°K, E = 3.22 $\pm$ 0.65 eV and $\phi$ = 5.3 to 4.6 eV; in the range 1700°-1884°K, E = 3.56 $\pm$ 0.70 eV and $\phi$ = 4.6 to 4.5 eV. The behavior of chlorine on tungsten was shown to be similar to that of oxygen on tungsten in the temperature range studied (Silver and Witte, 1963, FEM).

Potassium and Hydrogen. - Molecular hydrogen did not appear to be chemisorbed on potassium at low temperatures. Atomic hydrogen interacts, probably by the formation of a hydride structure with K atoms outermost from the surface. The coadsorption of hydrogen and potassium on tungsten caused a decrease in work function over that caused by potassium alone, and increased the temperature range required for potassium surface diffusion on tungsten. These facts were explained in terms of a surface complex WHK in which H is negatively charged relative to K (Schmidt and Gomer, 1965b, FEM).

Rubidium. - The binding energy and pre-exponential factor of rubidium atoms was found to be 2.60 $\pm$ 0.1 eV and 2.5 x $10^{-13}$ sec (Hughes, 1959, PB). The binding energy and pre-exponential factor for $Rb^+$ was reported as 1.90 eV and 3.5 x $10^{-12}$ sec (Hughes and Levinstein, 1959, PB) and 2.07 eV and 3.4 x $10^{-12}$ sec (Husmann, 1965, PP).

Sodium. - It was shown that for small coverages adsorption of sodium lowered the work function of all planes of tungsten. The most abrupt and greatest lowering was observed on the (110) faces which was related to the higher concentration of sodium on this face and to the initially high work function of the face (Shrednik and Snezhko. 1964, FEM).

Measurements were made of the work function as a function of coverage and temperature. A curve was calculated for the mean heat of evaporation. Field desorption measurements made it possible to obtain an independent value for the heat of adsorption in this stage. The zero coverage heat of adsorption was found to be 2.4 eV and the minimum work function was ~1.9 eV (Shrednik and Snezhko, 1964, FEM). The binding energy and pre-exponential factor for ionic desorption was found to be 2.33 eV and $6.3 \times 10^{-13}$ sec respectively (Husmann, 1965, PP).

Strontium. - A study of the migration of strontium on tungsten by field electron emission techniques revealed two modes. In the first mode, for $\theta > 1$, no boundary was observed and the surface diffusion activation energy was found to be $0.79 \pm 0.06$ eV. For the second mode the surface diffusion activation energy was measured at $1.44 \pm 0.08$ eV (Barnaby, et al, 1964, FEM).

The activation energy for the thermal desorption of strontium from tungsten falls from $4.21 \pm 0.22$ eV at zero strontium coverage to $1.78 \pm 0.13$ eV at "monolayer" coverage. The latter value approached the heat of sublimation of bulk strontium (1.69 eV). The desorption energies found using field electron emission techniques deviate markedly from the extrapolated thermionic results of Moore and Allison. A linear relationship was found to exist between the activation energy for desorption and the logarithm of the pre-exponential factor in the rate equation (Madey, et al, 1965a, FEM).

The energy of desorption was reported to be 3.56 eV and the monolayer surface coverage and work function were $4.89 \times 10^{14}$ atom/cm$^2$ and 2.2 eV respectively (Moore and Allison, 1955, RT). A study of work

function vs coverage gave a work function decrease of 2.1 eV at $4 \times 10^{14}$ atom/cm$^2$ with a constant work function decrease of 1.8 eV at $8 \times 10^{14}$ atom/cm$^2$ (Zingerman, et al, 1961, TE).

Strontium Oxide. - Below 1150°K evidence was given for the dissociation of SrO and migration of Sr to the (110) edges where clusters of crystallites were formed. Two modifications of field electron emission patterns associated with the (Sr-O-W) complex within 1150-1550°K were tentatively identified with the basic and normal tungstate; apparently the first goes over to the second with an activation energy of 2.6 eV as determined from desorption data. An unusually sharp decrease in Fowler-Nordheim work function to 2.6 eV occurred during this reaction. In the later stages of desorption above 1550°K patterns identifiable with an oxygen-tungsten surface were obtained. Desorption at this stage took place with an activation energy of 6.1 eV (Cape and Coomes, 1960, FEM).

Thorium- Field desorption of thorium occurs in the 200 mV/cm range (Muller, 1956, FEM-FD) and (Young, 1965, FIM). The (111) planes have the strongest adsorbing force for thorium atoms while the (211) planes have the weakest. The field electron emission current from a (111) plane has a maximum value (goes through a minimum work function) while the current from a (211) plane changes monotonically (no minimum work function). This phenomena was explained by a balance between the diffusion of thorium atoms from the interior of tungsten and the evaporation of thorium from the surface. The lowest work function was 2.9 eV. The surface diffusion energy of thorium atoms along the tungsten surface and the desorption energy were measured and found to be 2.8 and 7.4 eV respectively (Sugata and Kim, 1961, FEM).

The minimum work function of thorium on tungsten was found to be 3.0 eV by field electron emission techniques and $3.31 \pm 0.02$ eV by the Richardson method (Zubenko and Sokol'shaya, 1961, FEM).

A study of the (100) and (411) planes showed that the work function

goes through a minimum for both planes at a coverage of $4.2 \times 10^{14}$ atoms/$cm^2$. A monolayer coverage was found at $9 \times 10^{14}$ atoms/$cm^2$. The (100) plane has an initial work function of 4.52 eV, a minimum of 3.35 eV. The (411) plane has an initial work function of 4.41 eV, a minimum of 3.05 eV and a saturated value of 3.35 eV (Estrup, et al., 1966, LEED).

Titanium. - It was found that upon adsorption of titanium the work function decreased monotonically to a value of 3.9 eV and no minimum work function was observed. The rate of vaporization of titanium from tungsten carbide was lower than from tungsten, while the heat of vaporization was approximately the same at $5.4 \pm 0.2$ eV (Zubenko, 1963, FEM).

Xenon. - Adsorption of Xe lowered the work function by 1.38 eV. The work function diminished monotonically with Xe coverage even after more than a single layer is formed. Binding is believed similar to argon on tungsten. Observations of changes in electron emission with temperature yield a heat of desorption of 0.35 eV for Xe, as well as the following values for the activation energy for surface diffusion: Over the (310) toward the (100) = 0.16 eV and over the (111) = $0.07 < E_d < 0.15$ eV (Ehrlich and Hudda, 1959, FEM).

It was found that the work function decreased 1.4 eV for saturated monolayers when measured at $4.2^{\circ}$K. Work function changes were most pronounced near the (100) faces. Multilayer adsorption also occurred. It appears that dipole-dipole repulsions suffice to make the first layers gas-like (Gomer, 1958b, FEM).

The adsorption of xenon shows a distinct topographic dependence. Heats of adsorption for the (400) plane were reported as 0.33 eV and 0.22 eV for the (111) plane (Rootsaert, et al., 1962, FEM).

Zirconium. - Both electron and ion (deuteron and proton) field emission patterns were observed. It was found that zirconium lowered the work function markedly on the (100) plane. It was shown by best image ion voltage measurements that Zr on W roughens the surface around the

(100) plane thereby changing the field factor, especially for high concentrations of Zr. The work function for a monolayer of Zr on W was found to be 2.62 eV which fell to 2.2 eV as more Zr was added. The latter lowering was attributed to a field factor change. A (100) plane adherence was postulated by means of a hard sphere fit of Zr atoms (3.16 Å diameter) on the (100) planes of W (3.16 Å lattice const.) (Shrednik, 1961, FEM-FIM).

TABLE I - WORK FUNCTIONS

| Substrate | Adsorbate | $\phi_o$(eV) | $\phi_m$(eV) | $\Delta\phi_m$(eV) | Worker |
|---|---|---|---|---|---|
| Al | O | | | -0.05 | Huber and Kirk, 1966, CP |
| Be | Cs | 3.67 | 1.94 | | Wilson, 1966, LD |
| Cr | Cs | 3.90 | 1.71 | | Wilson, 1966, LD |
| | O | | | 2.1 | Quinn and Roberts, 1964, TFCP |
| Cu | BaO | 4.3 | 2.1 | | Ptushinskii, 1960, TFCP |
| | CO | | | -0.315 | Pritchard, 1962, TFCP |
| | Cs | 4.42 | 1.64 | | Wilson, 1966, LEED |
| | H | | | 0.35 | Pritchard, 1962, TFCP |
| | O | | | 1.46 | Quinn and Roberts, 1964, TFCP |
| Cu(100) | H | | | 0 | Lee and Farnsworth, 1965, LEED |
| Au | CO | | | -0.805 | Pritchard, 1962, TFCP |
| | H | | | 0.193 | Pritchard, 1962, TFCP |
| Ir | Cs | 5.27 | 1.79 | | Wilson, 1966, LD |
| Fe | Cs | 4.2-4.6 | | | Wilson, 1966, LD |
| | N | | | -0.27 | Suhrmann, et al., 1963, TFCP |
| | O | | | 1.55 | Quinn and Roberts, 1964, TFCP |
| Mo | Cs | 4.20 | 1.50±0.05 | 2.70 | Swanson, et al., 1964, FEM |
| | Cs | 4.0-4.3 | 1.61 | | Wilson, 1966, LD |
| | Hg | 4.2 | 4.60 | 0.40 | Swanson, 1967, FEM |
| | O | | | 1.46 | Quinn and Roberts, 1964, TFCP |
| Mo(111) | Ba | 4.15±0.05 | 2.3±0.1 | | Azizov, et al., 1966, TEM-FEM |
| Ni | Ba | | | -2.2 | Ptushinskii, 1961, TFCP |
| | BaO | | | -2.9 | Ptushinskii, 1961, TFCP |
| | Cs | | | -2.9 | Ptushinskii, 1961, TFCP |
| | Cs | 4.4-4.86 | 1.6-2.4 | | Wilson, 1966, LD |
| | Cs | | 1.38 | 3.62 | Bennette, et al., 1967, FEM |
| | O | | | 1.4 | Quinn and Roberts, TFCP |
| Ni(110) | CO | | | 0.3 | Park and Farnsworth, 1964b, LEED |
| Nb | CO | | | 0.7 | Klein and Little, 1964, FEM |
| | Cs | 4.19 | 1.44 | | Wilson, 1966, LD |
| Os | Cs | 4.83 | 1.44 | | Wilson, 1966, LD |

| Substrate | Adsorbate | $\phi_o$ (eV) | $\phi_m$ (eV) | $\Delta\phi_m$ (eV) | Worker |
|---|---|---|---|---|---|
| Pt | Cs | 5.6-5.8 | 1.59 | | Wilson, 1966, LD |
| Re | Cs | 4.96 | 1.51 | | Wilson, 1966, LD |
| | Cs | 4.85 | 1.45+0.05 | | Swanson, et al., 1964, FEM |
| | N | 4.9 | 4.5 | | Klein and Little, 1967, FEM |
| | Th | 4.85 | 3.15 | | Anderson, et al., 1963, FF-TEM |
| Ta | CO | | | 0.8 | Klein and Leder, 1963, FEM |
| | Cs | | 1.6 | | Gorbatyi and Ryabchenko, 1965, FEM |
| | Cs | 4.25 | 1.69 | | Wilson, 1966, LD |
| | O | | | 0.1 | Boggio and Farnsworth, 1964, LEED |
| Ti | Cs | 3.65-4.3 | 1.33 | | Wilson, 1966, LD |
| W | Cs | | | 2.92 | Bennette, et al., 1967, CP |
| | Ar | | | -0.80 | Gomer, 1958b, FEM |
| | Ar | | | -0.89 | Ehrlich and Hudda, 1959, FEM |
| | Ba | 4.5 | 2.0 | | Zingerman, et al., 1961, TEM |
| | Ba | | 2.1 | | Zubenko and Sokol'skaya, FEM |
| | Be | | | 0 | Zingerman, et al., 1961, TEM |
| | Br | 4.5 | 4.1 | | Duell and Moss, 1965, FEM |
| | Ca | | 2.6 | -1.9 | Zingerman, et al., 1961, TEM |
| | CO | | | 1.1 | Swanson and Gomer, 1963, FEM-FD |
| | Cs | | 1.70 | | Taylor and Langmuir, 1933, LD |
| | Cs | 4.52 | 1.53 | 3.00 | Swanson, 1964a, FEM |
| | Cs | 4.52 | 1.60 | 0.23 | Wilson, 1966, LD |
| | Cu | 4.52 | 4.75 | 0.31 | Bennette, et al., 1966, FEM |
| | Cu | 4.52 | 4.83 | | Jones, 1964, FEM |
| | H | 4.54 | 5.0 | 0.46 | Eisinger, 1958, FF |
| | H | | | 0.63 | Hopkins and Pender, 1966b, FF-MS-CP |
| | Hg | 4.52 | 4.92 | 0.40 | Swanson, 1967, FEM |
| | I | | | 0.4 | Duell and Moss, 1965, FEM |
| | Kr | | | -1.18 | Ehrlich and Hudda, 1959, FEM |
| | Mg | | 3.6 | | Zingerman, et al., 1961, TEM |
| | Ne | | | -0.15 | Gomer, 1958b, FEM |
| | N | 4.50 | | -0.18 | Holscher, 1966, FEM |
| | NO | | | 1.85+0.10 | Yates and Madey, 1966, FF-FEM-MS |
| | O | | | 2.4 | George and Stier, 1962, FEM |
| | O | | | 1.9 | Ptushinskii and Chuikov, 1967, FF-MS |

| Substrate | Adsorbate | $\phi_o$(eV) | $\phi_m$(eV) | $\Delta\phi_m$(eV) | Worker |
|---|---|---|---|---|---|
| W | K | 4.50 | 1.78 | | Schmidt and Gomer, 1966, FEM |
| | Na | | 1.9 | | Schrednik and Snezhko, 1964, FEM |
| | Sr | | 2.4 | | Zingerman, et al, 1961, TEM |
| | SrO | | 2.6 | | Cape and Coomes, 1960, FEM |
| | Th | | 2.9 | | Sugata and Kim, 1961, FEM |
| | Th | | 3.0 | | Zubenko and Sokol'skaya, 1961, FEM |
| | Xe | | | -1.38 | Ehrlich and Hudda, 1959, FEM |
| | Xe | | | -1.4 | Gomer, 1958b, FEM |
| | Zr | | 2.62 | | Schrednik, 1961, FEM-FIM |
| W(100) | Cs | | 1.60 | -3.10 | Bennette, et al., 1966, FEM |
| | H | | | 0.9 | Estrup and Anderson, 1966, LEED |
| | H | | | 0.88 | Armstrong, 1966, LEED |
| | H | | | 0.54 | Hopkins and Pender, 1966b, FFD-MS |
| | N | | | -0.9 | Holscher, 1966, FEM |
| | N | | | -0.4 | Delchar and Ehrlich, 1965, FF |
| | O | 5.11±0.02 | 6.25 | 1.14 | Hopkins and Pender, 1966a, CP |
| | O | | | 1.6 | Swanson, et al., 1966, FEM |
| | K | 4.82 | 2.1 | | Schmidt and Gomer, 1966, FEM |
| | Th | 4.52 | 3.35 | | Estrup, etal., 1966, LEED |
| W(110) | Cs | | 1.47 | -4.49 | Bennette, etal., 1966, FEM |
| | H | | | 0 | Armstrong, 1966, LEED |
| | H | | | -0.14 | Hopkins and Pender, 1966b, FF-MS-CP |
| | Li | 5.2 | 2.2 | | Gavrilyuk and Medvedev, 1966, FEM |
| "110 zone" | N | 4.40 | | -0.13 | Holscher, 1966, FEM |
| | O | 4.65±0.04 | 6.25 | 1.60 | Hopkins and Pender, 1966a, CP |
| | O | | | 1.9 | Swanson, et al., 1966, FEM |
| | K | 5.85 | 1.7 | | Schmidt and Gomer, 1966, FEM |
| W(111) | H | | | 0.15 | Armstrong, 1966, LEED |
| | H | | | 0.30 | Hopkins and Pender, 1966b, FF-MS |
| | Li | | | 2.7 | Gavrilyuk and Medvedev, 1966, FEM |
| | N | 4.40 | | 0.30 | Holscher, 1966, FEM |
| | N | | | 0.15 | Delchar and Erlich, 1965, FF |
| | O | | | 1.8 | Swanson, et al., 1966, FEM |

WORK FUNCTIONS (cont.)

| Substrate | Adsorbate | $\phi_o$(eV) | $\phi_m$(eV) | $\Delta\phi_m$(eV) | Worker |
|---|---|---|---|---|---|
| W(111) | K | 4.41 | 1.95 | | Schmidt and Gomer, 1966, FEM |
| | Th | | 2.7 | | Sugata and Kim, 1961, FEM |
| W(211) | H | | | 0.65 | Armstrong, 1966, LEED |
| | K | 4.85 | 1.8 | | Schmidt and Gomer, 1966, FEM |
| | Li | 4.6 | 2.65 | 2.75 | Gavrilyuk and Medvedev, 1966, FEM |
| | O | | | 2.2 | Swanson, et al., 1966, FEM |
| (310) | N | 4.35 | | 0.39 | Holscher, 1966, FEM |
| (311) | H | | | 0.43 | Hopkins and Pender, 1966b, FF-MS |
| | N | 4.50 | | 0.26 | Holscher, 1966, FEM |
| (411) | Th | 4.41 | 3.05 | | Estrup, et al., 1966, LEED |
| (611) | N | 4.30 | | 0.29 | Holscher, 1966, FEM |

TABLE II

HEATS OF DESORPTION

| Substrate | Adsorbate | $E_{initial}$(eV) | $\tau_o$ | Worker |
|---|---|---|---|---|
| Al | O | 9.2 (Integral) | | Brennan, et al., 1960, TFC |
| Cr | $CO_2$ | 3.5 (Integral) | | Brennan and Hayward, 1965, TFC |
| | O | 7.05 (Integral) | | Brennan, et al., 1960, TFC |
| Co | CO | 2.0 | | Brennan and Hayward, 1965, TFC |
| | $CO_2$ | 1.6 | | Brennan and Hayward, 1965, TFC |
| | O | 4.35 | | Brennan, et al., 1960, TFC |
| Cu | H | 0.74 | | Pritchard, 1962, TFCP |
| Fe | CO | 2.0 | | Brennan and Hayward, 1965, TFC |
| | $CO_2$ | 3.0 | | Brennan and Hayward, 1965, TFC |
| | O | 5.9 | | Brennan, et al., 1960, TFC |
| Ir | H | 1.04 | | Mimeault and Hansen, 1960, FFD |
| Mn | CO | 3.4 | | Brennan and Hayward, 1965, TFC |
| | O | 6.5 | | Brennan, et al., 1960, TFC |
| Mo | Ag | $1.9 \pm 0.3$ | | Von Goeler and Peacock, 1963, RT |
| | Au | $4.2 \pm 0.2$ | $0.5 \times 10^{-13}$ | Von Goeler and Luscher, 1963, RT |
| | CO | 3.2 | | Brennan and Hayward, 1965, TFC |
| | $Cs^+$ | 1.72 | $12.0 \times 10^{-13}$ | Husman, 1965, PP |
| | $Cs^+$ | $2.4 \pm 0.1$ | | Swanson, et al., 1964c, FEM |
| | $Cs^+$ | $2.1 \pm 0.1$ | | Swanson, et al., 1964c, FEM |
| | H | 1.74 | | Brennan and Hayward, 1965, TFC |
| | Hg | $1.82 \pm 0.05$ | | Swanson, 1967, FEM |
| | Ni | $2.10 \pm 0.05$ | | McIrvine and Bradley, 1957, FEM |
| | O | 7.5 | | Brennan, et al., 1960, TFC |
| | O | 2.6, 4.8 | | Redhead, 1964, EID |
| Mo(111) | Ba | 3.90, 4.00 | | Azizov, et al., 1966, FEM-TEM |
| Ni | Ag | $1.6 \pm 0.3$ | | Von Goeler and Peacock, 1963, RT |
| | CO | 0.15, 0.28, 2.28 | | Degras, 1965, FF |
| | CO | 1.83 | | Brennan and Hayward, 1965, TFC |
| | $Cs^+$ | $2.2 \pm 0.2$ | | Bennette, et al., 1967, FEM |
| | Cs | $3.1 \pm 0.2$ | | Bennette, et al., 1967, FEM |
| | H | $2.0 \pm 0.13$ | | Wortman, et al., 1957a, FEM |

HEATS OF DESORPTION (cont.)

| Substrate | Adsorbate | $E_{initial}$(eV) | $\tau_o$ | Worker |
|---|---|---|---|---|
| Ni | H | 0.95 (Integral) | | Brennan and Hayes, 1964, TFC |
| Ni(110) | H | 1.2 | | Germer and McRae, 1962a, LEED |
| Nb | N | 2.4 | | Pasternak, et al., 1966, TFC |
| | O | 9.0 | | Brennan, et al., 1960, TFC |
| Pd | CO | 1.9 | | Brennan and Hayward, 1965, TFC |
| | O | 3.0 | | Brennan, et al., 1960, TFC |
| Pt | CO | 2.1 | | Brennan and Hayward, 1965, TFC |
| | H | 1.13 | | Wiesendanger, 1963, FFD |
| | O | 3.0 | | Brennan, et al., 1960, TFC |
| Re | $Ba^+$ | $4.74 \pm 0.21$ | $0.6 \pm 0.4 \times 10^{-13}$ | Scheer and Fine, 1963a, PB |
| | $Cs^+$ | 1.96 | $1.93 \times 10^{-13}$ | Taylor, 1964a, LD |
| | $Cs^+$ | 2.2 | $11.4 \times 10^{-13}$ | Husmann, 1965, PP |
| | $Cs^+$ | $2.04 \pm 0.04$ | $(1.9 \pm 0.9) \times 10^{-13}$ | Scheer and Fine, 1963a, PB |
| | $Cs^+$ | $2.0 \pm 0.1$ | | Swanson, et al., 1963b, FEM |
| | Cs | 3.8 | | Swanson, et al., 1963b, FEM |
| | $K^+$ | $2.33 \pm 0.03$ | $1.0 \pm 0.3 \times 10^{-13}$ | Scheer and Fine, 1963b, PB |
| | $Na^+$ | $2.75 \pm 0.03$ | $(0.2 \pm 0.1) \times 10^{-13}$ | Scheer and Fine, 1963b, PB |
| | $Rb^+$ | $2.28 \pm 0.03$ | $0.8 \pm 0.3 \times 10^{-13}$ | Scheer and Fine, 1963b, PB |
| | Th | $8.30 \pm 0.15$ | | Anderson, et al., 1963, FFD-TEM |
| Rh | CO | 2.0 | | Brennan and Hayward, 1965, TFC |
| | H | 0.78 | | Mimeault and Hansen, 1966, FF |
| | O | 4.45 | | Brennan, et al., 1960, TFC |
| Ta | CO($\alpha$) | 0.17 | | Klein and Leder, 1963, FEM |
| | CO | 5.85 | | Brennan and Hayward, 1965, TFC |
| | $Cs^+$ | 1.65 | $1.8 \times 10^{-9}$ | Husmann, 1965, PP |
| | $K^+$ | 2.05 | $41.6 \times 10^{-13}$ | Husmann, 1965, PP |
| | O | 9.2 | | Brennan, et al., 1960, TFC |
| | $Rb^+$ | 1.81 | $23.6 \times 10^{-13}$ | Husmann, 1965, PP |

HEATS OF DESORPTION (cont.)

| Substrate | Adsorbate | $E_{initial}$(eV) | $\tau_o$ | Worker |
|---|---|---|---|---|
| W | Ba | 3.6 | | Moore and Allison, 1955, RT |
| | Ba | 4.68 | | Zingerman, et al., 1961, TEM |
| | Ba | 4.7 | | Gavrilyuk and Medvedev, 1963, FF |
| | $Cs^+$ | 1.91 | | Taylor and Langmuir, 1933, LD |
| | $Cs^+$ | 2.04 | $1.1 \times 10^{-12}$ | Scheer and Fine, 1962b. PB |
| | $Cs^+$ | 2.73 | $2.4 \times 10^{-15}$ | Taylor, 1964a, LD |
| | $Cs^+$ | 1.95 | $1.77 \times 10^{-12}$ | Husmann, 1965, PP |
| | $Cs^+$ | 2.4±0.1 | | Strayer, et al., 1962, FEM |
| | Cs | 3.0±0.1 | | Strayer, et al., 1962, FEM |
| | Cu | 3.17 | | Bennette, et al., 1966, FEM |
| | Au | 3.6±0.5 | | Godwin and Luscher, 1965, FF |
| | $K^+$ | 2.2 | $2.3 \times 10^{-13}$ | Husmann, 1965, PP |
| | $K^+$ | 2.6 | $10^{-12}$ | Haumovets, 1964, FEM |
| | Rb | 2.6± 0.1 | $2.5 \times 10^{-13}$ | Hughes, 1959, PB |
| | $Rb^+$ | 2.07 | $3.4 \times 10^{-12}$ | Husmann, 1965, PP |
| | $Rb^+$ | 1.90±0.05 | $3.5 \times 10^{-12}$ | Hughes and Levenstein, 1959, PB |
| | Na | 2.4 | | Shrednik and Snezhko, 1964, FEM |
| | $Na^+$ | 2.33 | $6.3 \times 10^{-13}$ | Husmann, 1965, PP |
| | Sr | 4.21±0.22 | | Madey, et al., 1965a, FEM |
| | Sr | 3.56 | | Moore and Allison, 1955, RT |
| | CO | 2.3 | | Klein, 1959, FEM |
| | CO | 1.26, 2.56, 3.02, 3.28 | | Redhead, 1961, FF |
| | CO | 0.87, 3.26, 4.35 | | Ehrlich, 1961b, FF |
| | CO | 2.3, 3, 3, 4.3 | | Ehrlich, 1962, FEM |
| | CO | 0.87, 2.6, 3.04, 4.35 | | Rootsaert, et al., 1962, FEM |
| | CO | 0.91, 2.70, 4.00 | | Gavrilyuk and Medvedev, 1963, FF |
| | CO | 1.0, 2.74, 3.35, 3.9 | | Rigby, 1964, FF |
| | CO | 1.0, 2.6 | | May and Germer, 1966, LEED |
| | $CO_2$ | 5.3 | | Hayward and Gomer, 1959, FEM |
| | H | 1.35, 2.9 | | Hickmott, 1960, FF |
| | H | 0.61, 1.48 | | Ageev, et al., 1964, FF |
| | H | 1.10, 1.26, 1.22 | | Rigby, 1956b, FF |
| | H | 1.52 | | Mimeault and Hansen, 1966, FF |

HEATS OF DESORPTION (cont.)

| Substrate | Adsorbate | $E_{initial}$(eV) | $\tau_o$ | Worker |
|---|---|---|---|---|
| W | H | 2.78 | | Gomer, et al., 1957, FEM |
| | Hg | 1.92±0.18 | | Swanson, 1967, FEM |
| | N | 0.39, 0.87, 3.5 | | Ehrlich, 1961a, FF |
| | N | 3.2 | | Rigby, 1965, FF |
| | N | 2.4, 6.5 | | Ustinov and Ionov, 1966, FF |
| | O | 2.5, 5 | | Becker and Brandes, 1956, FEM |
| | O | 8.4 | | Brennan, et al., 1960, TFC |
| | O | 5.6 (0) 4.4 (oxide) | | McCarroll, 1967, FF |
| | O | 6.25 (0), 4.95(oxide) | | Schissel and Trulson, 1965, FF |
| | O | 6(0), 4.2 (oxide) | | Ptushinskii and Chuikov, 1966, FF-MS |
| | Xe | 0.35 | | Ehrlich and Hudda, 1959, FEM |
| W(110) | O | 4.8 | | Zingerman and Ischuk, 1966, EID |
| W(411) | Xe | 0.33 | | Rootsaert, et al., 1962, FEM |
| W(111) | Xe | 0.22 | | Rootsaert, et al., 1962, FEM |
| W(211) | H | 2.0 | | Rootsaert, et al., 1962, FEM |

TABLE III

Room Temperature Sticking Probabilities and Surface Coverage

| System | s | $\sigma \times 10^{14}$ (molec/cm$^2$) | Worker |
|---|---|---|---|
| Cr-CO | 0.2 | | Haque and Farnsworth, 1964, LEED |
| Cr-N | 0.003 | | Haque and Farnsworth, 1964, LEED |
| Cr-O | 0.3 | | Haque and Farnsworth, 1964, LEED |
| Mo-H | 0.35 | 4.1 | Pasternak and Wiesendanger, 1961, FF |
| Mo-N | 0.7 | 2.2 | Pasternak and Wiesendanger, 1961, FF |
| Nb-N | 0.4 | 3.5 | Pasternak, 1965, FF |
| Nb-O | 0.8 | 6.5 | Pasternak and Evans, 1967, FF |
| Pt-H | 0.001 | | Wiesendanger, 1963, FF |
| Re-N | 0.009 | 0.7 | Scheer and McKinley, 1966, FF |
| W-CO | 0.2 | 7.5 | Eisinger, 1957, FF-CP |
| W-CO | 0.49 | 9.5 | Redhead, 1961, FF |
| W-CO | 0.50 | 4.5 | Ehrlich, 1961, FF |
| W-CO | 0.48 | 5.8 | Gavrilyuk and Medvedev, 1963, FF |
| W-CO | 0.27 | 10.1 | Ricca, et al., 1962, FF |
| W-H | 0.2 | 7.5 | Eisinger, 1958, FF |
| W-H | 0.1 | | Hickmott, 1960, FF |
| W(100)-H | 0.1 | | Armstrong, 1966, LEED |
| W(211)-H | 0.3 | | Armstrong, 1966, LEED |
| W(111)-H | 0.01 | | Armstrong, 1966, LEED |
| W(110)-H | $< 10^{-3}$ | | Armstrong, 1966, LEED |
| W-NO | 0.8 | 14.0 | Yates and Madey, 1966, FF |
| W-N | 0.33 | 5.6 | Eisinger, 1958a, FF |
| W-N | 0.35 | 1.72 | Kisliuk, 1959, FF |
| W-N | 0.33 | 2.8 | Ehrlich, 1961a, FF |
| W-N | 0.22 | 1.2 | Ustinov and Ionov, 1966, FF |
| W-N | 0.10 | 4.5 | Ricca, et al., 1962, FF |
| W-O | 0.8 | | George and Stier, 1962, FEM-FIM |

TABLE IV

Surface Migration Energies

| System | $E_d$ (eV) | Worker |
|---|---|---|
| Mo-Cs | 0.43 ± 0.1 | Bennette, et al., 1966, FEM |
| Mo-Ni | 1.48 ± 0.06 | McIrvine and Bradley, 1957, FEM |
| Mo-Hg | 0.63 ± 0.08 | Bennette, et al., 1966, FEM |
| Ni-$H_2$ | 0.30 ± 0.04 | Wortman, et al., 1957a, FEM |
| Re-Cs | 0.36 ± 0.03 | Swanson, et al., 1963b, FEM |
| Ta-C | 2.3 | Klein and Leder, 1963, FEM |
| Ta-CO | 1.7 | Klein and Leder, 1963, FEM |
| W-Ar | 0.04 | Ehrlich and Hudda, 1959, FEM |
| W-Ba | 0.41 (110) regions | Utsugi and Gomer, 1962a, FEM |
| | 0.83 (123) | Utsugi and Gomer, 1962a, FEM |
| W-CO | 1.56 (111) | Klein, 1959, FEM |
| | 1.44 (111) | Swanson and Gomer, unpublished, FEM |
| | 0.89 (123) | Swanson and Gomer, unpublished, FEM |
| | 1.48 (100) | Swanson and Gomer, unpublished, FEM |
| W-Cs | 0.76 (123) | Swanson, et al., 1963b, FEM |
| | 0.50 (110) regions | Swanson, et al., 1964b, FEM |
| | 0.61 | Langmuir and Taylor, 1932, LD |
| W-Cu | 0.87 | Melmed, 1966, FEM |
| | 1.15 | Bennette, et al., 1966, FEM |
| W/O-Cu | 1.21 | Melmed, 1966, FEM |
| W/N-Cu | 1.17 | Melmed, 1966, FEM |
| W-Ge | 0.2 | Sokolo'skaya and Mileshkina, 1964, FEM |
| W-$H_2$ | 0.26±0.04 ($\theta$=1) | Gomer, et al., 1957, FEM |
| | 0.41±0.04 ($\theta$<1) | Gomer, et al., 1957, FEM |
| | 0.78±0.01 ($\theta$=0) | Gomer, et al., 1957, FEM |

Surface Migration Energies (cont.)

| System | Ed (eV) | Worker |
|---|---|---|
| W-Hg | 0.51 (111) | Swanson, et al., 1967, FEM |
| | 0.40 (123) | Swanson, et al., 1967, FEM |
| | 1.00 (100) | Swanson, et al., 1967, FEM |
| W-K | 0.3 ($\theta$ = 0) | Schmidt and Gomer, 1965a, FEM |
| | 0.8 ($\theta$ = 0.6) | Schmidt and Gomer, 1965a, FEM |
| W-$N_2$ | $\sim$0.87 (110) (111) | Ehrlich and Hudda, 1960, FEM |
| | $\sim$1.28 (116) (120) | Ehrlich and Hudda, 1960, FEM |
| W-$O_2$ | 1.04$\pm$0.06 ($\theta$=1) | Gomer and Hulm, 1957, FEM |
| | 1.3 ($\theta$ = 0) | Gomer and Hulm, 1957, FEM |
| W-Sr | 0.79$\pm$0.06 ($\theta > 1$) | Barnaby, et al., 1964, FEM |
| | 1.44$\pm$0.08 ($\theta < 1$) | Barnaby, et al., 1964, FEM |
| W-Th | 2.8 | Sugata and Kim, 1961, FEM |
| W-Xe | $\sim$0.16 | Ehrlich and Hudda, 1959, FEM |

## SECTION A - REFERENCES


1. C. Davisson and L. H. Germer, Phys. Rev, 30, 705 (1927).

2. H. E. Farnsworth, Numerous articles appearing in Physical Review between 1929 and 1936.

3. J. J. Lander, Recent Progress in Solid State Chemistry, (Pergemon Press, London, 1965) Vol. 2 p. 26.

4. H. E. Farnsworth, Advan. in Catalysis 15, 31 (1964).

5. J. W. May, Industrial and Engineering Chem. 57, No. 7, 19 (1965).

6. A. U. MacRae, Surface Science 2, 516 (1964).

7. L. H. Germer, Fundamental Phenomena in the Materials Sciences, (Plenum Press, 1966) 2, 23.

8. J. C. Helmer, Varian Associates Research Report No. VR-28.

9. A. U. MacRae, Science 139, 379, No. 3553 (1963).

10. J. J. Lander and J. Morrison, J. Appl. Phys. 34, 3517 (1963).

11. G. Ehrlich, Annual Review of Physical Chemistry (Annual Reviews, Inc., 1966) Vol. 17, p. 317.

12. E. A. Wood, J. Appl. Phys. 35, 1306 (1964).

13. R. L. Park and H. E. Farnsworth, Surface Science 2, 527 (1965).

14. J. J. Lander, J. Morrison, and F. Unterwald, Rev. Sci. Inst. 33, 782 (1962).

15. K. Fujiwara, K. Hayakawa, and S. Miyake, Jap. J. Appl. Phys. 5, 295 (1966).

16. C. W. Tucker, J. Appl. Phys. 35, 1897 (1964).

17. G. Ehrlich, Advances in Catalysis 14, 255 (1963).

18. P. A. Redhead, J. P. Hobson, and E. V. Kornelson, Advances in Electronics and Electron Physics, (Academic Press, New York, 1962) Vol. 17, p. 323.

19. L. J. Rigby, Can. J. Phys. 42, 1256 (1964).

20. T. E. Madey, J. T. Yates, and R. C. Stern, J. Chem. Phys. 42, 1372 (1965).

21. F. Ricca, A. G. Nasini and G. Saini, J. Catalysis 1, 458 (1962).

22. D. A. Degras, Paper presented at the Third International Congress of Vacuum, June 28 to July 2, 1965.

23. P. Kisliuk, J. Chem. Phys. 30, 174 (1959).
J. A. Becker, Solid State Physics (Academic Press, New York, 1958, Vol. 7, p. 379.

24. P. A. Pasternak and B. Evans, Trans. Metallurgical Socl of AIME 233, June 1965.

25. T. W. Hickmott and G. Ehrlich, J. Phys. Chem. Solids, 5, 47 (1958).

26. R. Gibson, B. Bergsnov-Hansen, N. Endow and R. A. Pasternak, Tenth National Vacuum Symposium, (1963) p. 88.

27. G. Ehrlich, J. Appl. Phys. 32, 4 (1961).

28. P. A. Redhead, Vacuum 12, 203 (1962).

29. P. Marmet and J. D. Morrison, J. Chem. Phys. 36, 1238 (1953).

30. J. R. Young, J. Appl. Phys. 31, 921 (1959).

31. G. E. Moore, J. Appl. Phys. 32, 1241 (1961).

32. D. A. Degras. L. A. Peterman and A. Schram, Nat'l. Vac. Tech. Trans. 9, 497 (1962).

33. P. A. Redhead, Can. J. Phys. 42, 886 (1964).

34. G. E. Fischer and R. A. Mack, J. Vac. Sci. Tech. 2, 123 (1965).

35. S. O. Dean, Paper presented at the Annual Sherwood Vacuum Conference, U. S. Atomic Energy Commision, Jan. 30-31, 1964.

36. D. Menzel and R. Gomer, J. Chem. Phys. 41, 3311 (1964).

37. L. A. Peterman, Nuovo Cimento Suppl. 1, 601 (1963).

38. C. H. Hinrichs, Ph. D. Thesis, Washington State University, (1966).

39. D. Lichtman, R. B. McQuistan, T. R. Kirst, Surface Sci. 5, 120 (1966).

40. C. J. Bennette, et al., NASACR-72117 (Field Emission Corp., McMinnville, Ore., 1967).

41. R. Gomer, Field Emission and Field Ionization (Harvard Univ. Press, 1961).

42. R. H. Good, Jr., and E. W. Muller, Handbuch der Physik 21, 176 (1956).

43. A. Melmed and R. Gomer, J. Appl. Phys. 34, 1802 (1961).

44. W. P. Dyke and J. P. Barbour, J. Appl. Phys. 27, 1802 (1961).

45. L. D. Schmidt and R. Gomer, J. Chem Phys. 45, 1605 (1966).

46. L. W. Swanson, R. W. Strayer and F. M. Charbonnier, Surface Science, 2, 177 (1964).

47. L. Schmidt and R. Gomer, J. Chem. Phys. 42, 3573 (1965).

48. E. Wolf, 25th Annual Conf. on Physical Electronics, Mass. Inst of Tech. (to be published).

49. L. W. Swanson, et al., Final Report for NASA Contract NAS3-2596 (Field Emission Corp., 1964).

50. L. W. Swanson, R. Strayer and F. Charbonnier, Surface Science 2, 177 (1964).

51. H. Utsugi and R. Gomer, J. Chem. Phys. 37, 1706 (1962).

52. L. Swanson and R. Gomer, J. Chem. Phys. 39, 2813 (1963).

53. E. Muller, Phys. Rev. 102, 618 (1956).

54. R. Gomer and L. Swanson, J. Chem. Phys. 38, 1613 (1963).

55. L. Swanson and R. Gomer, J. Chem. Phys. 39, 2813 (1963).

56. A. Melmed, J. Chem. Phys. 38, 1444 (1963).

57. R. Gretz, 24th Annual Conf. on Physical Electronics (MIT), p. 80 (1964).

58. J. R. Oppenheimer, Phys. Rev. 31, 66 (1928).

59. E. W. Muller, Z. Physik 106, 541 (1937).

60. E. W. Muller, in Advances in Electronics and Electron Physics, ed. by L. Marton (Academic Press, New York, 1960) 13, 83.

61. G. Ehrlich, Advances in Catalysis 14, 255 (1963).

62. J. F. Mulson and E. W. Muller, J. Chem. Phys. 38, 2615 (1963).

63. R. V. Culver and F. C. Tompkins, Advances in Catalysis 11, 67 (1959).

64. C. Herring and M. H. Nichols, Revs. Mod. Phys. 21, 185 (1949).

65. D. O. Hayward and B. M. W. Trapnell, Chemisorption (Butterworths, London, 1964).

66. A. L. Reimann, Thermionic Emission (Chapman and Hall, London, 1934).

67. G. L. Weissler, Handbuch der Physik (Springer-Verlag, Berlin, 1956) Vol. XXI, p. 304.

68. R. H. Fowler, Phys. Rev. 38, 45 (1931).

69. C. W. Oatley, Proc. Roy. Soc. (London) A155 218 (1936); Proc. Phys. Soc. (London) 51, 318 (1939).

70. G. L. Weissler and T. N. Wilson, J. Appl. Phys. 24, 472 (1953).

71. L. Dobretsov, Electronic and Ionic Emission (NASA Technical Translation F-73, 1963).

72. W. B. Nottingham, Handbuch der Physik (Springer-Verlag, Berlin, 1956) Vol. XXI, p. 1).

73. D. E. Meyer and W. H. Wade, Rev. Sci. Inst. 32, 1283 (1962).

74. A. A. Holscher, Surface Sci. 4, 89 (1966).

75. R. D. Young, Phys. Rev. 113, 110 (1959).

76. R. D. Young and E. W. Muller, Phys. Rev. 113, 115 (1959).

77. D. M. Young and A. D. Crowell, Physical Adsorption of Gases (Butterworths, Washington, 1962).

78. D. Brennan, D. O. Hayward, and B. M. W. Trapnell, Proc. Roy. Soc. (London) 256 A, 81 (1960).

79. P. Kisliuk, J. Chem. Phys. 31, 1605 (1959).

80. J. B. Taylor and I. Langmuir, Phys. Rev. 44, 423 (1933).

81. O. K. Husmann, Phys, Rev. 140, A546 (1965).

82. M. D. Scheer and J. Fine, J. Chem. Phys. 37, 107 (1962).

## SECTION B - BIBLIOGRAPHY OF AUTHORS REFERENCED IN EXPERIMENTAL RESULTS


Ageev, V. N. and N. I. Ionov, and Yu. K. Ustinov, Soviet Physics-Tech. Phys. 9, 1581 (1965).

Anderson, J., W. E. Danforth and A. J. Williams, III, J. Appl. Phys. 34, 2260 (1963).

Armstrong, R. A., 25th Ann. Conf. Physical Electronics, 209 (1965).

Armstrong, R. A. Can. J. Phys. 44, 1753 (1966).

Arthur, J. R., Jr., and R. S. Hansen, J. Chem. Phys. 36, No. 8, 2062 (1962).

Azizov, U. V., V. M. Vaknidov, V. M. Sulmanov, B. M. Sheinberg, and G. N. Shuppe, Soviet Physics-Solid State, 7, No. 9, 2232 (1966).

Barnaby, B. E., T. E. Madey, A. A. Petrauskas and E. A. Coomes, J. Appl. Phys. 35, No. 6, 1759 (1964).

Becker, J. A., and R. G. Brandes, J. Chem. Phys. 23, 1323 (1956).

Bell, A. E. and R. Gomer, J. Chem. Phys. 44, No. 3, 1065 (1966).

Bennette, C. J., R. W. Strayer, L. W. Swanson and E. C. Cooper, NASA Contract NAS3-5902, Report No. 54704, 18 February (1966).

Bennette, C. J., R. W. Strayer, L. W. Swanson and E. C. Cooper, NASA Contract NAS3-8900, Report No. 72117, 25 April (1967).

Boggio, J. E., and H. E. Farnsworth, Surface Science 1, 399 (1964).

Brennan, D., F. H. Hayes, Trans. Faraday Soc. 60, 589 (1964).

Brennan, D., D. O. Hayward, Phil. Trans. A(GB) 258, 375 (1965).

Brennan, D., D. O. Hayward and B. M. W. Trapnell, Proc. Roy. Soc. A256 81 (1960).

Cape, J. A. and E. A. Coomes, J. Chem. Phys. 32, 210 (1960).

Cerny, S., V. Ponec, and L. Hlodek, J. Catalysis 5, 27 (1966).

Degras, D. A., 3 eme Congres International du Vide, Stuttgart, (28 June-2 July, 1965).

Delchar, T. A. and G. Ehrlich, J. Chem. Phys. 42, 2686 (1965).

Duell, M. J. and R. L. Moss, Trans. Faraday Soc. 61, Pt. 10, 2262 (1965).

Ehrlich, G., J. Chem. Phys. 34, 29 (1961a).

Ehrlich, G., J. Chem. Phys. 34, 39 (1961b).

Ehrlich, G., T. W. Hickmott and F. G. Hudda, J. Chem. Phys. 28, 506 (1958a).

Ehrlich, G., T. W. Hickmott and F. G. Hudda, J. Chem. Phys. 28, 977 (1958b).

Ehrlich, G. and F. G. Hudda, J. Chem. Phys. 30, 493 (1959).

Ehrlich, G. and F. G. Hudda, J. Chem. Phys. 32, 942 (1960).

Ehrlich, G. and F. G. Hudda, J. Chem. Phys. 35, 1421 (1961).

Ehrlich, G. and F. G. Hudda, J. Chem. Phys. 36, 3233 (1962).

Ehrlich, G., J. Chem. Phys. 36, 1171 (1962).

Eisinger, J., J. Chem. Phys. 27, 1206 (1957).

Eisinger, J., J. Chem. Phys. 28, 165 (1958a).

Eisinger, J., J. Chem. Phys. 29, 1154 (1958b).

Estrup, P. J. and J. Anderson, J. Chem. Phys. 45, 2254 (1966).

Estrup, P. J., J. Anderson and W. E. Danforth, Surface Science 4, 286 (1966).

Gasser, R. P. H., and D. E. A. Schuftan, Vacuum 13, 146 (1963).

Gavrilyuk, V. M. and V. K. Medvedev, Soviet Physics-Solid State, 4, 1737 (1963).

Gavrilyuk, V. M. and V. K. Medvedev, Soviet Physics-Solid State 8, 1439 (1966).

George, T. H. and P. M. Stier, J. Chem. Phys. 37, No. 9, 1935 (1962).

Germer, L. H. and A. U. MacRae, J. Chem. Phys. 37, 1382 (1962a).

Germer, L. H. and A. U. MacRae, J. Appl. Phys. 33, 2923 (1962b).

Godwin, R. P. and E. Luscher, Surface Science 3, 42 (1965).

Gomer, R. and J. K. Hulm, J. Chem. Phys. 27, No. 6, 1363 (1957).

Gomer, R., R. Wortman and R. Lundy, J. Chem. Phys. 26, 1147 (1957).

Gomer, R., J. Chem. Phys. 28, 168 (1958a).

Gomer, R., J. Chem. Phys. 29, 441 (1958b).

Gorbatyi, N. A. and E. M. Ryabchenko, Soviet Physics-Solid State 7, No. 4, 921 (1965).

Haas, T. W. and A. G. Jackson, J. Chem. Phys. 44, 2921 (1966).

Haque, C. A. and H. E. Farnsworth, Surface Science 1, 378 (1964).

Haque, C. A. and H. E, Farnsworth, Surface Science 4, 195 (1966).

Haumovets, A. G., Soviet Physics-Solid State 5, No. 8, 1688 (1964).

Hayward, D. O., and R. Gomer, J. Chem. Phys. 30, 1617 (1959).

Hickmott, T. W., J. Chem. Phys. 32, 810 (1960).

Hill, M. P. and B. A. Pethica, J. Chem. Phys. 36, No. 11, 3095 (1962).

Holscher, A. A., J. Chem. Phys. 41, 579 (1964).

Hopkins, B. J., and K. R. Pender, Surface Science 5, 155 (1966a).

Hopkins, B. J., and K. R. Pender, Surface Science 5, 316 (1966b).

Huber, E. E., Jr., Applied Phys. Letters 8, No. 7, 169 (1966).

Huber, E. E., Jr., and C. T. Kirk, Jr., Surface Science 5, 447 (1966).

Hughes, F. L., Phys. Rev. 113, 1036 (1959).

Hughes, F. L. and H. Levinstein, Phys. Rev. 113, 1029 (1959).

Husmann, O. K. Phys. Rev. 140, A546 (1965).

Jones, J. P., Proc. Royal Soc. 284A, 469 (1964).

Kisliuk, P., J. Chem. Phys. 30, 174 (1959).

Klein, R., J. Chem. Phys. 31, 1306 (1959).

Klein, R. and L. B. Leder, J. Chem. Phys. 38, No. 8, 1866 (1963).

Klein, R. and J. W. Little, Surface Science 2, 167 (1964).

Klein, R. and J. W. Little, Surface Science 6, 193 (1967).

Langmuir, I. and J. B. Taylor, Phys. Rev. 40, 463 (1932).

Lawson, R. P. W. and G. Carter, Applied Phys. Letters 9, No. 2, 85 (1966).

Lee, R. N. and H. E. Farnsworth, Surface Science 3, 461 (1965).

Lichtman, D., R. B. McQuistan, and T. R. Kirst, Surface Science 5, 120 (1966).

Madey, T. E., A. A. Petrauskas, and E. A. Coomes, J. Chem. Phys. 42, 479 (1965a).

Madey, T. E., J. T. Yates and R. C. Stern, J. Chem. Phys. 42, 1372 (1965b).

May, J. W. and L. H. Germer, J. Chem. Phys. 44, 2895 (1966).

McCarroll, B., J. Chem. Phys. 46, 863 (1967).

McIrvine, E. C. and R. C. Bradley, J. Chem. Phys. 27, No. 3, 646 (1957).

Melmed, A. J. and R. Gomer, J. Chem. Phys. 34, No. 5, 1802 (1961).

Melmed, A. J., J. Appl. Phys. 36, No. 11, 3691 (1965a).

Melmed, A. J., J. Chem. Phys. 43, No. 9, 3057 (1965b).

Melmed, A. J., J. Appl. Phys. 37, No. 1, 275 (1966).

Menzel, D. and R. Gomer, J. Chem. Phys. 41, No. 11, 3311 (1964a).

Menzel, D. and R. Gomer, J. Chem Phys. 41, No. 11, 3329 (1964b).

Mimeault, V. J. and R. S. Hansen, J. Chem. Phys. 45, 2240 (1966).

Moore, G. E. and H. W. Allison, J. Chem. Phys. 23, 1609 (1955).

Moore, G. E. and F. C. Unterwald, J. Chem. Phys. 40, 2626 (1964).

Moss, R. L. and C. Kimball, Trans. Faraday Soc. 56, No. 454, Part 10, 1487 (1960).

Muller, E. W., Phys. Rev. 102, No. 3, 618 (1956).

Mulson, J. F. and E. W. Muller, J. Chem. Phys. 38, No. 11, 2615 (1963).

Naumovets', A. G., Ukrainiskii Fizichnii Zuhurnal 8, No. 1, 65 (1963).

Park, R. L. and H. E. Farnsworth, J. Appl. Phys. 35, 2220 (1964a).

Park, R. L. and H. E. Farnsworth, J. Chem. Phys. 40, 2354 (1964b).

Pasternak, R. A., Transactions, Eighth Annual Conference on Vacuum Metallurgy, (June 1965).

Pasternak, R. A., N Endow, and Bergsnov-Hansen, J. Phys. Chem. 70, 1304 (1966a).

Pasternak, R. A., B. Evans and Bergsnov-Hansen, J. Electrochemical Soc, 113, 731 (1966).

Pasternak, R. A., and B. Evans, J. Electrochemical Society 114, 452 (1967).

Pasternak, R. A., and H. U. D. Wiesendanger, J. Chem. Phys. 34, 2062 (1961).

Pritchard, J. Nature 194, 38 (1962).

Ptushinskii, Yu. G., Radiotekhn i Elektron 5, 1663 (1960).

Ptuchinskii, Yu. G., Radiotekhn i Elektron 6, 382 (1961).

Ptushinskii, Yu. G., and B. A. Chuikov, Surface Science 6, 42 (1967).

Quinn, C. M. and M. W. Roberts, Trans. Faraday Soc. 60, 899 (1964).

Redhead, P. A., Trans. Faraday Soc. 57, 641 (1961).

Redhead, P. A., Can. J. Phys. 42, 886 (1964a).

Redhead, P. A., Appl. Phys. Letters 4, 166 (1964b).

Ricca, F., A. G. Nasini and G. Saini, J. Catalysis 1, 458 (1962).

Ricca, F., R. Medana and G. Saini, Trans. Faraday Soc. 61, 1492 (1965).

Rigby, L. J., Can. J. Phys. 42, 1256 (1964).

Rigby, L. J., Can. J. Phys. 43, 532 (1965a).

Rigby, L. J., Can. J. Phys. 43, 1020 (1965b).

Rootsaert, W. J. M., L. L. van Reijen, W. M. H. Sachtler, J. Catalysis 1, 416 (1962).

Scheer, M. D., and J. Fine, J. Chem. Phys. 37, 107 (1962a).

Scheer, M. D. and J. Fine, J. Chem. Phys. 36, 1647 (1962b).

Scheer, M. D. and J. Fine, J. Chem. Phys. 38, 307 (1963a).

Scheer, M. D. and J. Fine, J. Chem. Phys. 39, 1752 (1963b).

Scheer, M. D. and J. D. McKinley, Surface Science 5, 332 (1966).

Schissel, P. O. and O. C. Trulson, J. Chem. Phys. 43, 737 (1965).

Schmidt, L. D. and R. Gomer, J. Chem. Phys. 42, 3573 (1965a).

Schmidt, L. D. and R. Gomer, J. Chem. Phys. 43, 95 (1965b).

Schmidt, L. D. and R. Gomer, J. Chem. Phys. 43, 2055 (1965c).

Schmidt, L. D. and R. Gomer, J. Chem. Phys. 45, 1605 (1966).

Shrednik, V. N., Soviet Physics-Solid State 3, No. 6 (1961).

Shrednik, V. N. and E. V. Snezhko, Soviet Physics-Solid State 6, No. 5, 1173 (1964).

Shrednik, V. N. and E. V. Snezhko, Soviet Physics-Solid State, 6, No. 11 (1965).

Silver, M. and R. S. Witte, J. Chem. Phys. 38, 872 (1963).

Sokolo'skaya, I. L. and N. V. Mileshkina, Soviet Physics-Solid State 6, No. 6, 1401 (1964).

Strayer, R. W., E. C. Cooper, L. W. Swanson and F. M. Charbonnier, NASA Contract NASr-19, 30 April (1962).

Sugata, E. and H. Kim, Eighth Annual Field Emission Symposium, (1961).

Suhrmann, R., U. Richter and G. Wedler, Naturwissenschaften, 50, 641 (1963).

Swanson, L. W., R. W. Strayer and L. E. Davis, Submitted to Surface Science, 1967.

Swanson, L. W. and R. Gomer, J. Chem. Phys. 39, No. 11, 2813 (1963a).

Swanson, L. W., R. W. Strayer, E. C. Cooper, F. M. Charbonnier, NASA Contract NASw-458, 30 April (1963b).

Swanson, L. W., R. W. Strayer, and F. M. Charbonnier, Proceedings of the Twenty-Fourth Annual Conference on Physical Electronics 120 (1964a).

Swanson, L. W., R. W. Strayer, and F. M. Charbonnier, Surface Science 2, 177 (1964b).

Swanson, L. W., R. W. Strayer, C. J. Bennette and E. C. Cooper, NASA Contract NAS3-2596, Report No. 54106, 2 June (1964c).

Swanson, L. W., A. E. Bell, L. C. Crouser, and B. E. Evans, NASA Contract NASw-1082, November (1966).

Taylor, J. B. and I. Langmuir, Phys. Rev. 44, 423 (1933).

Taylor, L. H. Surface Science 2, 188 (1964a).

Taylor, N. J., Surface Science 2, 544 (1964b).

Tucker, C. W., Jr., Surface Science 2, 516 (1964a).

Tucker, C. W., Jr., J. Appl. Phys. 35, 1897 (1964b).

Ustinov, Yu. K., and N. I. Ionov, Sov. Phys.-Tech. Phys., 10, 1607 (1966).

Utsugi, H. and R. Gomer, J. Chem. Phys. 37, No. 8, 1706 (1962a).

Utsugi, H. and R. Gomer, J. Chem. Phys. 37, No. 8, 1720 (1962b).

von Goeler, E., and E. Luscher, J. Phys. Chem. Solids 24, 1217 (1963).

von Goeler, E., and R. N. Peacock, J. Chem. Phys. 39, 169 (1963).

Wiesendanger, H. U. D., J. Catalysis 2, 538 (1963).

Wilson, R. G, Appl. Phys. 37, 2261 (1966a).

Wilson, R. G., Appl. Phys. 37, 3161 (1966b).

Wilson, R. G., Appl. Phys. 37, 3170 (1966c).

Wilson, R. G., Appl. Phys. 37, 4125 (1966d).

Wortman, R., R. Gomer, and R. Lundy, J. Chem. Phys. 26, 1334 (1957a).

Wortman, R., R. Gomer, and R. Lundy, J. Chem. Phys. 27, 1099 (1957b).

Yates, J. T., Jr., and T. E. Madey, J. Chem. Phys. 43, 1055 (1965).

Yates, J. T., Jr., and T. E. Madey, J. Chem. Phys. 45, 1623 (1966).

Young, R. D., J. Appl. Phys. 36, 2656 (1965).

Zingerman, Ya. P., V. Z. Ishchuk, and V. A. Morozovskii, Soviet Physics-Solid State 2, 2030 (1961).

Zingerman, Ya. P., and V. A. Ischuk, Soviet Physics-Solid State 8, 728 (1966).

Zingerman, Ya. P., and V. A. Ischuk, Soviet Physics-Solid State 8, 2394 (1967).

Zubenko, Yu. V. and I. L. Sokolo'skaya, Soviet Physics-Solid State 3, No. 5, 1133 (1961).

Zubenko, Yu. V., Radio Engng. and Elect. Phys. 8, No. 7, 1208 (1963).